DEVELOPMENT AND TESTING AN INTELLIGENT HYBRID POLYMERIC COMPOSITE BEAM WITH HEALING ABILITY EMBEDDED WITH Ni-Ti SHAPE MEMORY ALLOY

WAMBURA MWIRYENYI MWITA

BELLVILLE-CAPE TOWN

REPUBLIC OF SOUTH AFRICA

DECEMBER - 2010

DEVELOPMENT AND TESTING AN INTELLIGENT HYBRID POLYMERIC COMPOSITE BEAM WITH HEALING ABILITY EMBEDDED WITH Ni-Ti SHAPE MEMORY ALLOY

by

WAMBURA MWIRYENYI MWITA (BSc (Hons) Mech Eng UDSM)

Thesis submitted in fulfillment of the requirement for the degree

Master of Technology in Mechanical Engineering

in the Faculty of Engineering

at the Cape Peninsula University of Technology

Supervisor: Dr. O Philander
Co-supervisor: Dr. S Mahoi

Bellville-Cape Town

Republic of South Africa

DECEMBER 2010

DECLARATION

I, Wambura Mwiryenyi Mwita, declare that the contents of this thesis represent my own unaided work, and that the thesis has not previously been submitted for academic examination towards any qualification. To the best of my knowledge, it contains no copy or paraphrase of work published by another person, except where dully acknowledged in the text. Furthermore, it represents my own opinions and not necessarily those of the Cape Peninsula University of Technology.

W M Mwita *Dec 2010*

Signed **Date**

ABSTRACT

Hybrid polymeric composites (HPC) are widely used for the design of aerospace, automobile and civil engineering structures. One of the major challenges posed by these materials and structures is their brittle nature. When subjected to impact and dynamic loads, the polymeric composite structures undergo micro cracking. The cracks coalesce, propagate and can lead to catastrophic failure of the material and structures.

In this thesis, an intelligent hybrid polymeric composite (IHPC) beam with healing ability was developed and tested. The IHPC beam developed consisted of a 3% prestrained 1mm diameter Ni-Ti shape memory alloy (SMA) wire actuator embedded in the polymeric host matrix. The function of the embedded Ni-Ti shape memory alloy was to enhance intelligence and healing ability to the IHPC beam.

Upon electric current resistance heating, the Ni-Ti SMA actuator responds by contracting as a result of detwinned martensite → austenite phase transformation. Contraction of the SMA in the IHPC beam was utilized to stiffen and enhance healing by retarding crack growth and recovery of the strain induced in the loaded IHPC beam. This can result to increase of the flexural stiffness EI (defined as the product of the Young's Modulus E of the material and the moment of inertia I of the geometry of the beam) and mode I fracture stress intensity factor K_{IC} of the IHPC beam.

One (1) mm diameter Ni-Ti SMA wire was used in the experimental work in this thesis. The wire was cut into 35 pieces, 200 mm long each. Ni-Ti SMA wires were heated in the furnace to a temperature of 250ºC for ten (10) hours then were left to cool in the ambient air. The heat treatment was aimed to release any residual stress and to stabilize the austenite start (A_S) and austenite finish (A_f) transformation temperatures of the Ni-Ti SMA.

After heat treatment, the Ni-Ti SMA wires were prestrained by 3% (based on a gauge length of 150mm) on a tensile testing machine. Prestraining of the Ni-Ti SMA wires was aimed to induce detwinned martensite volume fraction in them hence increasing the transformation strain and recovery force of the Ni-Ti SMA actuator.

Intelligent hybrid polymeric composite (IHPC) beams and polymeric virgin (PV) beams, all of dimensions 150mmx25mmx10mm were manufactured by casting 60D polyurethane thermosetting epoxy resin in a silicon mould. The casting process was done using the MCP

Vacuum cast System in the Rapid Prototyping Development Laboratory in the Department of Industrial Engineering, University of Stellenbosch.

Six (6) IHPC beams, each with Ni-Ti SMA embedded wire along the neutral axis were manufactured for a pullout test. Three (3) of them were tested at temperature T1 below austenite start (A_S), the remaining three (3) were tested at temperature T2 of austenite finish (A_f).
Six (6) un-notched IHPC beams with Ni-Ti SMA wire embedded 7mm off the neutral axis and three (3) un-notched PV beams were manufactured. The manufactured beams were tested to determine the effect of actuated Ni-Ti SMA on the flexural stiffness EI of un-notched IHPC beam under a bending load.

Six (6) notched IHPC beams with Ni-Ti SMA wire embedded 7mm off the neutral axis and three (3) notched PV beams were manufactured. The manufactured beams were tested to determine the effect of actuated Ni-Ti SMA on mode I fracture stress intensity factor K_{IC} of the notched IHPC beam under a bending load.

A pullout test was performed to determine the SMA-matrix interfacial pullout load at two temperature conditions (T1 below austenite start A_S and T2 of austenite finish A_f).The test results showed that the pullout load at the elevated temperature T2 decreased by 50% compared to the pullout load at room temperature T1. This behaviour was due to softening of the SMA-matrix interface upon heating the Ni-Ti SMA wire. The softened interface created a weaker bond hence a lower pullout load.

A four point bending test was performed on un-notched IHPC and PV beams to determine the effect of Ni-Ti SMA on the flexural stiffness EI of un-notched IHPC beams and was compared to the value of EI for un-notched PV beams. Two tests were done at two temperature conditions, (T1 below austenite start A_S and T2 of austenite finish A_f).The results showed that actuation of the Ni-Ti SMA increased the flexural stiffness EI of un-notched IHPC beams at elevated temperature T2 by 4.3% over the value of EI for un-notched PV beams at room temperature T1.

A four point bending test was performed on notched IHPC and PV beams to determine the effect of actuated Ni-Ti SMA on mode I fracture stress intensity factor K_{IC}. Two tests were done at two temperature conditions, at T1 (below austenite start A_S) and (T2 of austenite finish A_f). The results showed that actuation of the Ni-Ti SMA increased the fracture stress intensity factor K_{IC} of notched IHPC beams at T2 by 41% over the value of K_{IC} for notched IHPC beams at T1.

The value of K_{IC} of notched IHPC beams at T2 was 189% over that of notched PV beams at T1.The increase of fracture stress intensity factor was enhanced by suppression of crack propagation in the notched IHPC beams.

Results from an analytical model of un-notched IHPC and PV beams were compared with experimental results. The Lin and Rogers (1991) model equation was applied to predict the martensite volume fraction in the Ni-Ti SMA as a function of temperature.

The Brinson (1993) model equation was implemented to predict the recovery stress and force generated by the Ni-Ti SMA as functions of actuating temperature. A constitutive relation for the bending strain and flexural stiffness EI of un-notched IHPC and PV beams as functions of actuating temperature was developed. A C++ program was formulated and used for the computation.

The results showed that increasing the temperature of the NI-Ti SMA from T1 below austenite start A_S to T2 of austenite finish A_f, decreased the martensite volume fraction and increased the Ni-Ti SMA recovery force. The results showed that the flexural stiffness EI of un-notched IHPC beam increased with the increase of temperature by 6% at T2 over the value of EI for un-notched PV beam at T1.

A comparison between experimental and analytical results on the bending load versus strain showed good agreement for un-notched IHPC and PV beams at T1 (below austenite start A_S). For the un-notched IHPC beam at T2 (of austenite finish A_f), the experimental flexural stiffness EI was relatively lower than the value of EI determined based on the analytical model. This was contributed by softening and debonding of the SMA-matrix interface upon heating the Ni-Ti SMA wire. For the analytical model to agree with experimental results, the effect of heating the Ni-Ti SMA wire from T1 to T2 on the analytical model was taken into account. A bonding factor K_b =0.8 was introduced to the analytical bending strain equation. Experimental and analytical results on the bending load versus strain showed good agreement.

The results achieved in this thesis indicate that application of the Ni-Ti shape memory alloy increased flexural stiffness EI and mode I fracture stress intensity factor K_{IC} of the IHPC beam. The embedded Ni-Ti SMA significantly stiffened and enhanced healing in the IHPC beam by retarding crack growth and recovery of strain induced by the applied load. The results promise that the use of shape memory alloy can improve in-service safety and reliability of hybrid polymeric composites and structures.

TABLE OF CONTENTS

CHAPTER FOUR: EXPERIMENTAL PROCEDURE AND RESULTS

CHAPTER FIVE: ANALYTICAL MODELING OF UN-NOTCHED IHPC AND PV BEAMS

CHAPTER SIX: DISCUSION OF RESULTS

CHAPTER SEVEN: CONCLUSION AND RECCOMMENDATIONS

ACKNOWLEDGEMENTS

First of all, I thank God for giving me strength and endurance towards completion of this thesis.

I am deeply indebted to my supervisor Dr. O Philander, Lecturer and Head of Smart Materials-Centre for Research in Applied Technology (CRATECH), Mechanical Engineering Department, Cape Peninsula University of Technology. He provided me guidance, encouragement, moral and material support for the successful completion of this thesis. For any assistance required, technical or financial, he acted on time.

Thanks shall go to the followings for their inputs to this work:
Dr. S Mahoi, my co-supervisor for his guidance in the preliminary experimental work. Mr. B. Deez, head of Rapid Product Development Laboratory, Department of Industrial Engineering, University of Stellenbosch. On behalf of the institution, Mr. Deez facilitated the MCP vacuum casting machine for manufacturing the IHPC and PV beams. Ms Liezel Van Zyl, Administrative Assistant, Smart Alignment Research Group. She played a big role in the coordination and procurement of various materials required for my research work. Mr. W Kohlhofer, lecturer in Mechanical Engineering Department for his assistance on the use of strain gauges. My colleague A Ayodele, M. Tech. student for his tireless assistance and cooperation he offered during the experimental work.

Lastly but not least, special thanks shall go to the Cape Peninsula University of Technology (CPUT) for the appreciated financial support it provided towards the accomplishment of my research work.

LIST OF SYMBOLS

SYMBOL	EXPLANATION	UNITS (SI)
a	length, crack length	m
A	area	m^2
A	austenite	-
A_f	austenite finish temperature	K
A_S	austenite start temperature	K
b,	Length (beam)	m
B	width(beam)	m
C_A	Ni-Ti SMA stress constant in austenite phase	$N/m^2.K$
E	Young's modulus	N/m^2
E_A	Young's modulus of austenite	N/m^2
E_C	Young's modulus of the composite	N/m^2
E_m	Young's modulus of the epoxy matrix	N/m^2
E_M	Young's modulus of the martensite	N/m^2
E_S	Young's modulus of Ni-Ti SMA wire	N/m^2
F	bending force	N
F_C	critical (fracture) force	N
F_{re}	recovery force	N
H, h	Height (beam)	m
I	sectional second moment of area (beam)	m^4
K_I	stress intensity factor	$N/m^{3/2}$
K_b	bonding factor	-
K_{IC}	critical (fracture) stress intensity factor	$N/m^{3/2}$
L	Length (beam)	m
ΔL	change in length	m

SYMBOL	EXPLANATION	UNITS (SI)
M	Martensite	-
M_f	martensite finish temperature	K
M_S	martensite start temperature	K
M[d]	detwinned martensite	-
M[t]	twinned martensite	-
Ni-Ti	nickel-titanium alloy	-
Q	shear force	N
PE	pseudoelasticity	-
SMA	shape memory alloy	-
SME	Shape memory effect	-
t	time	S
T	temperature	K
T1	temperature below austenite start A_S	K
T2	temperature equal to austenite finish A_f	K
T_O	initial temperature.	K
T_g	glass transition temperature of the epoxy matrix	K
V_m	volume fraction of epoxy matrix	-
V_S	volume fraction of Ni-Ti SMA wire	-
x	Length (beam)	M
y	Length (beam)	M
Y	compliance function	-
σ	axial stress	N/m^2
σ_b	bending stress	N/m^2
σ_{me}	mechanical axial stress	N/m^2
σ_{th}	thermal stress	N/m^2

SYMBOL	EXPLANATION	UNITS (SI)
σ_{re}	recovery stress	N/m^2
σ_{tr}	transformation stress	N/m^2
ε	axial strain	-
ε_O	initial prestrain in Ni-Ti SMA	-
ε_L	recovery strain at temperature above A_f	-
ε_T	recovery strain at temperature T	-
ε_{max}	maximum transformation strain of Ni-Ti SMA	-
ξ	martensite volume fraction in Ni-Ti SMA	-
ξ_o	initial martensite volume fraction in Ni-Ti SMA	-
ξ_S	stress induced martensite volume fraction in Ni-Ti SMA	-
ξ_T	temperature induced martensite volume fraction in Ni-Ti SMA	-
Ω	SMA transformation modulus	N/m^2
Θ	modulus of thermal expansion	N/m^2. K
IHPC	Intelligent Hybrid Polymeric Composite	-
PV	Polymeric Virgin	-

LIST OF FIGURES

LIST OF TABLES

CHAPTER ONE

INTRODUCTION

1.1 Problem statement

Hybrid polymeric composites (HPC) are materials that result from a combination of at least two (polymer and polymer or polymer and non polymer) chemically distinct materials with a distinct interface separating the components. At least one of the materials of the composite acts as a reinforcing agent, this can be in the form of particles (powder), fibers or laminates (sheets) and usually is embedded in the other material called the matrix. A correctly manufactured composite combines the strength of the reinforcement with that of the matrix and possesses desirable properties that cannot be achieved by any of the individual components of the composite (Trask and Bond, 2006; Collister, 2003).

Hybrid polymeric composites are characterized by their high corrosion resistance against chemical and other environmental attacks, high strength to weight ratio, lightness in weight and relatively poor thermal and electrical conductance. In order to improve the mechanical properties and to achieve certain functionalities, polymeric materials are reinforced with carbon fibers, glass fibers, shape memory alloys (SMAs) and ceramics. Due to the above mentioned desirable characteristics; hybrid polymeric composites are widely used for the design of aerospace, automobile and civil engineering structures (Auricchio et al. 2003; Collister, 2003; Crane and Charles, 1984).

One of the major challenges posed by HPC material structures is their brittle nature. They possess low strain-to-failure characteristics. Their inability to deform plastically results in energy absorption via creation of defects and damages. When subjected to impact and dynamic loads, these structures undergo micro cracking and delaminations. The cracks coalesce, propagate and can lead to catastrophic failure (Burton et al, 2006; Kessler et al, 2003). Much effort is required to detect the cracks in polymeric composite structures. In some cases the cracks can be difficult to detect and even difficult to repair. Currently, some

cracks formed in the composite parts and structures can be inspected manually to determine the extent of damage. For critical parts advanced non destructive testing methods can be used. This may include ultrasonic, infrared thermography, X-ray tomography and computerised vibro thermography (Kessler et al, 2003).

Based on specific desired properties, Hybrid Polymeric Composites have found their way into engineering applications. However their brittle nature makes them unpredictable in service and thus limits their overall integration and performance. There has been a need to develop "intelligence" and "healing" ability for these materials to overcome unpredictable fracture due to their brittle nature.

In this thesis, an intelligent hybrid polymeric composite (IHPC) beam with healing ability embedded with the Ni-Ti shape memory alloy is to be developed and tested. Intelligence and healing ability of the IHPC beam will be enhanced by the contraction of the embedded Ni-Ti shape memory alloy actuator. Contraction of the Ni-Ti SMA results from Ni-Ti SMA material phase transformation from detwinned martensite to austenite phase upon heating from a temperature T1 below austenite start A_S to the temperature T2 of austenite finish A_f.

In this thesis the following meanings will apply to "intelligence" and "healing" of IHPC beam:
"Intelligence" of the IHPC beam is the behaviour of the intelligent hybrid polymeric composite beam to contract as a result of contraction of the embedded SMA actuator. Contraction of the SMA is due to its sensing and response to applied electric current resistive heat.

"Healing" of the IHPC beam is the ability of the intelligent hybrid polymeric composite beam to stiffen as a result of contraction of embedded SMA actuator. Contraction of the IHPC beam will enhance healing by retarding crack growth and recovery of the strain induced by applied load.

The healing ability of the IHPC beam will be quantitatively tested through determination of the flexural stiffness EI and mode I fracture stress intensity factor K_{IC} of the IHPC beam. Each of the values EI and K_{IC} will be determined at two temperature conditions, T1 below austenite start A_S and T2 of austenite finish A_f.

1.2 Objectives of the thesis

1.2.1 Main Objective

Development and testing an intelligent hybrid polymeric composite (IHPC) beam with healing ability embedded with Ni-Ti shape memory alloy.

1.2.2 Specific Objectives

1.2.2.1 Heat treatment and prestraining of Ni-Ti SMA wire specimens.

1.2.2.2 Manufacture of IHPC and Polymeric Virgin (PV) beams.

1.2.2.3 Determination of the Ni-Ti SMA - matrix interfacial pullout load.

1.2.2.4 Determination of the effect of actuated Ni-Ti SMA on the flexural stiffness EI of un-notched IHPC beams.

1.2.2.5 Determination of the effect of actuated Ni-Ti SMA on retarding crack growth and mode I fracture stress intensity factor K_{IC} of notched IHPC beams.

1.2.2.6 Analytical modeling of un-notched IHPC and PV beams.

1.2.2.7 Determination of the effect of Ni-Ti SMA actuation temperature on the Ni-Ti SMA-epoxy interfacial bond.

1.3 Literature Review

1.3.1 Shape memory alloys (SMAs)

Shape memory alloys fall in a group of materials known as smart materials. Smart materials are engineering intelligent adaptive materials that are capable of sensing and responding to environmental stimuli such as strain, force, temperature in a predetermined behaviour and recover their original state when the stimuli are removed (Michaud, 2004; Poon et al. 2005). Shape memory alloys are material alloys with ability to undergo large strains while recovering their initial configuration at the end of the deformation process spontaneously or by heating without any residual deformation (Michaud, 2004).

Recently a number of shape memory alloys such as Ni-Ti, Cu-Al-Zn , Ni-Mn-Ga, Cu-Ni-Al have been utilised in various engineering and medical applications (Auricchio et al. 2003). Due to their high actuation property, SMAs are used in the manufacturing industry for making fastening devices, temperature sensing valves and vibration damping plates, also they can be used as active actuators to control the shape of structural elements or as passive actuators to stiffen the structural elements (Rustighi et al., 2005; Zang et al.2005; and Burton et al., 2006). SMAs are applied in the medical sciences for making artificial organs, in mechanical and marine engineering and also for new applications in civil engineering specifically in structural seismic protection and structural health monitoring of buildings and bridges (Muthumani, 2002).

Shape memory alloys are used to reinforce polymer composite structures in a form that is compatible with the composite processing route (Zeng et al, 2004). In order to achieve the best response from SMA effect, thin wires span the entire composite component, where as for damping or electrical properties, particles of foams could be suitable (Burton et al, 2006;

Yang, 2000). Most SMA composites have been designed for shape change, recent developments in fabrication techniques of SMA wires to be embedded in composites have produced high quality wires, with thin oxide layers (Tompson et al. 2001). This has facilitated the integration of SMA wires into fiber reinforced polymer materials enhancing their structural

integrity of the matrix. It has been found that reinforced composites with prestrained SMAs exhibits higher reversible strains, higher damping capacity, increase in mechanical and physical properties and most importantly, the ability to generate extremely high recovery stresses (Poon et al. 2005).

1.3.2 Memory phenomena of shape memory alloys (SMAs)

Depending on the temperature, in general, Ni-Ti SMA can exist in two different crystal structures, the martensitic phase B19' (at low temperature with monoclinic lattice) and the austenitic phase B2 (at high temperature with a cubic lattice) (Nasser and Guo, 2006).

The memory phenomena of SMAs are associated to a solid-solid phase transformation which can be stress or thermally induced (Wenyi et al., 2002; Eggeler et al., 2005; Khalil et al., 2005; and Tsoi et al., 2006). Stiffening and healing of the matrix is accomplished either by the shape memory effect (SME) or by pseudo - elasticity effect (PEE) of the Ni-Ti SMA wire in which the SMA wire gains extreme large elastic compressive stress (Nasser and Guo, 2006).

1.3.2.1 Shape memory effect (SME) of Ni-Ti SMA

Martensite variants orientations denoted by M[t] and M[d] for twinned and detwinned martensites are illustrated in figure1.1 (a) and (b) respectively. Consider a stress-strain-temperature diagram for Ni-Ti SMA wire (see figure 1.2). At a relatively lower temperature than the austenite start A_s and subjected to an external load, the initial parent phase (twinned-martensite) denoted by M[t] transforms into (detwinned-martensite) phase denoted by M[d] accompanying an apparent macroscopic plastic deformation. At this phase, the material can accommodate a significant elongation ΔL in the direction of the applied force. Upon unloading, the material may remain in detwinned martensite state with residual strain.

When the material is heated to a certain temperature, the detwinned-martensite transforms to austenite with the material regaining its original dimensions (figure1.1c). This process is termed the shape memory effect (SME) and accompanies a reduction in macroscopic deformation. The critical temperature at which the de-twinned martensite transformed to austenite is the austenitic start temperature A_s, and the temperature at which all the de-twinned martensite fully transforms to austenite is termed the austenitic finish temperature A_f

Upon cooling the austenite transforms back to original martensite. The critical temperature at which austenite transformed to martensite is termed martensite start temperature M_s, and the temperature at which all the austenite fully transforms to martensite is termed the martensite finish temperature M_f (Bhattacharyya and Lagoudas, 1997). Figure1.3 shows the metallurgical microscopic images of twinned and austenite of Ni-Ti SMA.

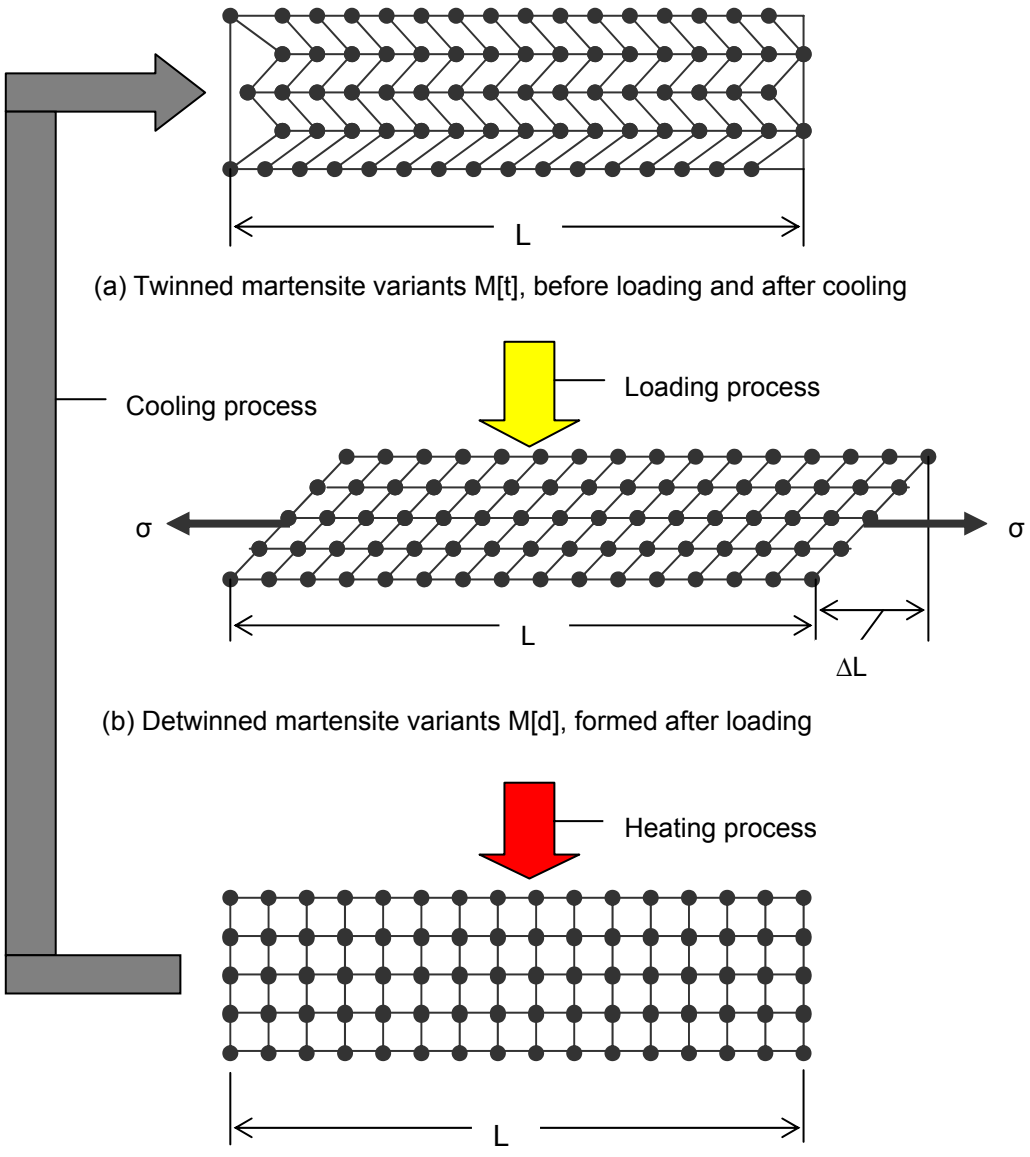

(a) Twinned martensite variants M[t], before loading and after cooling

(b) Detwinned martensite variants M[d], formed after loading

(c) Formation of austenite phase A, after heating detwinned martensite.

Figure1.1: Schematic diagram-Shape memory effect (SME) of the Ni-Ti.

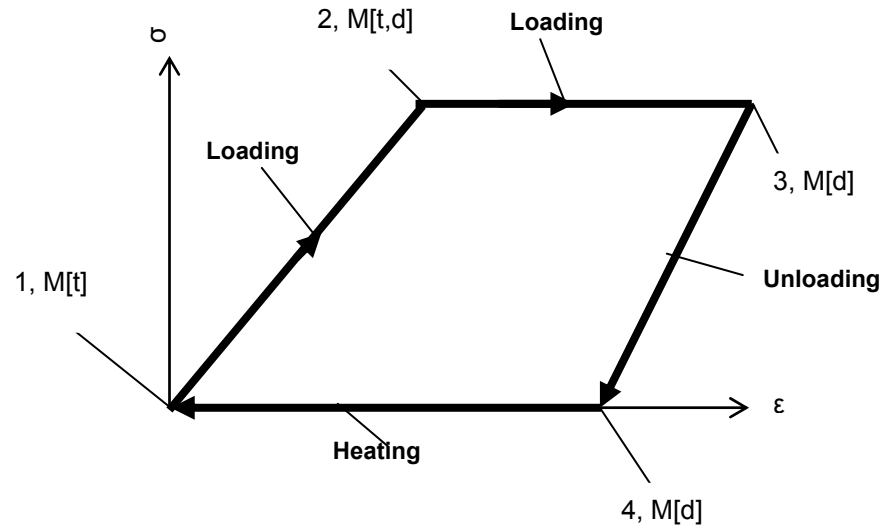

Figure1.2: **Shape memory effect-stress-strain behaviour of the Ni-Ti SMA. Processes: 1-2-3 loading path, 3-4 unloading path, 4-1 heating followed by cooling path.**

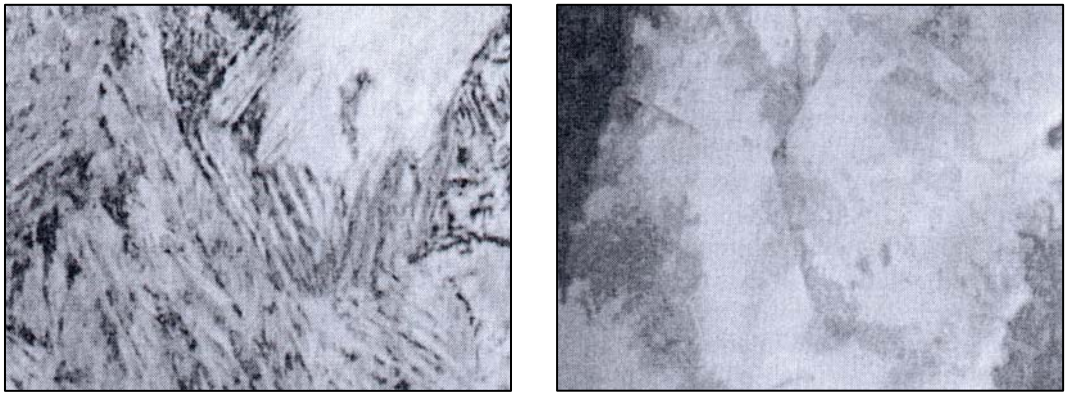

(a) (b)

Figure1.3: Metallurgical phases observed in Ni-Ti shape memory alloys. These images were obtained using transmission electron microscopy (TEM). (a)The low temperature martensite phase showing different twinned variants, and (b) the high temperature austenite phase. (Philander, 2004)

1.3.2.2 Pseudo elasticity (supper elasticity) effect (PEE) of Ni-Ti SMA

Consider a stress-strain diagram (see figure1.4) of the parent material in the austenite phase A, when loaded at a temperature relatively higher than the austenite finish A_f, the material will perform elastically until certain yielding value of stress is reached. The austenite will now transform to detwinned martensite M[d] and again induce an apparent macroscopic plastic deformation. But martensite phase is not stable at this temperature, consequently, the martensite phase will transform in reverse to austenite during partial unloading while recovering the prior deformation. Upon complete unloading the material returns to its original austenite state and all deformation is recovered. This extraordinary recoverable deformation

behaviour is called super elasticity or pseudo elasticity because in the loading-unloading process, material restores its original state and a hysteresis loop occurs (Muller and Seelecke, 2001). Figure 1.5 (a) and (b) illustrates pseudo -elasticity (super elasticity effect) of Ni-Ti SMA.

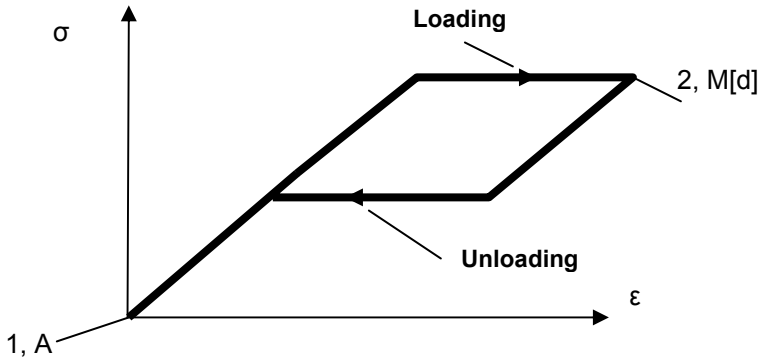

Figure1.4: Stress-strain diagram showing pseudo elasticity (supper elasticity) effect of Ni-Ti SMA.1-2 loading path, 2-1 unloading path

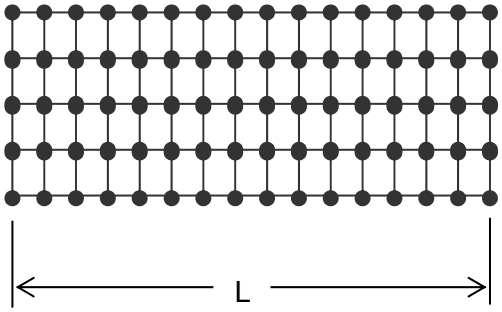

(a) Austenite phase of Ni-Ti at elevated temperature

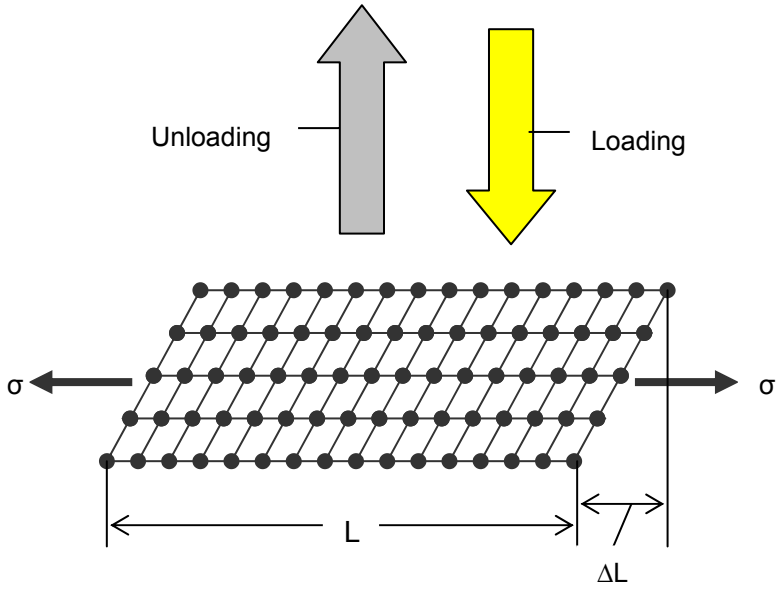

(b) Detwinned martensite M[d], formed after loading

Figure1.5: Schematic diagram-Pseudo-elasticity (supper elasticity) effect of Ni-Ti SMA

The reverse transformations of the shape memory effect (upon heating) and the energy dissipation due to the pseudo-elastic behaviour produce actuation forces that could be harnessed for various actuator applications in mechanical systems (**Philander, 2004**). The induced compressive stress is to be utilised to stiffen the IHPC beam by retarding crack growth and recovery of the strain induced.

1.3.3 Review of Ni-Ti Shape Memory Alloys recovery (clamping) force

The high recovery / clamping force generated by the SMA wire in the heating stage is critical in order to heal the composite effectively (Tsoi et al., 2003; Nasser and Guo, 2006; and Burton et al., 2006). Figure1.6 shows a thermo mechanical loading path laid on the Ni-Ti SMA wire phase diagram. The graph of change in temperature versus clamping force in the SMA wire is plotted (Burton et al. 2006). The terms M_f, M_s, A_s and A_f stands for martensite finish, martensite start, austenite start and austenite finish temperatures respectively. Before loading the SMA wire, it is recommended that the wire is prestrained between 1% and 6% to achieve detwinned martensite M[d] from twinned martensite M[t].

Upon application of the force the wire undergoes a plastic deformation (plastic strain). The wire is then heated to initiate healing by reverse transformation from detwinned martensite to austenite. The temperature of the SMA must be raised to well above the austenite finish temperature A_f to effectively transform the martensite to austenite, thus achieving a more clamping force. During cooling back to M_f temperature, there is an initial increase in clamping force/compressive stress due to increasing matrix properties. This is followed by a decrease in clamping force/stress as the austenite transforms to martensite. The martensite volume fraction increases slightly during the cooling process, but the wire remains mostly austenite and is able to exert a clamping force on the composite matrix.

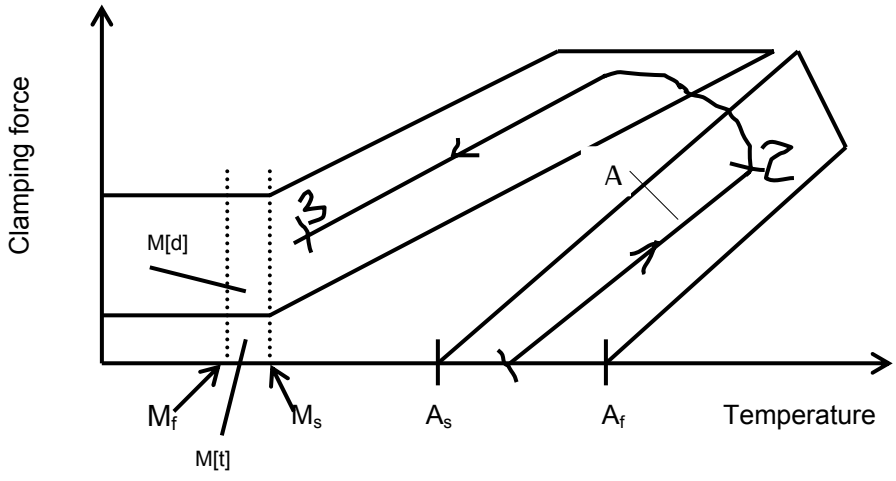

Figure1.6: Clamping force vs. temperature for Ni-Ti

Processes:

1-2: heating process-the SMA undergoes reverse transformation from martensite to austenite. It results in increase of clamping (compressive) force in the matrix.

2-3: cooling process- the austenite transforms to martensite. During the cooling process, there is an initial increase in clamping/compressive force in the matrix followed by a decrease in the force. The martensite fraction increases slightly but the SMA wire remain mostly austenitic and is able to exert a compressive force in the matrix. Residual compressive force remains after cooling to martensite finish temperature M_f.

Tsoi et al. (2003) worked on thermo-mechanical characteristics of Ni-Ti and Ni-Ti-Cu SMAs. The study focused on the basic thermo mechanical behaviour of SMA wires and to determine what sort of wire was suitable to be embedded into a constraining matrix. Extensive tests on series of different bare wires were performed.

The stress versus strain behaviour and the effect of temperature on both stress and strain were investigated. The SMA wires were actuated using electric current resistive heating. In the stress versus strain behaviour, it was found that the maximum plateau strain was dependent on the temperature. It showed that with increasing temperature, the maximum plateau strain value also increased. This was due to the fact that at low temperature, the SMA is in its soft martensitic phase thus it is easy to deform. As the temperature increases to austenitic finish temperature, the structure in the austenitic phase becomes stiffer, therefore more difficult to deform. A strain versus temperature behaviour showed that a small hysteresis in SMAs (compared to a large hysteresis) is preferable for actuation purposes for it provides better recovery stresses with a small temperature range. A small hysteresis has small temperature differences during heating and cooling, therefore enables faster transformation of the SMA wire. The stress versus temperature behaviour study was performed. SMA wires were heat treated in the oil bath to 110°C in order to establish zero percent strain (0%). The wires were subsequently cooled to room temperature. Different wire samples prestrained at 1, 3 and 6% were prepared and underwent a thermo cycling process between 110°C and room temperature in an oil bath. Resulting recovery stresses were determined. It was observed that the rate of recovery stress generated changed with prestrain value. The higher prestrain value, the slower the recovery stress generated. Maximum recovery stresses were higher for 3 - 6% prestrain of SMA wires.

Zheng et al. (2004) produced design guidelines for SMA/epoxy smart composites based on experimental results. The study focused on the effect of the temperature, curing process of the matrix and the prestraining of Ni-Ti-Cu SMA on actuating ability and reliability of a shape memory alloy hybrid composite. A ternary Ni-Ti-12wt%Cu SMA of 0.15mm diameter wire, glass fiber reinforced epoxy and Kevlar 29 fiber reinforced epoxy composites were prepared. The SMA/ glass fiber/epoxy composites were cured in an autoclave at 413K for 20 minutes. The SMA/Kevlar fiber/epoxy composites were cured at 343K for 12 hours, and then post cured at 413 for 4hours. A frame was used to align the SMA wires and to maintain the wires at a constant strain during curing process. The transformation behaviour of SMA wires was determined using a differential scanning calorimeter (DSC) with a helium cell purge.

The stress-temperature behaviour of the SMA wire and the composites was investigated. Strain, force and temperature of the samples were measured. Results showed that Ni-Ti-Cu alloy composites had a very small hysteresis during thermal cycling which could be approximated by linear functions. The Ni-Ti-Cu SMA wire with a high prestrain (above 6%) induced high recovery stresses hence a high internal stress resulting in weak SMA wire-matrix interface and low actuation ability.

The Ni-Ti-Cu wire-epoxy matrix interface of the Kevlar fiber composite could survive to a higher temperature than the glass fiber composite because Kevlar fiber have a negative temperature expansion coefficient. Therefore the Kevlar fiber/epoxy composite was found more suitable as a matrix for SMA composites than glass fiber/epoxy composite. It was found that the working temperature during curing process of the epoxy should be below the glass transition temperature T_g of the epoxy to avoid softening of the matrix.

1.3.4 Review of Thermo Mechanical Treatment of Ni-Ti SMA

The literature shows that extensive work has been done to investigate the effects of thermo-mechanical treatments on performance of Ni-Ti SMAs in terms of shape memory effect, pseudo elasticity, transformation temperatures and strains. The main goal being the utilization of shape memory alloys application.

Jackson, (1972) found that the process of drawing Ni-Ti wires imparts large plastic strains into the alloy while in the martensite state. The drawing process creates texturing in the wire specimens that affect the thermo mechanical properties such as the maximum transformation strain higher than that of cast specimens. Wenyi et al. (2003) demonstrated that thermo mechanical cycling can lead to plastic strain development at a relative low stress

levels and can raise the internal stress state such that martensite variants remain in the micro structure upon thermal transformation to the austenite.

Miller and Lagoudas (2001) studied the influence of cold work and heat treatment on the shape memory effect and plastic strain development for the thermally induced phase transformation of Ni-Ti shape memory alloy under constant applied stress. Full annealed SMA wire specimens with same chemical composition were cold rolled to reduction of specimen width by 10, 20, 30 and 40% of the original wire diameter and then annealed at 300, 400 or 500°C for 15 minutes. Thermally induced phase transformations under constant applied stress at various levels from 0, 50, 100, 150, 200 up to 500 MPa were performed on the SMA. The aim was to identify the effect of cold work percentage and the annealing temperature on the development of the transformation and plastic strains in the SMA. Each single specimen was sequentially subjected to a thermal cycle at each stress level and the complete loading paths for the specimens were plotted. It was observed that each constant stress cycle began at an elevated temperature in the austenitic region. The specimen was then cooled below the martensite finish temperature, and then heated to a temperature above the austenitic finish temperature. Upon completing the thermal cycle, the specimen was loaded to the next stress level and the thermal cycle was repeated.

The results showed that increasing both annealing temperature and cold work percentage resulted in dislocations associated with high levels of plastic deformation. This state generates internal stresses which restricts the martensite from transforming to austenite. This martensite phase remains pinned in the microstructure until the dislocations are removed through an annealing process. It was found that higher annealing temperature (transformation softening) increased the transformation strain at a given stress level. An increase in annealing temperature lowers the stress level at which the maximum transformation strain can occur. Higher levels of cold work (transformation hardening) require a larger applied stress to achieve a given level of transformation strain. Increased cold work at a constant annealing temperature raised a stress level for the on set of the plastic strain and decreased development of more plastic strain. Also a reduction in annealing temperature at a constant cold work percentage raised the stress level for the onset of plastic strain and decreased development of more plastic strain. An increase in annealing temperature increased the plastic strain accumulation and an increase of cold work decreased the plastic strain accumulation.

Lahoz and Puertolas (2004) studied a two-way shape memory effect on a Ni-Ti SMA. The study applied a training procedure based on a constant stress load applied on a Ni-Ti wire in

the temperature range of the parent-martensite transformation. From the results, a maximum of two shape memory strain was obtained for a stress training of 115MPa independently of the number of training cycles.

The A_S and A_f transformation temperatures presented a positive shift, M_S and M_f a negative shift with increasing training stress. All the transformation temperatures decreased with the increase of the training cycling.

Chen and Si (2006) studied the effect of the thermo mechanical training deformations of the two-way shape memory effect in Ni-Ti-Cu alloy spring. Ni-Ti-Cu SMA spring showed various two-way shape memory effect recovery rates through thermo mechanical training processes when five different training deformations were employed. Results showed that the two- way shape memory recovery rate increased from a training deformation of 70mm to a maximum value at a deformation of 250mm and then started decreasing up to a deformation of 280mm. Also it was found that, after training and thermo cycling; the austenite transformation temperatures (austenite start temperature A_s, and austenite finish temperature A_f) were lower than those of the un-trained specimen. The martensite starting temperature M_s and the martensite finish temperature M_f were affected slightly.

Mukhawana (2005) experimentally studied the effect of 250ºC aging temperature on the transformation temperatures of thermo-mechanical cycled Ni-Ti SMA with the use of dilatometer. The SMA specimens of length 10mm and diameter 3mm un-aged were heated in the furnace chamber to a temperature of 120ºC and left to cool in the furnace. During heating and cooling processes, a temperature versus expansion curve was plotted by the computerized system built on the dilatometer machine. Using the curve, the transformation temperatures were determined. Next the SMA specimens were aged at 250ºC by heating in the furnace to a temperature of 250ºC and left to cool in the furnace. During the heating and cooling process, a temperature versus expansion curve was plotted. Results for 250ºC aging temperature are presented in table 1.1. Mukhawana found that at an aging temperature of 250ºC, the austenite starting temperature was 45.72 ºC, compared to 46.07ºC of un-aged specimens and there was a decrease of 0.35ºC of the austenite start transformation temperature. The austenite finish temperature was 53.48 ºC, compared to 54.74ºC of un-aged specimens and there was a decrease of 1.26 ºC of the austenite start transformation temperature. The martensite start temperature was 40.72 ºC, compared to 40.11 ºC of un-aged specimens and there was an increase of 0.61ºC of the martensite start transformation temperature. The martensite finish was found to be 34.10ºC with a decrease of 1.68 ºC when compared to that of un-aged specimens.

Results showed that un-aged specimens had variations in the austenite start temperature of up to 16ºC. For austenite finish temperature the variation was up to 9ºC and martensite start and finish temperatures had variations of about 11ºC.

These results implied that an actuator made of this un-treated material would have poor performance because of a wide difference in operating temperatures. The specimens subjected to thermo-mechanical cycling and aged at 250ºC showed a decrease of variation in austenite start and austenite finish temperatures of 4ºC and 7ºC respectively.

Table 1.1: Transformation temperatures of Ni-Ti SMA aged at 250ºC, Mukhawana (2005)

	A_S		A_f		M_S		M_f	
	Temp. (ºC)	% vol. change	Temp. (ºC)	% vol. change	Temp. (ºC)	% vol. change	Temp. (ºC)	% vol. change
Average	45.72	0.11	53.48	0.25	40.72	0.24	34.10	0.11
Minimum	43.00	0.06	49.00	0.14	36.00	0.17	27.00	0.07
Maximum	47.00	0.17	56.00	0.81	44.00	0.36	38.00	0.2
Variances	4.00	0.11	7.00	0.67	8.00	0.19	11.00	0.13
Std dev.	1.16	0.03	1.74	0.12	1.93	0.05	2.40	0.03

1.3.5 Review of healing of polymeric composites

Fusion of the failed surfaces has been one of the methods of healing polymeric composites. In this method polymeric composite materials possessing selective cross-links between polymer chains that can be broken by applied forces and then reformed by heat or pressure have been reported to offer a significant healing efficiency (Chen et al. 2002).

Zako and Takano, (1999) have developed a polymeric healing method where the material hosts a second solid state polymer phase that migrates to the damage site under the action of heat. Hayes et al. (2005) developed a two- phase, solid state self repairable polymer by mixing a thermoplastic healing agent into a thermosetting epoxy matrix to produce a homogeneous matrix which contrasts with the discrete particles of uncured epoxy. These systems offer the capacity for self healing, but they require means of damage sensing, some form of response via feedback loops and heating requirements. All these make the methods difficult to implement.

The use of hollow glass fibers embedded in a composite laminate was experimented by Bleay and colleagues (Bleay et al. 2001). In this work, commercial hollow fibers were consolidated into lamina then manufactured into composite laminates. The healing agent is stored in the hollow fibers and is dispersed to the surrounding composite cracks by fracturing

of the fibers. The main limitations of this method are the relatively large diameter of the fibers required, the need for the fiber to fracture and the need for maintaining the low viscosity of the healing resin to facilitate fiber and damage infusion.

Kesler et al., (2003) developed a method of self healing of an epoxy composite in which arrest and retardation of cracks were achieved by microencapsulated dicyclopentadiene (DCPD) agent and Grubbs' first generation Ru catalyst. A healing agent is released into the crack plane by the propagating crack, where it polymerizes to form a polymer wedge generating a crack tip shielding mechanism.

The specimen was tested to fatigue failure. It was found that the healing ability increased with an increase in healing temperature. Also the healing efficiency was dependant on the healing time and the fatigue crack's retardation was limited to the applied range of the cyclic stress intensity factor ΔK_I. Other disadvantages of this technology are the need for the microcapsule's fracture, the resin to encounter the catalyst prior to any repair occurring, in adequate of the catalyst supply to provide uniform healing. Also some voids are created in the composite after the healing resin is consumed.

Lee et al. (2004) considered healing polymers using nano particles dispersed in polymer films to behave at a damage site in a similar fashion to blood clotting. The nano particles are dispersed in polymer films within a multilayer composite and are studied by computer simulations. The model comprises a brittle layer containing a nano crack sand witched between two polymer films. Self healing is achieved by nano particles congregating at the nano crack. The mechanical properties of composites repaired with this method could range between 75%-100% of the virgin material strength. The healing method is applicable to display technologies and biomedical engineering. The suitability of this technology for use in structural composite materials is limited by the fact that the healing capacity is rather on a miniature scale.

The use of shape memory alloys in healing polymeric composites has been reported to offer a significant healing ability (Thompson Loughlan, 2000; Burton et al, 2006; Zeng et al, 2004). In this method, the reverse transformations of the shape memory effect (SME) (upon heating) and the energy dissipation due to the pseudo-elastic behaviour (PEE) produce actuation forces that could be harnessed to stiffen, retarding crack growth and recovery of the strain in deformed polymeric composite structures.

Thompson and Loughlan (2000) utilized Ni-Ti actuators in controlling buckling and post buckling of the plate by positioning the SMA wires in the tubes, the tubes were embedded in the composite matrix. The wires were constrained between the boundaries. The method aimed to ensure that there is no direct interface between the SMA wires and the matrix. The performance of the adaptive composite was successful. The main limitation with this approach is that the loading planes or axes of the SMA and the matrix may not coincide hence the matrix lacks an effective healing developed by the SMA recovery force, it has a little application to conventional designs.

Burton et al. (2006) did a finite element simulation on a self healing composite using Ni-Ti shape memory alloy. In this study, SMA wires were not embedded in the metal matrix to avoid debonding, instead they were fixed on the surfaces of the matrix. A crack was allowed to propagate during the loading process. Healing of the composite was achieved by simple heating of SMA wires that reverses transformation of martensite to austenite of Ni-Ti wires which brought the crack faces into contact. It was found that the use of prestrained SMA wires resulted in greater closure force and the softening of the matrix by heating gave full crack closure. The main limitation of this approach is that fixing SMA wires on the surface of the matrix may have little practical application to polymeric composites structures.

1.3.6 Review of the fiber-matrix interface strength

One of the most important factors which lead to failure of the smart composite materials is the fiber-matrix interfacial debonding. When the shear stress along the interface increases beyond the interfacial shear strength, interfacial debond starts immediately. It is generally accepted that the higher the critical debonding strength, the stronger the composite will be (Wang et al., 2004; Poon et al., 2005; and Zhou et al., 2005). The stress distribution in embedded SMA actuators and the resulting in plane actuation force on a hybrid composite beam has been investigated for various boundary conditions (Lin and Rogers, 1991) and with reference to various micromechanics on composites texts (Baz and Tampe, 1989).

The stress transfer between the SMA and the matrix material occurs primarily through interfacial shear around the periphery of the SMA wire and will be greatest at its ends.The failure of the SMA-matrix interface in a pullout as explained with a shear lag model (Gao, 1988; Wang and Hu, 2004) is illustrated in figure 1.7. In the pullout of a prestrained SMA wire from a composite beam, when an externally applied tensile force F is lower than the recovery force F_{re} induced by the actuated SMA , the matrix is under compressive force. If the applied force is continuously increased up to the magnitude of the SMA wire recovery force i.e $F = F_{re}$, the interfacial shear force Q at loading ends becomes zero.

The shear force is moderated by the actuating force induced by the SMA wire. If the load is increased until it exceeds the recovery force i.e. $F > F_{re}$, there is a maximum force at which interfacial debonding occurs . The magnitude of this force is called the critical interfacial debonding (pullout) load F_c.

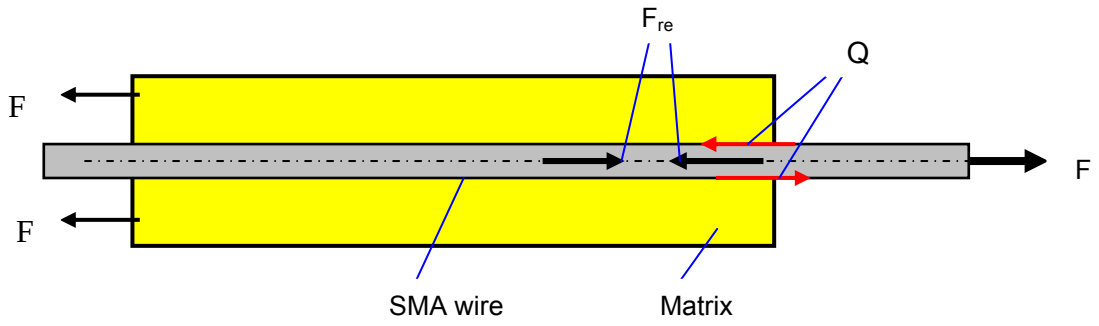

Figure 1.7: Longitudinal section- failure mode of SMA-matrix interface

Some work has been done to develop methods of reducing interfacial debonding in SMA-polymeric composites. Umezaki, (2000) did a performance comparison between twisted (spiral shape) and linear (straight) SMA wires embedded in the epoxy matrix. The performance was based on the effect of the magnitude and mode of the current supply to the SMA wire on the heat generated to the composite matrix, the crack closure of the epoxy matrix and the degree of debonding (separation) of the SMA-epoxy interface. In this study, a Ni-Ti alloy wire of 0.5 mm diameter, austenite finish temperature A_f 58°C was used in crack closure of the epoxy matrix.

1A, 1.5A, 2A and 2.5A of (direct current DC) were applied to the SMA wire in order to generate heat. In each current setting, the rise of temperature in the SMA wire was observed. The temperature of the SMA wire was raised above the austenite finish temperature A_f (58°C) to completely recover the SMA shape.

The results showed that a current supply of more than 1.5 A produced complete shape recovery and that 2.5 A produced the fastest shape recovery in all four cases. The temperature was almost constant after the first 10 seconds. An abnormal memory property was observed for the 2.5 A current.

A supply of 1.5-2A current for which the recovery was complete for the first 7-4 seconds was recommended and used. It is generally recommended, that since the heat generation can affect the matrix and result in interfacial debonding between SMA and matrix, an intermittent supply of electric current is advisable.

The epoxy resin plates embedded with spiral and linear SMA wires were fabricated. The plates were used as specimens for crack closure and pullout tests. The pullout loads on the specimens embedded with the spiral and linear SMA wires were measured without supply of electric current to the SMA. The pull out load was defined as the maximum load at which the spiral and the linear SMA wires were completely removed from the epoxy matrix.

Results showed that the spiral SMA wire, compared with the linear SMA wire, improved greatly in resisting the pullout of the SMA wire from the matrix. It was found that the effect of heat generated by the spiral SMA wire on the epoxy matrix was similar to that caused by the linear SMA wire. However, the maximum recovery stress of the spiral SMA wire was 15% lower than that of the linear SMA wire. It is therefore deduced that the amount of recovery force depends on the shape of the SMA wire.

Tompson et al. (2001) experimentally investigated the effect of the SMA wire surface treatment before they are embedded in the polymer matrix. They measured and compared recovery stresses between sandblasted and plain SMA actuators. In this study, two sample wires of Ni-Ti (49.8-50.0 Ni) SMA of 0.3 mm diameter were prepared, one sand blasted and the other one plain.

Samples were subjected to thermal cycling process of alternately heating and cooling. After that the recovery stress of each sample was determined. It was found that plain SMA wire could generate more recovery stress than the sandblasted one. This degradation in recovery stress when the entire SMA periphery was sandblasted was likely due to the SMA surface material loss. Sandblasting of the SMA surface improves interfacial bonding but degrades the SMA recovery stress.

1.3.7 Relevance of reviewed literature to the thesis

This section covers a summary of literature survey and its relevance to the thesis.

1. Reverse transformations of shape memory alloys (the shape memory effect, SME and pseudo-elastic, PEE) can produce forces that could be harnessed to actuate mechanical structures. In this thesis Ni-Ti recovery forces will be utilized to stiffen and heal the IHPC beam by retarding crack growth and recovery of the strain induced by applied load.

2. Performing thermo-mechanical treatment on SMA results to higher recovery stress/strains and stable transformation temperatures. (Tsoi et al, 2004; Cheng and Si, 2006; Mukhawana, 2005). In this thesis the Ni-Ti SMA will be aged at a temperature of 250ºC and prestrained at 3%.

3. The use of fusion method for healing the polymeric composites has posed the need for means of damage sensing, feedback loops for effective response and heating mechanism (Zako and Takano, 1999; Hayes et al, 2005). There is a need for embedded fibers to carry healing agent, maintaining low viscosity of the healing agent and mechanism of fracturing the fibers (Beay et al, 2001). Also in this category, the healing ability depends on healing temperature and time, it involves creation of voids in the matrix after a healing agent is consumed (Kesler et al, 2003). In this thesis the SMA will be applied to stiffen the beam by contracting as a response to electric current resistive heat.

4. Application of Shape memory alloys (SMA) reverse transformation recovery stress for healing the polymeric composites showed that healing the composite by embedding the SMAs in the composite via tubes (Thompson and Loughlan, 2000) results to the loading planes of the SMA and matrix not to coincide. The method lacks effective healing and has little practical application. In a finite element simulation of a self healing SMA composite (Burton et al, 2006), SMAs are embedded outside the matrix. This method may have a limited application to a conventional design. In this thesis polymeric composite beam specimens embedded with Ni-Ti SMA will be manufactured in the laboratory and tested.

5. To reduce bonding of SMA-matrix interface the working temperature of the Ni-Ti SMA actuator should not exceed the glass transition temperature T_g of the matrix material (Zeng et al.,2004). The intermittent supply of electric current is advisable during heating the SMA (Umezaki, 2000). In this thesis in order to reduce debonding of SMA-matrix interface, the pullout load at elevated temperature will be predetermined, intermittent heating of Ni-Ti SMA wire will be adopted. Selected Ni-Ti SMA will have austenite finish temperature (A_f) below the glass transition temperature T_g (75 ºC) for 60D epoxy -polymeric host matrix.

In this thesis a practical procedure for thermo-mechanical treatments involved to enhance performance of the Ni-Ti SMA actuator in the IHPC beam is provided. Also details of procedure for manufacturing polymeric composite beams embedded with Ni-Ti SMA in the laboratory are discussed. Attention will be taken on the control of the properties and performance of the resulting IHPC beam such as the reducing the interfacial debonding at elevated temperature, determination of SMA austenite transformation temperatures. Experimental work will be done to test the composite beam specimens. The test results will quantify the effect of actuated Ni-Ti SMA on stiffening and healing IHPC beam by retarding crack growth and recovery of strain. The healing test parameters will be flexural stiffness EI and mode I fracture stress intensity factor K_{IC}.

1.4 Scope of the thesis

In this thesis, an intelligent hybrid polymeric composite (IHPC) beam with healing ability is to be developed and tested. The IHPC beam consists of a 3% prestrained Ni-Ti shape memory alloy (SMA) wire actuator embedded in the polymeric host matrix. The use of Ni-Ti SMA in the host matrix is to contract, stiffen and enhance healing by retarding crack growth and recovery of the strain induced in the IHPC beam by applied load. The healing ability will be tested experimentally by determining flexural stiffness EI and mode I fracture intensity factor K_{IC} when the SMA is heated to austenite finish temperature A_f.

Chapter one covers the problem statement of the thesis, objectives of the thesis and the general understanding on Hybrid polymeric composite materials and shape memory alloys (SMAs). The chapter covers a selected literature survey on the shape memory effect (SME), pseudo elasticity effect (PEE), thermo-mechanical treatment of SMAs, approaches for healing of polymeric composites and SMA-matrix interface strength. The relevance of reviewed literature to the thesis is summarized.

Details on selection of Ni-Ti SMA, the heat treatment performed, prestraining procedures and determination of transformation temperatures of Ni-Ti SMA are presented in chapter two. Manufacturing process for un-notched IHPC and PV beams and notched IHPC and PV beam specimens are discussed in chapter three.

Chapter four discusses in detail experimental procedures done. A pullout test will be performed to determine the matrix-SMA interfacial strength at two temperature conditions, T1 below austenite start A_S and T2 of austenite finish A_f. A four point bending test will be performed to determine the effect of actuated Ni-Ti SMA on the flexural stiffness EI of un-notched IHPC beams. A four point bending test will be performed to determine the effect of actuated Ni-Ti SMA on retarding crack growth and mode I fracture stress intensity factor K_{IC} of notched IHPC beams.

Chapter five covers an analytical modeling of un-notched IHPC and PV beams done to compare with experimental results.

Chapter six covers a discussion of results. A detail discussion on experimental and analytical results is presented. A comparison between experimental and analytical results for un-notched IHPC and PV beams is discussed. Chapter seven covers a general conclusion and recommendations on performance of developed intelligent hybrid polymeric composite beam.

CHAPTER TWO

SELECTION AND TREATMENT OF Ni-Ti SHAPE MEMORY ALLOY

2.1 Selection of Ni-Ti shape memory alloy (SMA)

The author has made the choice to use Ni-Ti as an actuator for an IHPC beam for the following reasons: Experimentally, it has been found that Ni-Ti shape memory alloy can generate high recovery stresses (up to 700 MPa) for a specific actuator volume (Thompson and Loughlan, 2001). Such forces could be generated and quantified by prevention of the shape memory recovery phenomenon (Tsoi et al, 2004; Burton et al, 2006; Poon et al, 2005).

Tsoi et al. (2004) proved experimentally that for a 50.0-55.2 % Ni proportion in the Ni-Ti shape memory alloy, the ultimate recovery force depends mainly on the initial prestrain of the SMA. A small amount of prestrain of the Ni-Ti can induce a significant recovery force/stress.

Ni-Ti alloy, 1mm diameter wire was purchased from the manufacturer. Table 2.1 shows composition and active austenite finish transformation temperature of the SMA as obtained from the supplier.

Table 2.1: Ni-Ti SMA material composition

Dia. mm	Chemical Composition					Temper	Surface	Active A_f (^0C)
	Ni	Ti	C	O	Total All Others			
1	55.32	44.38	$\leq$ 0.05	$\leq$ 0.05	0.20	Straight Annealed	Oxide	60.7
All Others Are: Al, Co, Cr, Cu, Fe, Mn, Mo, Nb, Si, W								
Materials obtained from Johnson Matthey, 1070 COMMERCIAL ST., SUITE 110, SAN JOSE, CA 95112 USA								

The wire was cut into 35 pieces, 200 mm length each using a guillotine shearing machine in the workshop in Mechanical Engineering Department at Cape Peninsula University of Technology. It was essential to determine the four transformation temperatures of the Ni-Ti SMA wire i.e. martensite start temperature (M_S), martensite finish temperature (M_f), austenite start temperature (A_S) and austenite finish temperature (A_f).

In this thesis, the main interest was on the A_S and A_f values for martensite - austenite phase transformation during actuation (heating) process. It should be noted that the two phases austenite and martensite can coexist (overlap) at some intermediate temperatures. It is vital to have the knowledge of the values of the mentioned transformation temperatures of the particular shape memory alloy in application. For actuation purpose, the austenite finish temperature (A_f) is the most important.

Since the means of actuating the wire would be by electric current resistive heating, predetermined values of the transformation temperatures would predict the maximum required actuating/heating temperature of the SMA and the optimal electric current required to achieve the austenite finish transformation temperature (A_f).

2.2 Treatment of Ni-Ti SMA

Treatment of Ni-Ti SMAs was accomplished by thermo mechanical means prior to their application. Depending on the type of treatment applied on the alloy, it can yield lower transformation temperatures of the metallurgical phases and higher transformation strain (Tsoi et al.2004). The treatment can stabilise the reversible martensite-austenite phase transformation of Ni-Ti SMA (Mukhawana, 2005; Chen and Si, 2006; Nemat-Nasser and Wei-Guo, 2006).

In this thesis, the process of treating SMA material was aimed:

- To increase transformation strain in the SMA by prestraining the SMA wire specimens. Prestraining of the wire specimens induced detwinned martensite fraction in SMA.
- To release any residual stresses and attain negligible residual strain in the SMA wire specimens.
- To stabilize the austenite start and austenite finish transformation temperatures of SMA.

The treatment process involved aging of the SMA wire specimens followed by prestraining by 3%. SMA wire specimens were heated in the furnace to a temperature of 250°C for 10 hours and were left to cool in air.

2.3 Prestraining of Ni-Ti SMA

The purpose of prestraining the Ni-Ti SMA wire was to give higher transformation strain hence more recovery force. Prestraining converts the twinned martensite to detwinned martensite of the SMA. Experimental work done by (Tsoi et al. 2004 and Zheng et al. 2005)

found that prestraining of SMA can result to more actuating stress. But for SMA composites at a large prestrain such as 6%, the recovery stress level remains high even after several thermal cycles. This means that a large residual compressive stress will remain in the matrix if the embedded SMA wire has a large prestrain level. The residual compressive stress will improve the tensile stress of the composite but on the other hand it will exert a large shear stress along the matrix and SMA wire interface, thus making the interface more susceptible to debonding. The authors recommended that an effective prestraining of the Ni-Ti SMA actuator should be between 1% and 6%.

The process of prestraining Ni-Ti wires was carried out in the Strength Laboratory in Mechanical Engineering Department at Cape Peninsula University of Technology. SMA specimens were prestrained by 3% on a gauge length of 150mm using a 5 kN load cell on a tensile testing machine. The test was conducted at 25°C room temperature at a displacement rate of 5mm/minute. Figure 2.1 illustrates the layout of the test.

The prestraining load was predetermined by loading two equal lengths of Ni-Ti wire specimens up to fracture (see fracture curves in figure 2.2). After fracture, the load-extension curves were used to determine the load that could induce a plastic strain of 3% (4.5mm apparent-permanent elongation) in the wire specimens with a gauge length of 150mm. The detail of the elastic region of the fracture curves shown in figure 2.2 is presented in figure 2.3. On the load-extension graph, a straight line (see dotted line in figure 2.3) was drawn from 4.5mm point on the extension axis parallel to the linear (elastic) straight curves of the material. The points where the line meets the loading curves, the corresponding forces were taken and averaged as the prestraining value. A maximum average tensile force of 55 N was selected and was applied on each of the wire specimens until it was deformed to a plastic strain of 3%. After the prestraining process, using a micrometer screw gauge, the length of each wire specimen was measured to verify that the increase of length of the wire was 3%.

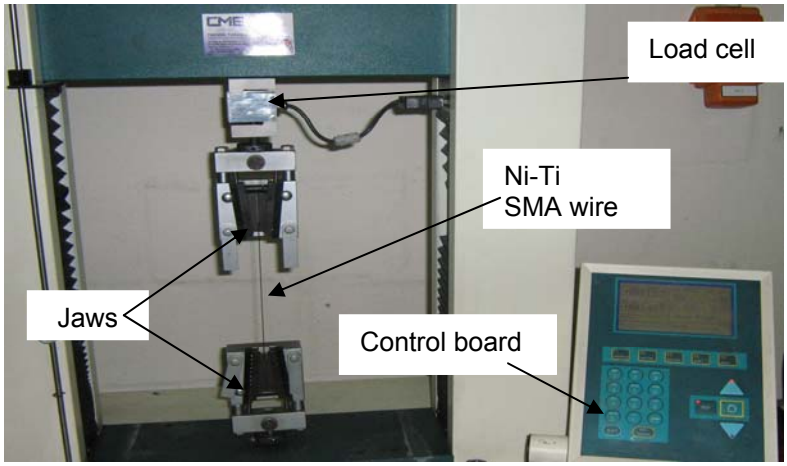

Figure 2.1: Layout of a tensile test for prestraining Ni-Ti SMA wires

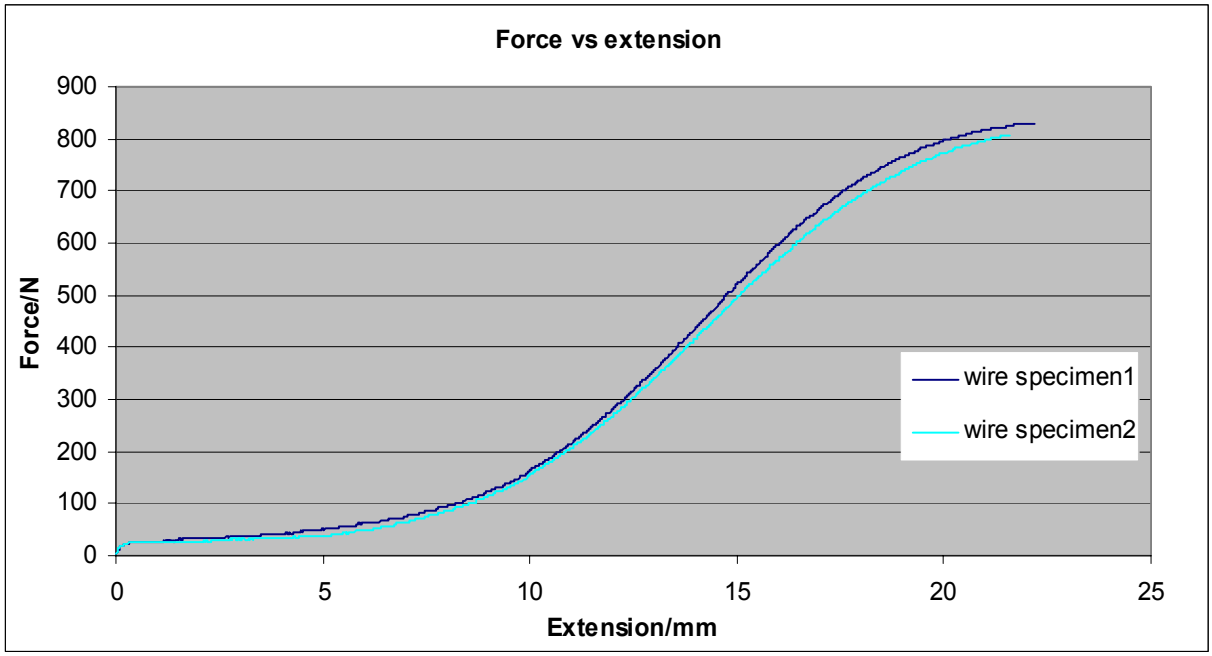

Figure 2.2: Load- extension fracture curves of Ni-Ti SMA wires 250ºC aged.

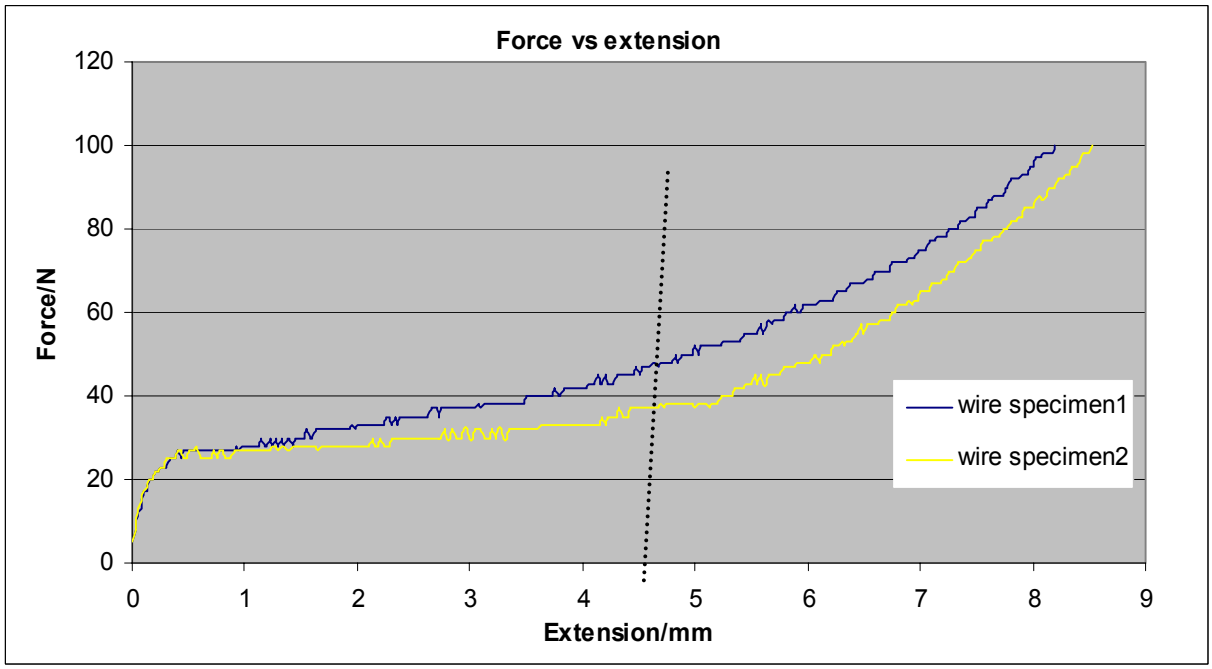

Figure 2.3: Detail of the elastic region of the load-extension fracture curves.

2.4 Transformation temperatures of Ni-Ti SMA.

The values of transformation temperatures A_S, A_f, M_S and M_f of the SMA material depend on the magnitude at which the material is prestrained and the training temperature. This phenomenon has been reported by Huang (1998). It has been found that, when prestraining the SMA enhances martensite orientations as a result of internal stresses that are generated

in the material in the same direction as the oriented martensite. Internal stresses create resistance to the martensite→austenite phase transformation and the values of transformation temperatures A_S, A_f may change.

In this thesis, a simple experiment was performed to determine transformation temperatures of prestrained SMA wires. Three prestrained SMA wire specimens were bent into several irregular shapes (see figure 2.4(a)) at 26ºC room temperature. For each wire, the ends of the wire were connected to the DC source terminals. An electric current of 3A was applied to the wire. The surface temperature of the wire was measured using a digital thermometer. As the temperature of the wire increased, the wire started to straighten as it was trying to recover its original straight shape until it was completely straight (see figure 2.4(b), (c)).The temperatures at which the wire specimens started to straighten and that at which they completely straightened are presented in table 2.2. Results indicated that the SMA wire started to straighten at an average temperature of 30 ºC. The specimens completely recovered their straight shape at an average temperature of 46 ºC. On these results, the austenite start and austenite finish temperatures for the SMA wire specimens were taken as 30 ºC and 46 ºC respectively.

Table 2.2: Transformation temperatures of straightening Ni-Ti SMA wire specimens

	A_S	**A_f**
	Temp.(ºC)	Temp.(ºC)
Specimen1	31.0	48.0
Specimen2	29.0	44.5
Specimen3	30.0	45.3
Average	**30.0**	**46.0**

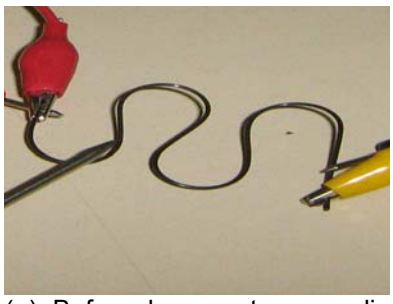

(a) Before dc current was applied on the SMA wire

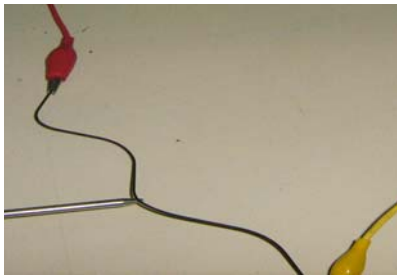

(b) After dc current was applied the SMA wires started to straighten at average temperature of 30 ºC

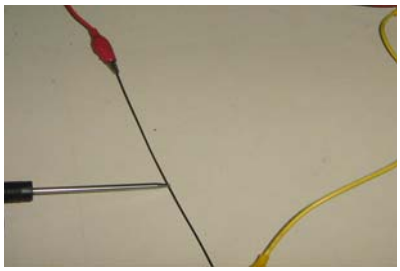

(c) The SMA wires were completely straight at an average temperature of 46 ºC

Figure 2.4: Straightening of the heated Ni-Ti SMA wires.

2.5 Experimental determination of the tensile Young's moduli of Ni-Ti SMA specimens in the martensite and austenite phases.

2.5.1 Objective of the test

The objective of this experiment was to determine the tensile modulus of Ni-Ti SMA material in both cases. The tensile modulus for the Ni-Ti SMA in the martensite phase at a temperature T1 below austenite start A_S and that of the Ni-Ti SMA in austenite phase at T2 of austenite finish A_f were determined.

The behaviour of shape memory alloys (SMAs) when loaded at an environmental temperature below austenite start A_S, based on the stress-strain curve is as follows; the SMA initially exhibits linear elastic behaviour while in twinned martensite phase. As the load increases, it transforms into stress induced (detwinned) martensite Upon unloading, the SMA can not recover its original shape unless it is subjected to heat at a temperature above to that of its austenite finish A_f.

When the SMA is loaded at an environmental temperature above the austenite finish A_f value the SMA initiates linear elastic deformation with the elastic modulus of the austenite. Upon reaching the critical stress, the austenite starts to transform into stress induced (detwinned) martensite phase. After finishing the transformation of stress induced martensite, it initiates linear elastic deformation of self-accommodated (twinned) martensite. When unloaded a hysteresis loop occurs and the martensite transforms into the austenite and the SMA material completely recovers its residual deformation.

2.5.2 Test procedures

The tensile test was performed in the Strength Laboratory of the Mechanical Engineering Department at Cape Peninsula University of Technology. Four Ni-Ti wire specimens, 1mm diameter, 200mm long each were tested on a tensile test machine. Their gauge length was 150mm. Prior to the tensile test, the wire specimens were aged at a temperature of 250ºC followed by prestraining of 3% on the same gauge length of 150mm. Two wire specimens were loaded up to fracture at room temperature T1 of 25°C below austenite start A_S to ensure that the Ni-Ti SMA material initially was in the martensite phase. The remaining two specimens were loaded up to fracture at temperature T2 of 46°C to ensure that the SMA material was in the austenite phase. Prestrained specimens were loaded to fracture on a tensile test machine using a 5 kN load cell at a displacement rate of 5mm/minute. Results of the tensile fracture tests at both temperatures T1 below A_S and T2 of austenite finish A_f were plotted and are presented in figure 2.5.

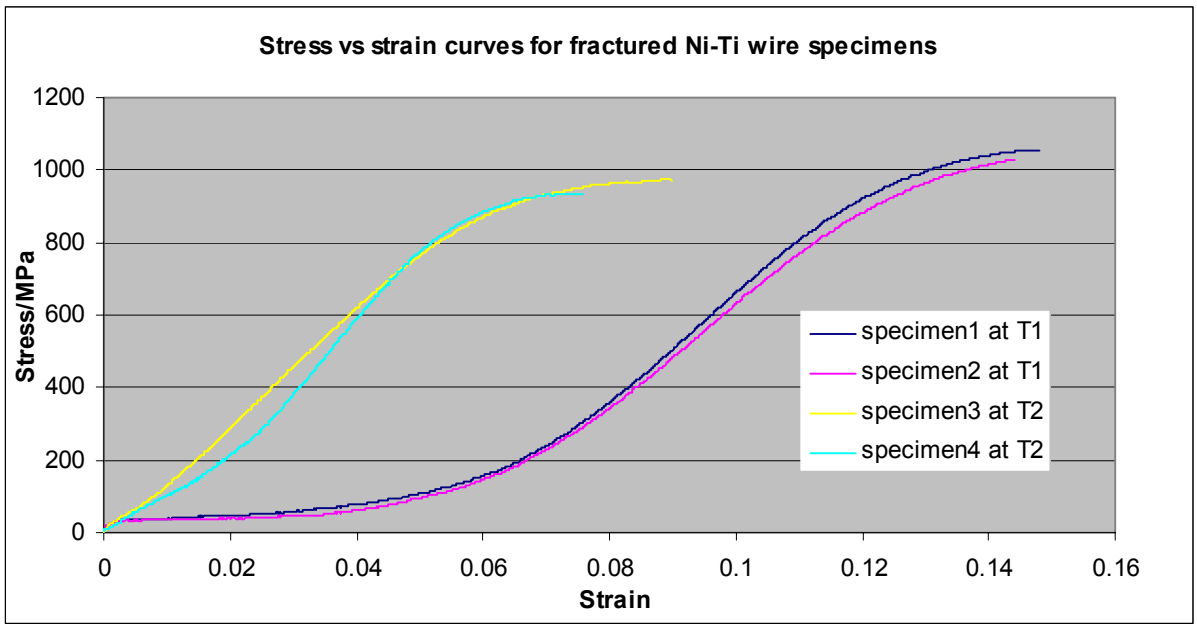

Figure 2.5: Stress-strain fracture curves for Ni-Ti SMA wires loaded at T1 and T2.

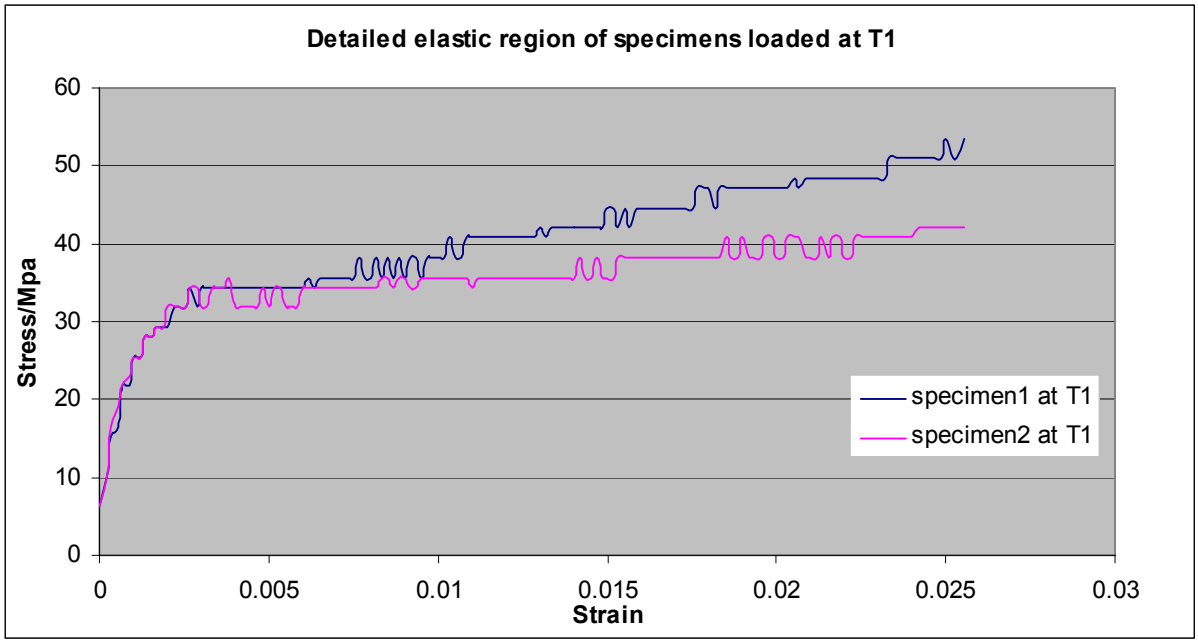

Figure 2.6: Detail of the martensitic elastic region of the stress-strain curves at T1.

2.5.3 Test results

The results presented in figure 2.5 show that specimens fractured at a temperatureT1 below the austenite start A_S initially were in the martensitic phase. When the load was increased, the specimens deformed elastically while in the martensitic phase up to a critical stress of about 32MPa; afterwards material started to transform to stress induced (detwinned) martensite with a more horizontal curve.(see figure2.6 for a detailed view). As the load increased, the martensite hardened until fracture occurred at an average load of 1042MPa.

Specimens fractured at a temperature T2 of the austenite finish A_f initially were not completely in the austenitic phase. Figure 2.5 shows that the initial temperature of the Ni-Ti SMA was below the austenite finish value hence the material was not wholly in the austenitic phase. However as the temperature increased by heating the Ni-Ti SMA during the loading process, the material was completely austenite at a load of 200MPa, the material exhibited elastic (linear) behaviour with a higher stiffness. As the load continued to increase up to about 800MPa the material started to transform from austenite to stress induced (detwinned) martensite with a more horizontal curve until fracture occurred at 950MPa.

The tensile modulus, E of the martensite at T1 and that of the austenite at T2 were determined by calculating the slopes of the lines between two points located on the elastic portions on the stress-strain curves. Calculated E values are presented in table 2.3.
The tensile (Young's) modulus for the martensite was taken as 11.50 GPa and that of the austenite was16.0 GPa.

Table 2.3: Calculation for the tensile modulus E of martensite and austenite

	SPECIMENS FRACTURED AT T1< A_S		SPECIMENS FRACTURED AT T2 = A_f	
SELECTED POINTS	Specimen1	Specimen2	Specimen3	Specimen4
A	0.00020, 10.192			
B	0.00187, 29.302			
C		0.00020, 10.192		
D		0.00187, 29.302		
E			0.0270, 405.640	
F			0.0390, 613.560	
G				0.0272,407.680
H				0.0396,581.960
SLOPE OF A LINE X 10^9	11.45	11.45	17.33	14.74
AVERAGE TENSILE MODULUS, E (GPa)	11.5		16.0	

CHAPTER THREE

MANUFACTURING THE IHPC AND PV BEAMS

3.1 Description of the IHPC and PV beam specimens

The beam specimens manufactured were of rectangular cross section with dimensions 150mmx25mmx10mm. The beam dimensions conform to the standard four point bending test (Measurements Group, 1982). The types of beams manufactured can be grouped into three categories. Category one consisted of intelligent hybrid polymeric composite (IHPC) beams with 1mm diameter Ni-Ti SMA wire embedded along the neutral axis. A total of six (6) IHPC beams were manufactured. These specimens were tested to determine the pullout load. Three were tested at room temperature T1 and three at elevated temperature T2.

Category two consisted of un-notched polymeric virgin (PV) beams (without SMA wire) and intelligent hybrid polymeric composite (IHPC) beams with 1mm diameter Ni-Ti SMA wire embedded 7mm off the neutral axis. A total of three (3) polymeric virgin (PV) beams and six (6) intelligent hybrid polymeric composite (IHPC) beams were manufactured. These specimens were tested to determine the flexural stiffness EI at temperatures T1 and T2. Figure 3.1(a) and (b) show the geometry and dimensions of the un-notched IHPC beams.

Category three consisted of notched polymeric virgin (PV) beams (without Ni-Ti SMA wire) and notched intelligent hybrid polymeric composite (IHPC) beams with 1mm diameter Ni-Ti SMA wire embedded 7mm off the neutral axis. A total of three (3) polymeric virgin (PV) beams and six (6) intelligent hybrid polymeric composite (IHPC) beams were manufactured all of them notched. These specimens were tested in order to determine the mode 1 fracture stress intensity factor K_{IC} at temperatures T1 and T2.

Thompson and Loughlan (2000) utilized Ni-Ti actuators in controlling buckling and post buckling of the plate by positioning the SMA wires in the embedded tubes in the composite matrix.. The use of tubes aimed to ensure that there is no direct interface between the SMA wires and the matrix. The main limitation with this approach was that loading planes or axes of the SMA and the matrix may not coincide during healing process.

The method adapted in this thesis is embedding the SMA wire within the matrix. This method was also applied by Thompson and Loughlan, (2001). The performance of the SMA in this method will depend on the level of bonding strength along the matrix-SMA interface.

Three polyurethane epoxies were available; 45D, 60D and Task3. Previous research done by the Smart Materials and Systems Research group found that Task3 has the highest glass transition temperature followed by 60D and 45D. It should be noted that the glass transition temperature of the epoxy composite limits the heating temperature during SMA actuation. Also it was found that Task3 has the least pullout debonding strength, followed by 60D and 45D. Task3 has the higher ultimate tensile strength followed by 60D and 45D. Much force is required to deform Task3 in order to obtain extensive readings during the testing process. The author preferred to work on 60D since it has desirable material properties i.e. moderate transition temperature, debonding strength and the material is easier to deform than Task3.

The beam specimens were manufactured by casting 60D polyurethane thermal setting plastic epoxy resin in the silicon mould. Ni-Ti SMA wires prestrained by 3% were embedded in the mould before casting the beam specimens. The SMA wires were prestained to achieve detwinned martensite to enhance a greater SMA transformation strain and recovery force. The average position of the SMA wire in the composite beam was 7.1mm away from the neutral plane such that for a given level of actuation of the SMA, the generated recovery force could demonstrate strengthening of the beam by resisting the bending moment induced by an external load.

3.2 Master part

The master part was obtained by machining a 160mmx30mmx15mm mild steel bar. Machining process was carried out on a shaper. The final dimensions of the part (see figure 3.2) are 150x25x10mm. Four, 2 mm diameter, 3mm deep holes were drilled on the bottom side of the part. The holes were used for inserting brazing rods on which the part stood on the base of the mould box. The surfaces of the master part were cleaned with a clean cloth dipped in methylated spirit. Part cleaning was aimed to remove oil and dust from the part. The prepared master part was used to cast the silicon mould.

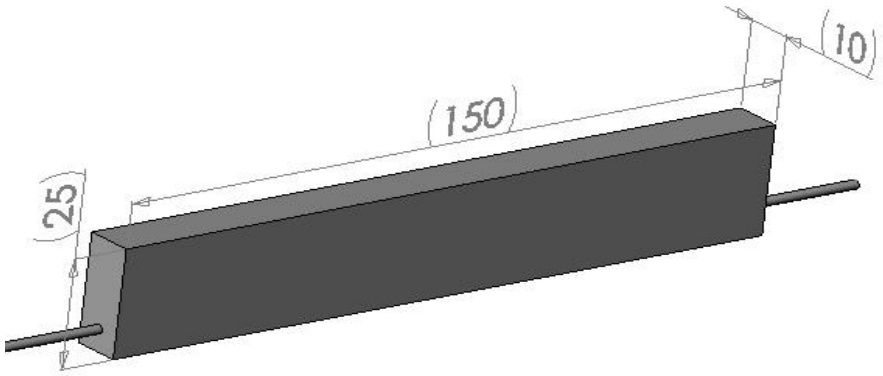

(a) Three dimensional view of the Ni-Ti composite beam

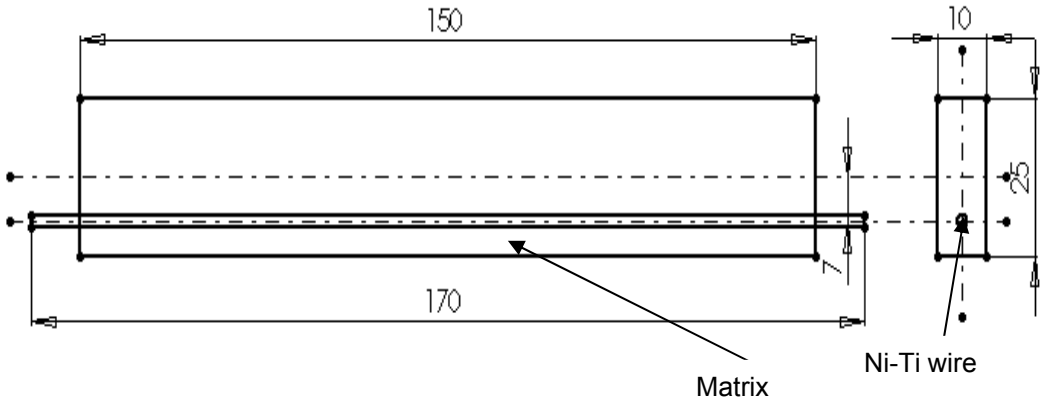

(b) Wire frame view of the Ni-Ti composite beam

Figure 3.1: Geometry and dimensions of the IHPC beam (all dimensions in mm)

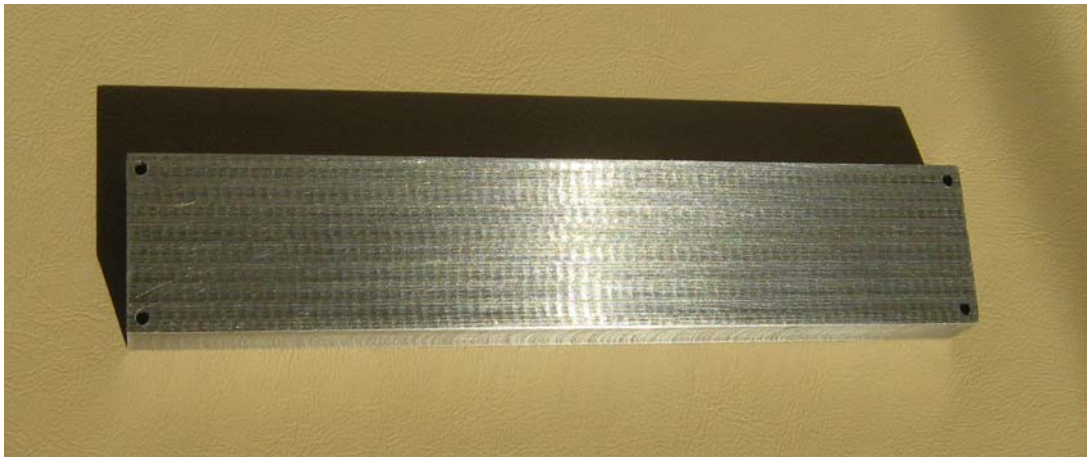

Figure 3.2: Master part

3.3 Mould box preparation

The mould box was made up of the base and four sides. The box was constructed using Melamine face Board, the smooth surface of this board detaches relatively easy from the silicone and glue. Four brazing rods were inserted in the holes on the bottom of the part. The part was inserted in the box such that the inside dimensions of the box was at least 25mm around the outer boundaries of the part. Extra 20 mm was added to the top of the mould box to allow for the silicone rise during casting. To assemble the mould box, the melamine boards were glued together using a glue gun.

A strip of board with same base length was prepared, on which a 12 mm diameter hole was drilled through. An ingate to the part was created by putting a glue stick of 12 mm diameter that tapered to 6 mm diameter. The glue stick was allowed to suspend and protrude at least 20 mm above the strip. The stick was pushed through the strip and placed on top of the box such that the tapered point was attached on the part while 25mm length from the box inside surfaces to the part was maintained. The glue stick was glued to the strip and the strip was glued on the top of the box.

The packaging tape that defines the parting plane on the master part was also taped to the inside of the mould box to prevent movement of the part during the casting process. The mould box without the part is shown in figure 3.3.

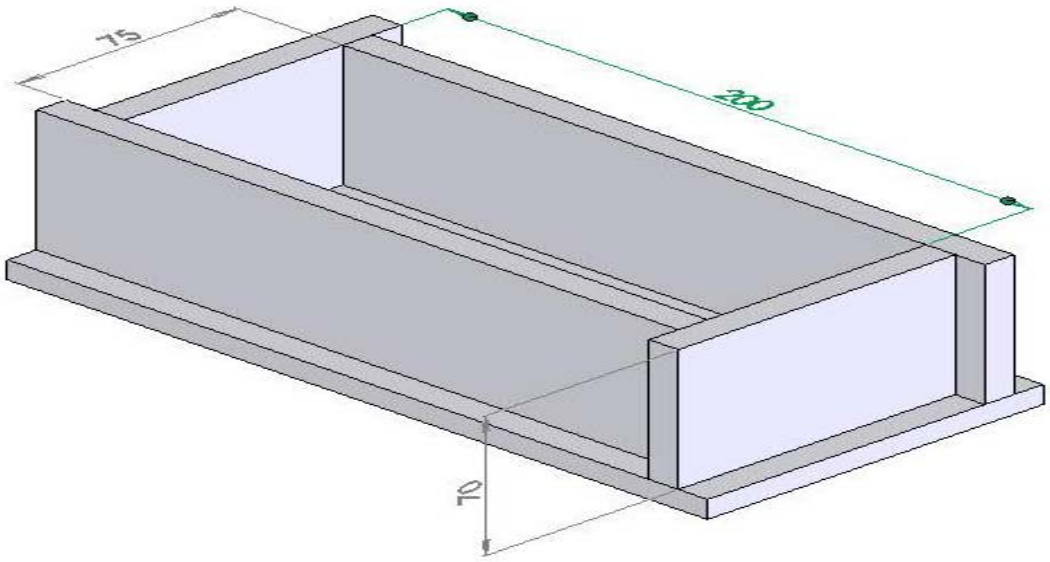

Figure 3.3: Mould box (all dimensions in mm)

3.4 Casting the silicone mould

Casting of the silicone mould was performed in the MK-Mini Vacuum Chamber in the CRATECH Laboratory for Smart Materials, department of Mechanical Engineering at the Cape Peninsula University of Technology. The silicone used was Wicker Silicone grade Elastosil (EL) M 4644A coupled with Wicker hardener grade Elastosil (EL) M 4644B. The density of the silicone used was 1140 kg/m^3. The casting mass of the silicone was determined by multiplying the density and the calculated volume of the box space. The silicone mass was weighed on a scale and poured in a 20 litres bucket. The corresponding mass of the hardener was weighed on the scale. The ratio of the silicone to the hardener was 10:1 by mass according to the manufacturer's recommendations. The hardener was mixed with the silicone and the mixture was stirred with a mixing paddle for ten (10) minutes. Afterwards, the mixture was kept in the vacuum chamber for degassing for 18 minutes then taken out and poured in the box cavity. The pouring process was done slowly to avoid trapping of air bubbles. The mould box was taken back to the vacuum chamber for degassing for 20 minutes. Then it was removed from the chamber and left to cure at room temperature for 18 hours. To remove the silicon mould from the box, the box boards were separated along the glued surfaces. The cast silicon mould is shown in figure 3.4.

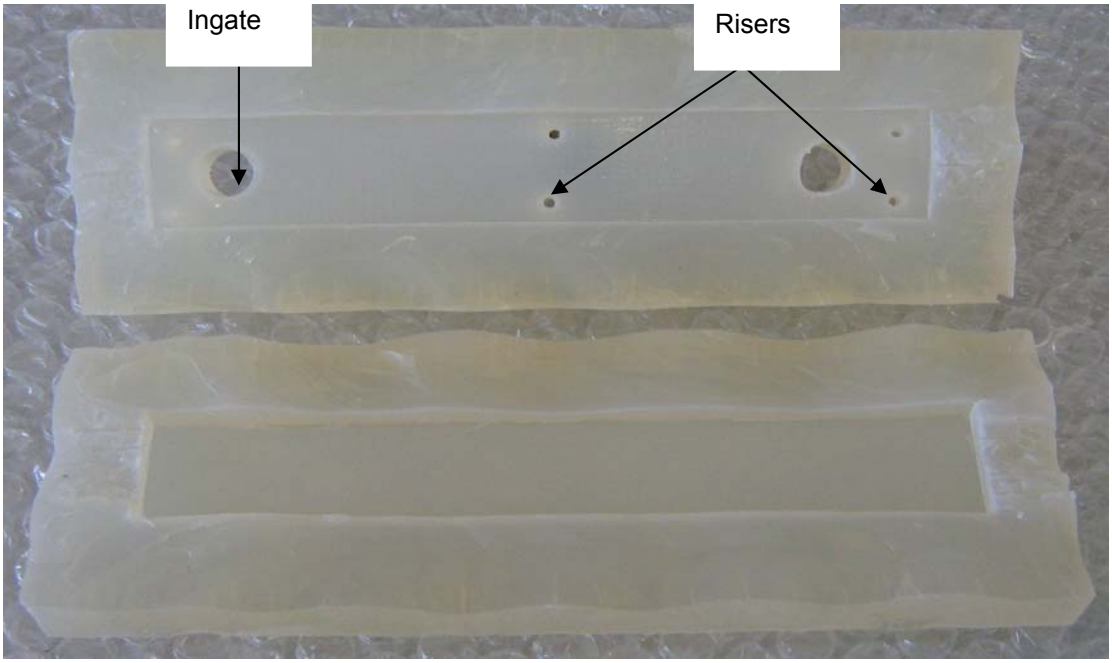

Figure 3.4: Silicon mould

3.5 Casting the IHPC and PV beams

Casting of the IHPC and PV beams was done in the Rapid Prototyping Development Laboratory, Department of Industrial Engineering at the University of Stellenbosch. The MCP vacuum cast system was used. Ni-Ti SMA wire prestrained by 3% was embedded in the silicon mould cavity for casting the IHPC beams. For casting PV beams, no SMA wire was embedded in the mould. Types, IHPC and PV beams were cast in the silicon mould from 60D polyurethane thermal setting epoxy resin.

The casting procedures were as follows; first the MCP Vacuum Chamber system was started for 20 minutes for the pump to warm up. Two plastic containers were prepared.
The casting of each beam was performed by mixing epoxy resin and the hardener in the ratio of 1:1 by mass. A mass of 50 g of epoxy resin was measured on the scale and put in cup B and another 50 g of hardener was measured and put in cup A. It was observed that the resin had a higher viscosity than the hardener.

The two cups A and B with the solutions were mounted on the fixtures in the vacuum chamber. The mixing blade was positioned for stirring the resin in cup B. The mould was placed in the chamber just below the resin cup B. A rubber hose was used to connect the mould and the pouring funnel. The chamber doors were closed and the vacuum pump was switched on until the chamber was at vacuum. The mixer was switched on so that the mixing blade could stir the resin in cup B. Mixing was done slowly so that the degassing process could be accelerated. This process took 15 minutes.

After degassing was complete i.e. the resin surface was free of air bubbles, the resin in cup A was poured in cup B and the mixture was stirred for 1.5 minutes. A pressure shot was released to burst air bubbles and maintain the mixture free of air bubbles for a better cast. The mixer was stopped and the mixture was poured in the mould through the funnel. The vacuum was drawn for 2 minutes then the mould was taken out of the vacuum chamber. The mould was taken out of the vacuum chamber for curing at room temperature for two hours. Afterwards the beam was removed from the mould cavity. Samples of manufactured IHPC and PV beams are presented in figure 3.5 (a) and (b) respectively.

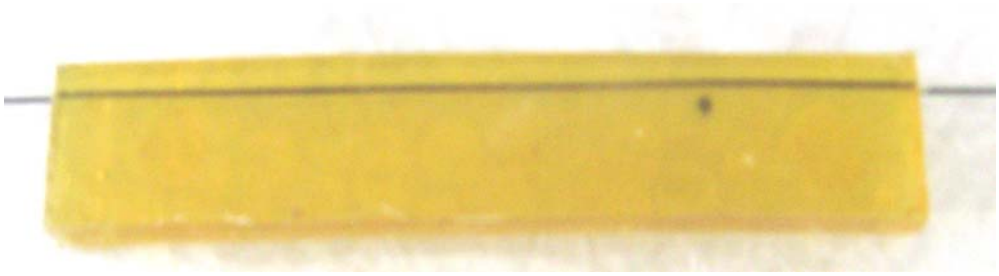

(a) IHPC beam

(b) PV beam

Figure 3.5: **Manufactured IHPC and PV beams.**

Notched IHPC and PV beams were obtained by cutting notches on the beams. Dimensions and loading of notched IHPC and PV beams were chosen according to the guidelines of the American Society for Testing and Materials (ASTM) for the bending of single edge notched specimens (Broek, 1986). The beam thickness H, beam width B and the loading span S are approximately related as: H= 0.25 B to 1B and S=4 B. The notches were cut with the use of a sharp razor blade. A notch of 2mm deep with a notch-tip angle of 60º was cut at the centre of each beam. The samples of notched beams are presented in figure 4.6 page 42. The procedure for cutting the notches and the initiation of cracks on the beams is discussed in detail in chapter four.

CHAPTER FOUR

EXPERIMENTAL PROCEDURE AND RESULTS

4.1 Pullout test

4.1.1 Objective of the experiment

The objective of the pullout test was to determine the strength of the matrix-SMA interface of the manufactured IHPC beam upon heating the Ni-Ti SMA to austenite finish temperature A_f. The critical load obtained was also used as a guideline to set the maximum bending load in the bending test.

The pullout test was preferred in this thesis since it is among the most popular mechanical testing methods to investigate the fiber-matrix interface strength. It has been quoted as the easiest method to use and is reported as being a satisfactory test method (Poon et al. 2005). In this test, the Ni-Ti SMA wire was pulled out from the matrix by an axial tensile force. The test resembles the work done by Poon et al. (2005) and is based on a traditional fiber pullout test model. The test specimen was an IHPC beam with a 1mm diameter Ni-Ti SMA wire embedded along the neutral axis. The embedded length of the Ni-Ti SMA wire was 150 mm. The Ni-Ti SMA wire was prestrained by 3% before was embedded in the matrix. The debonding strength was sought through the maximum load that could separate completely the Ni-Ti SMA wire from the matrix.

4.1.2 Test procedure

A schematic diagram of the pullout test is shown in figure 4.2. It consists of the Ni-Ti SMA reinforced polymeric composite beam positioned between the jaws of the tensile testing machine, a DC power source to supply electric current for the heating of the SMA wire, and a digital thermometer for monitoring the temperature of the SMA wire. The beam specimen was mounted on the pullout tensile testing machine. The lower jaws of the tensile machine (see bottom view of figure 4.1) were selected to ensure that clamping of the beam would not induce compressive force to the Ni-Ti SMA-epoxy matrix interface. The upper jaws of the machine clamped the upper free length of the Ni-Ti SMA wire. The test was performed using the 10KN load cell and at the crosshead displacement rate of 5mm/s.

Initially, the test was performed on three specimens at 28 °C room temperature below the austenite start (A_S) where no current was supplied to the Ni-Ti SMA wire.For each specimen, the load was increased until the maximum pullout load was determined. Next the test was performed on other three specimens at a temperature T2 of the austenite finish (A_f) value. The temperature of the Ni-Ti SMA was raised to 46°C by applying 3A of electric current for 30 seconds. The actuating temperature of the Ni-Ti SMA wire was maintained by heating the Ni-Ti SMA wire at intervals of 5 seconds. The digital thermometer was used to monitor the temperature of the Ni-Ti SMA wire. For each specimen, the load was increased until the maximum pullout load was determined.

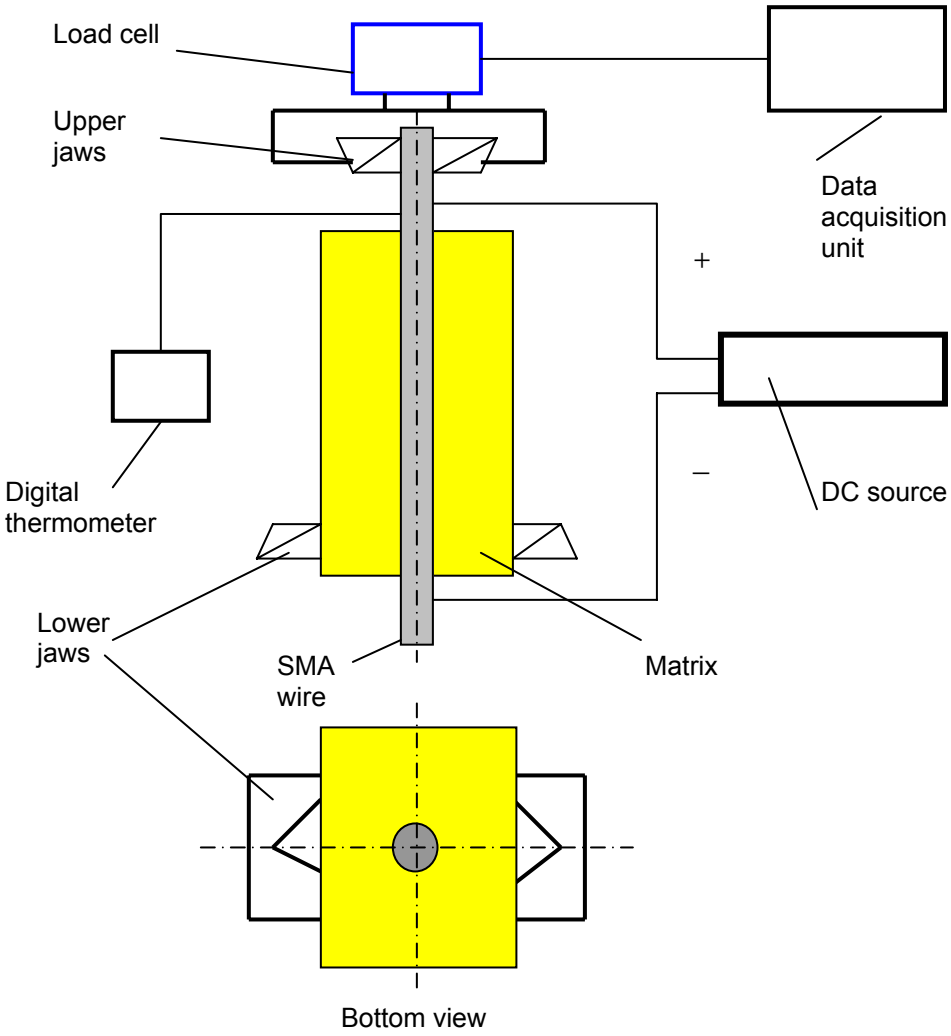

Figure 4.1: Schematic diagram, layout of the pullout test.

It was expected that the interface shear strength would decrease as the actuating temperature would increase towards the glass transition temperature of the composite matrix surrounding the Ni-Ti SMA wire. Throughout the pullout test, the actuating temperature was kept below the glass transition temperature T_g (75 ºC) of the host matrix.

The average load and displacement values of three specimens at each temperature were tabulated. The displacement was considered as the total distance traveled by the loading arm in the testing machine. The graphs of force versus displacement for the two testing temperatures were plotted and presented in figure 4.9 (see chapter 4.3).

4.2 Four point bending test

4.2.1 Objective of the experiment

The objective of the bending test was first to investigate the effect of embedded actuated Ni-Ti SMA on the flexural stiffness of un-notched IHPC beams. Secondly to investigate the effect of actuated Ni-Ti SMA on the mode I fracture stress intensity factor K_{1C} of the notched IHPC beams.

In this test, a four point bending load was preferred due to the fact that in four point bending, along the middle span on the beam specimen, the bending moment is uniform and the shear force is zero. The maximum temperature of the SMA wire was kept 46^0C below 75^0 C the glass transition temperature (T_g) of the polymeric matrix. Excessive heating of the SMA wire could be detrimental to the mechanical properties of the host matrix and the interfacial strength.

The loading dimensions of all tested beams were selected based on standard four point bending test (Measurements Group, 1982) as shown in figure 4.2. The dimensions of the beam were as follows, length 150 mm, width 25 mm and the thickness 10 mm .The beam was simply supported, loaded under four point bending. The middle span length of the beam was b=30 mm, the outer span lengths of the beam were a = 30 mm each, the free ends lengths were 30mm each. The bending test was conducted on a universal tensile testing machine at a displacement rate of 1mm/minute using a 10kN load cell. The test was done in the Strength Laboratory, Department of Mechanical Engineering at Cape Peninsula University of Technology.

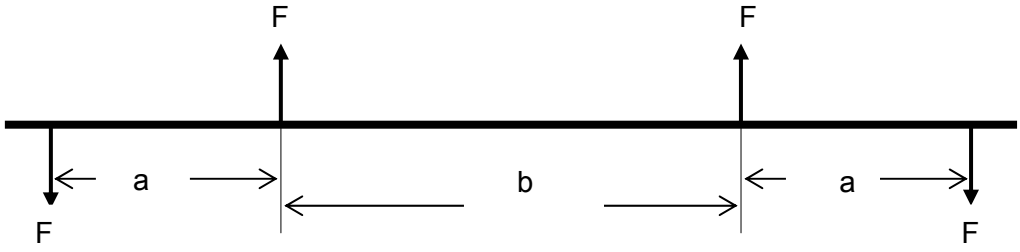

Figure 4.2: Four point bending loading dimensions

4.2.2 A bending fixture for four point bending test

A bending fixture was fabricated to suit the loading dimensions of the beam indicated in figure 4.2. The fixture was fabricated in the Welding Laboratory, Department of Mechanical Engineering, Cape Peninsula University of Technology. The top member of the fixture was used as the loading points on the beam and the bottom member of the fixture was used as the supporting points on the beam. Metal bushes were used to reduce friction forces between the fixture and the beam specimen on loading points. Two bushes were used on the loading member and other two on the supporting member. Four bolts were used to fix the bushes on members. A light clearance fit between the bush and the bolt was made. A drawing of the bending fixture is presented in figure 4.3.

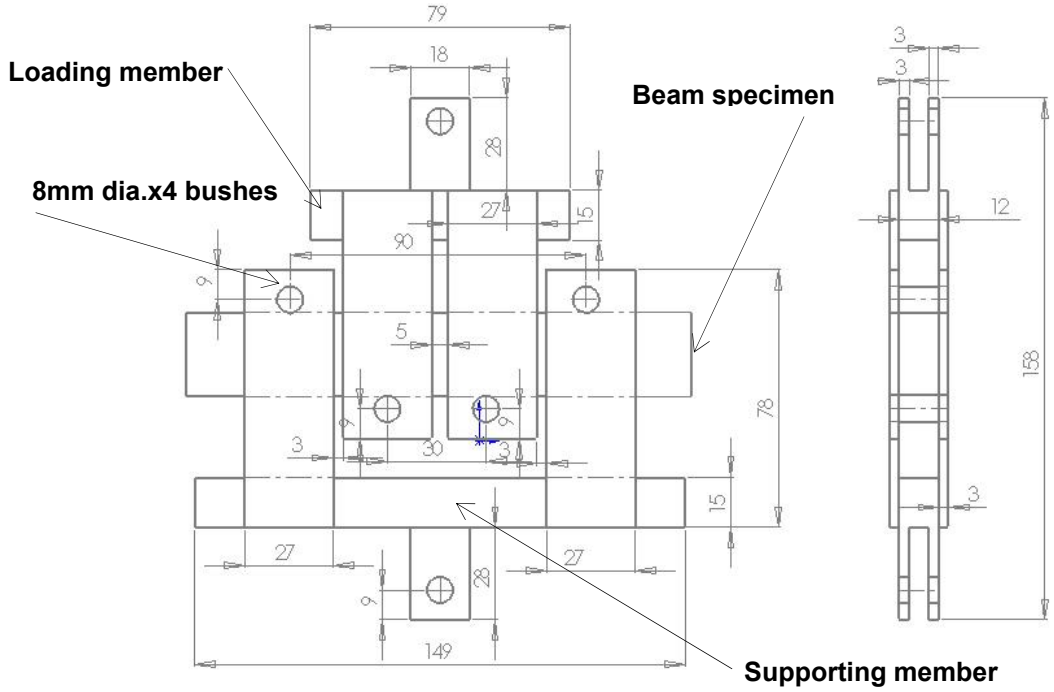

Figure 4.3: Drawing of fabricated bending fixture (all dimensions in mm)

4.2.3 Experimental determination of the flexural stiffness EI of un-notched IHPC and PV beams

4.2.3.1Test procedure

In this test, three (3) un-notched PV beams and three (3) un-notched IHPC beams were tested at room temperature T1. Also three (3) un-notched IHPC beams were tested at a temperature T2. Electrical resistance strain gauges were bonded on the mid points on the surfaces of un-notched IHPC and PV beam specimens to sense and measure the tensile bending strains (see figure 4.4). The gauges had a gauge factor of 2.085 and were supplied by Vishay Micro-measurements, Raleigh-North Carolina, USA. The strain gauges were bonded on the beams with Q-bond adhesive solution, soldered to conductor wires which connected them to the wheat stone bridge. In this test, a maximum bending load was chosen to be lower than the pullout load. The maximum bending force of 55N (equivalent to 27.5N on each of two loading points on the beam) was set on the test machine.

At room temperature of 26°C each of the three PV beams was subjected to the four point bending load. The bending load was increased from zero up to 27.5N. During the load application, values of the bending load F, strain ε and the transverse deflection of the beam δ were recorded. The values of the bending strains were read on the wheat stone bridge and that of the transverse deflections were displayed by the tensile test machine on the computerized data acquisition unit.

At room temperature of 25°C, each of the three IHPC beams was subjected to a four point bending load (see photo layout for test in figure 4.5). The load was increased from zero to 27.5N.The values of the bending load F, strain ε and the transverse deflection of the beam δ, were recorded.

Next, the bending test was performed on remaining three IHPC beams while the temperature of the Ni-Ti SMA was raised to 46°C to effectively transform the detwinned martensite to austenite. The Ni-Ti SMA wire was actuated by means of electric current resistive heating. 3A of electric current was supplied by the DC source for heating the Ni-Ti SMA wire. At temperature T2, the bending load was increased up to 27.5N and the values of the bending load F, strain ε and the transverse deflection of the beam δ were recorded.

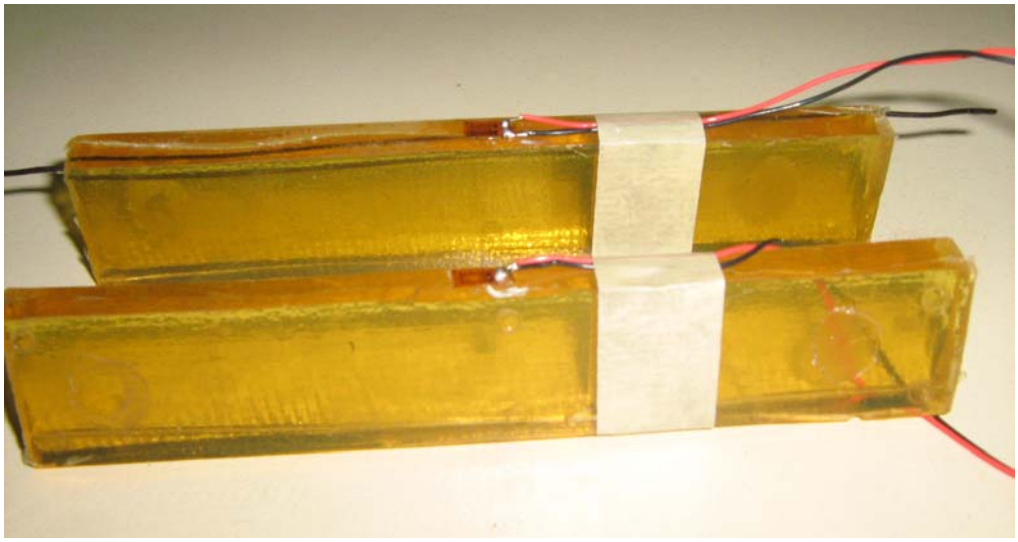

Figure 4.4: Strain gauges bonded on un-notched IHPC and PV beams

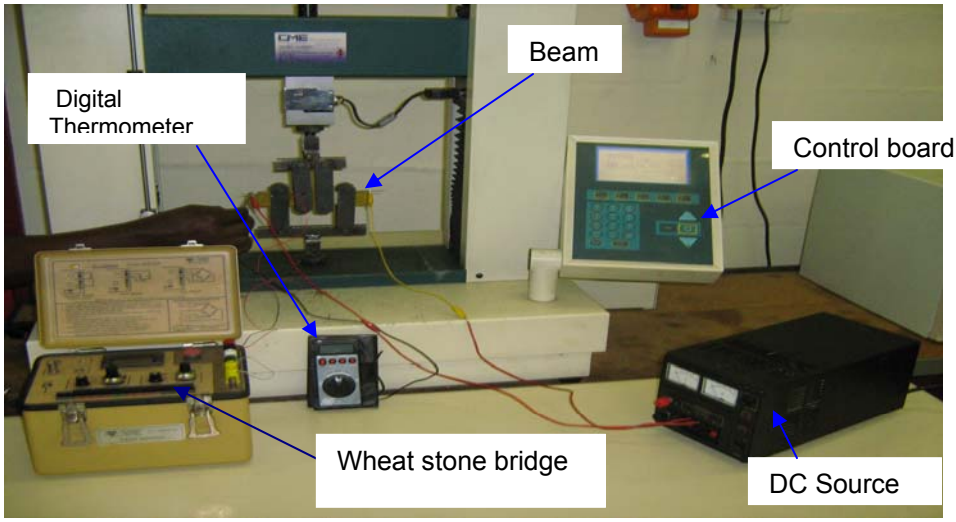

Figure 4.5: Layout of a four point bending test for un-notched IHPC and PV beams

Applying Hooke's law of elasticity, the bending stress can be obtained by the formula:

$\sigma_b=(M/I)y$ ----------(4.1)

But $\sigma_b = E\varepsilon$---------- (4.2)

There fore,

$\varepsilon= (M/EI)y$ ----------(4.3)

For a simply supported beam under a four point bending, the maximum bending moment,

M-max = F.a

$\varepsilon= (Fa/EI)\ y$ ---------- (4.4)

$F= (EI/ay)\ \varepsilon$ ---------- (4.5)

where by;

ε = bending strain

E= Young's modulus of the composite beam

I = second moment of area of the composite beam cross section.

y = distance from the neutral axis to the point of consideration

Flexural stiffness EI can be obtained from a force-strain curve, from which EI/ay is the slope of the curve. There fore EI can be expressed as:

EI= (slope).a.y

The average values of load, strain and deflection of three specimens at each temperature were tabulated and plotted. The graphs are presented in figures 4.10 -4.11 (see chapter 4.3).

4.2.4 Experimental determination of the fracture stress intensity factor K_{IC} of notched IHPC and PV beams

4.2.4.1Test procedure

In this test, three (3) IHPC and three (3) PV single edge notched beams were tested under a four point bending load, at temperature T1. Also three (3) notched IHPC beams were tested at temperature T2. The samples of notched beams are shown in figure 4.6. Using a sharp razor blade, a V-notch 2mm deep with a notch-tip angle of 60º was cut at the centre of each beam. A crack length of 1 mm was cut at the notch-tip, giving the value of an initial crack length a, as 3mm. Detail of the V-notch and the initial crack length is presented in figure 4.7.

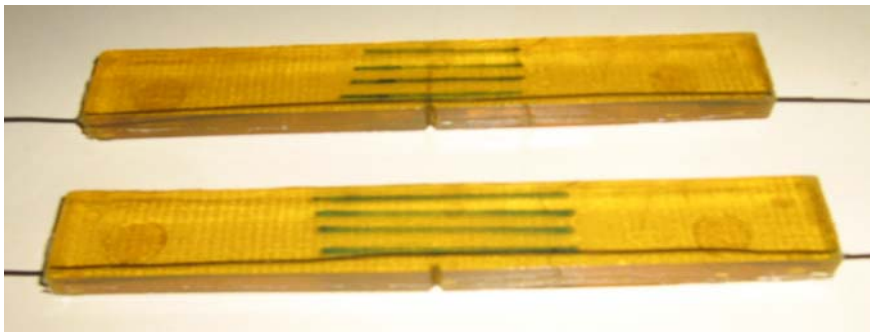

Figure 4.6: Notched IHPC beams

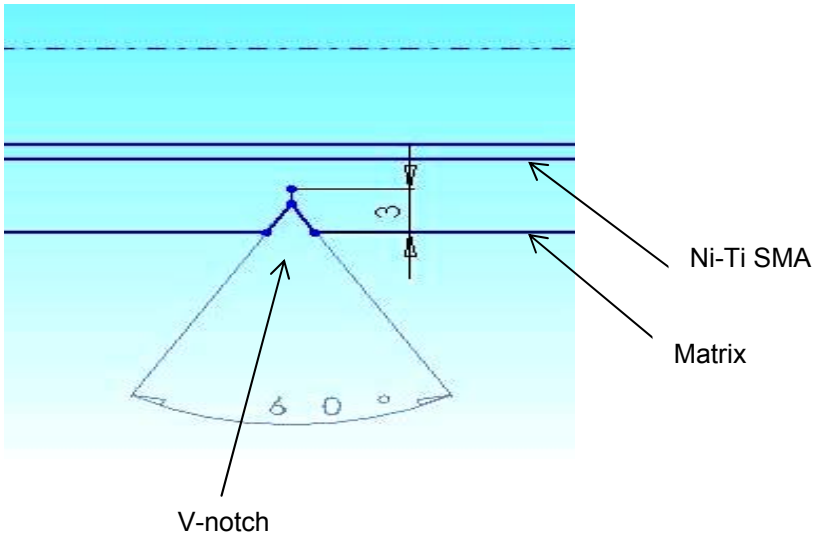

Figure 4.7: Detailed view of the V-notch with initial crack length of 3mm.

In order to measure the crack length induced by a given bending force, one face of each notched beam was marked with equally spaced parallel lines drawn longitudinally to the axis of the beam. A scale ruler was used to draw parallel lines equally spaced at 2mm apart. Each line on the specimen was marked its respective perpendicular length from initial crack tip. During the loading process, the instantaneous crack length was observed and recorded; simultaneously the corresponding bending force F, was recorded on the data acquisition unit.

At room temperature T1 of 24°C, each of the three PV notched beams and three IHPC notched beams was subjected to a four point bending load. The test was performed using a10kN load cell at a displacement rate of 1mm/minute. The load was increased until the crack started to propagate. The load increased further until the crack propagated across the width of the beam, hence complete fracture of the beam. The corresponding values of the bending load, crack length and the transverse deflection of the beam δ were recorded.

Next, the bending test was performed while the temperature of the Ni-Ti SMA was raised from 24°C to T2 of 46°C to effectively transform the detwinned martensite to austenite. The Ni-Ti SMA wire was actuated by means of direct current resistive heating. A magnitude of 3A of electric current was supplied by the DC source for the heating of the Ni-Ti SMA wire.

At temperature T2, a four point bending load was applied on each of the three (3) notched IHPC beams. The load was increased until the crack propagated across the width of the beam matrix. The values of the bending load, the transverse deflection of the beam δ and the crack length were recorded. The average experimental results of three beams at each temperature were used to determine the stress intensity factor K_I and the fracture stress

intensity factor K_{IC}. The fracture stress intensity factor K_{IC} is the value of K_I for which the crack was unstable and propagated completely across the beam to fracture.

Applying Irwin's mathematical model on a specimen with finite size under plane stress, the stress intensity factor K_I near the crack tip is obtained by the equation;

$K_I = \sigma Y(a)^{1/2}$ ----------(4.6)

where:

σ = bending stress in the beam (for a beam under bending load).

a = crack length,

H= un-cracked width in the crack plane.

Y = dimensionless compliance polynomial function of the ratio a/H.

The compliance function Y can be expressed as;

$Y=A(a/H)^{1/2}-F(a/H)^{3/2}+C(a/H)^{5/2}-D(a/H)^{7/2}+E(a/H)^{9/2}$----------(4.7)

For a four point bending, the constants A, F, C, D and E are: 1.99, 2.47, 12.97, 23.17 and 24.80 respectively (Hearn, 1997).

There fore the equation for stress intensity factor can be written as;

$K_I = (3PL/BH^{3/2})Y$ ----------(4.8)

where;

P =2F= total bending load on the beam,

L = distance between loading points,

B = beam specimen thickness

The fracture (critical) stress intensity factor K_{IC} is obtained when a fracture (critical) load F_C is substituted in equation (4.8).

Results for the experimental critical fracture load (F_C) and mode I fracture stress intensity factor (K_{IC}) of notched PV and IHPC beams were plotted and presented in figures 4.12-4.13 (see chapter 4.3).

4.3 Experimental results

Results obtained in the pullout test, bending test of un-notched IHPC and PV beams and bending test of notched IHPC and PV beams were plotted and presented in figures 4.8-4.13. A summary on the average values for the experimental pullout load, flexural stiffness (EI) of un-notched PV and IHPC beams , critical fracture load (F_C) and mode I fracture stress intensity factor (K_{IC}) of notched PV and IHPC beams are presented in tables 4.1,4.2 and 4.3.

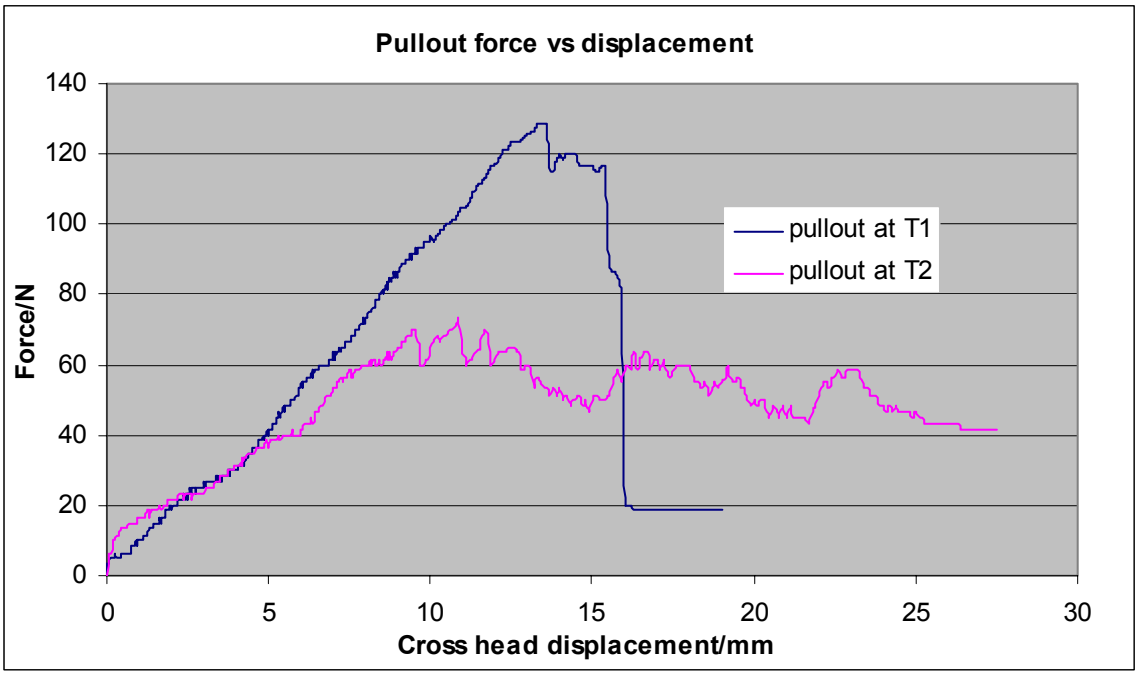

Figure 4.8: Pullout force versus displacement

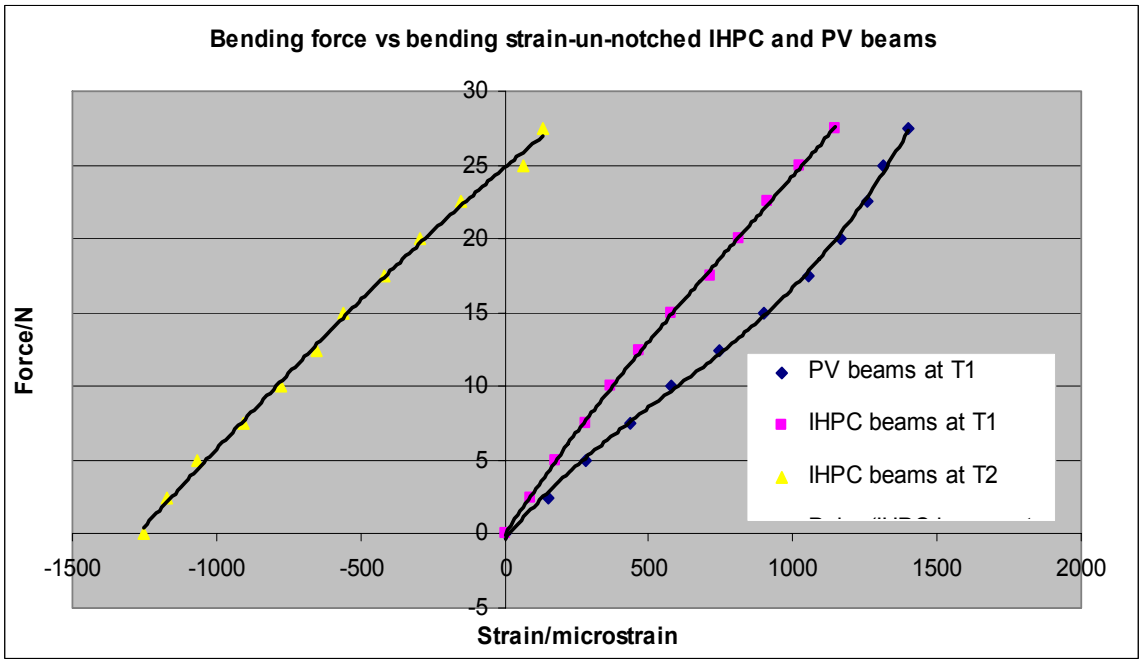

Figure 4.9: Bending force versus strain – un-notched beams

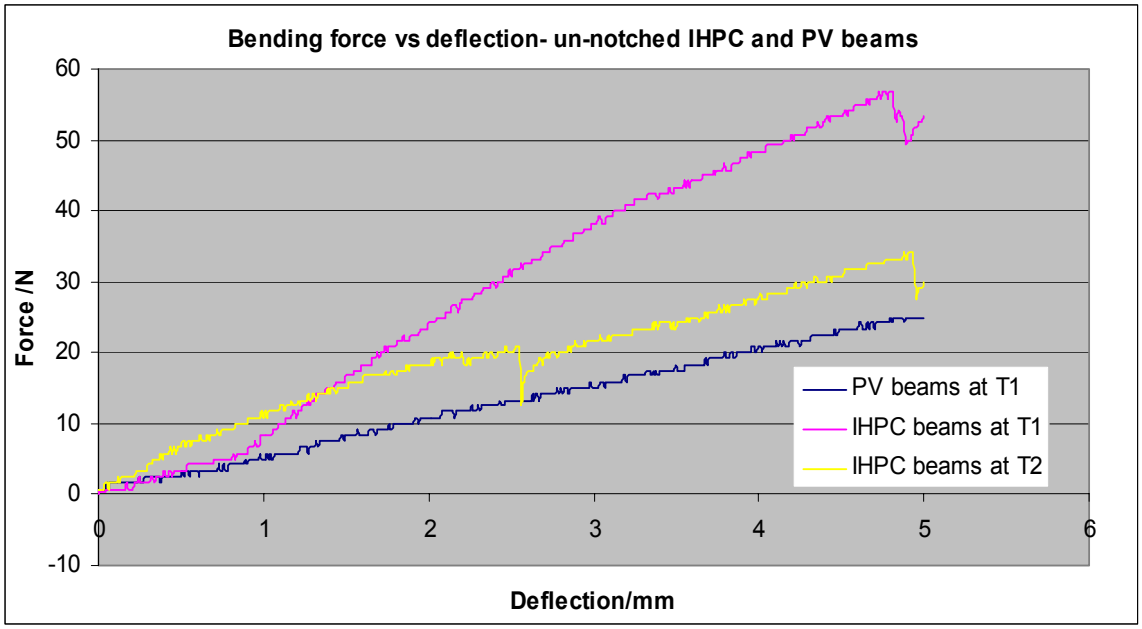

Figure 4.10: Bending force versus deflection – un-notched beams

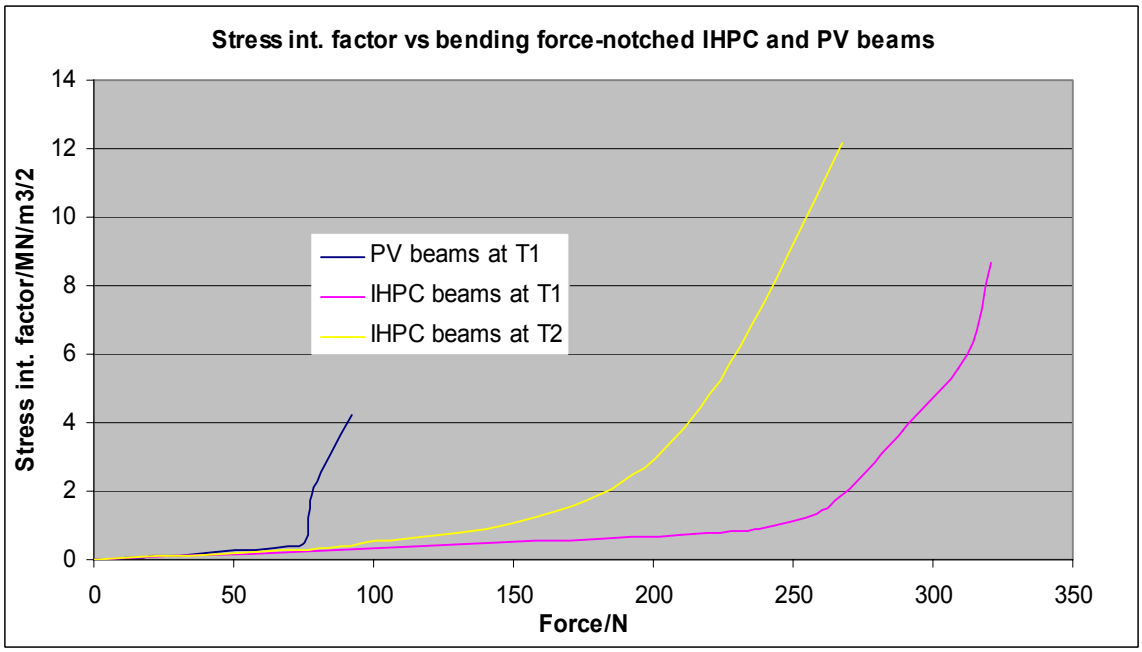

Figure 4.11: Stress intensity factor versus bending force- notched IHPC and PV beams

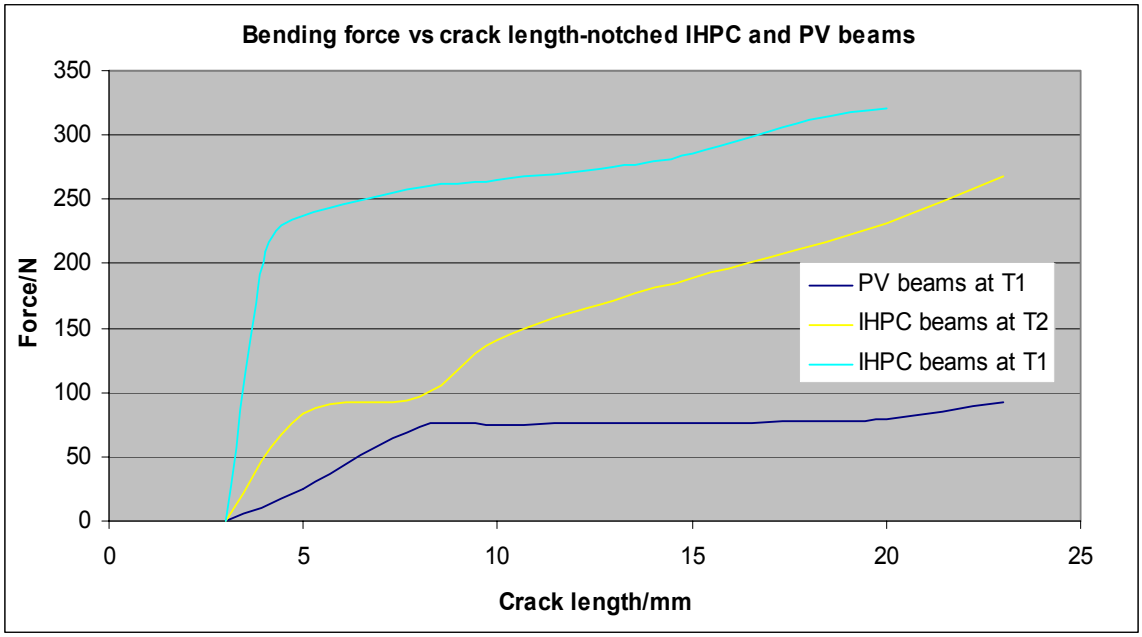

Figure 4.12: Bending force versus crack length- notched IHPC and PV beams

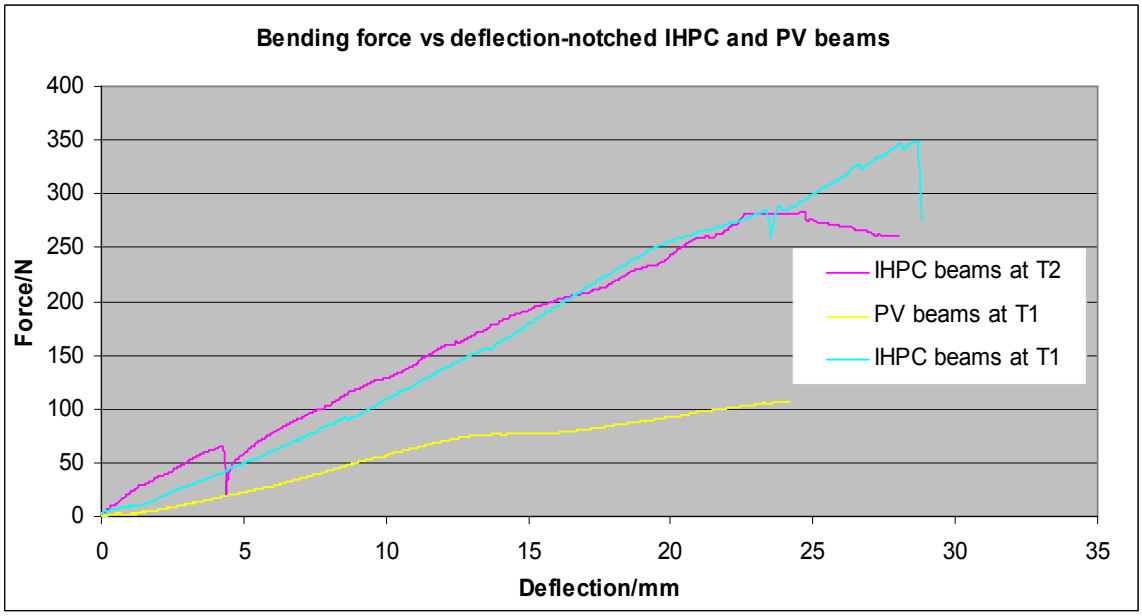

Figure 4.13: Bending force versus deflection- notched IHPC and PV beams

Table 4.1: Summary of experimental results- Pullout test

PULLOUT TEMPERATURE	PULLOUT LOAD (N)
IHPC beams at room temperature T1< A_S	120
IHPC beams at elevated temperature T2= A_f	60

Table 4.2: Summary of experimental results-bending of un-notched IHPC and PV beams

TYPE OF BEAM	FLEXURAL STIFFNESS, EI (Nm^2)
PV beams at room temperature T1< A_S	6.90
IHPC beams at room temperature T1< A_S	8.23
IHPC beams at elevated temperature T2= A_f	7.20

Table 4.3: Summary of experimental results- bending of notched IHPC and PV beams

TYPE OF BEAM	FRACTURE(CRITICAL) LOAD (N)	FRACTURE (CRITICAL) STRESS INTENSITY FACTOR, K_{IC} ($MN/m^{3/2}$)
PV beams at room temperature T1< A_S	93.0	4.21
IHPC beams at room temperature T1< A_S	321.0	8.64
IHPC beams at elevated temperature T2= A_f	268.0	12.17

CHAPTER FIVE

ANALYTICAL MODELING OF UN-NOTCHED IHPC AND PV BEAMS

5.1 Objectives of analytical modeling

In this chapter, analytical modeling of un-notched IHPC and PV beams was done to compare with experimental results. A constitutive relation of the bending force, Ni-Ti SMA recovery force, resulting bending strain and flexural stiffness EI of un-notched IHPC and PV beams were developed. The constitutive relation was used to predict the effect of actuated Ni-Ti SMA on increasing the flexural stiffness EI of un-notched IHPC beam under a bending load. First Ni-Ti SMA was modeled separately. Lin and Rogers (1991) model was applied to predict the martensite volume fraction in the Ni-Ti SMA at a given temperature. Brinson (1993) model was applied to determine the recovery stress and force that the Ni-Ti SMA can generate at a given temperature. The modeled Ni-Ti SMA was incorporated in modeling the un-notched IHPC and PV beams. The response of un-notched IHPC and PV beams in terms of the bending strain and the flexural stiffness under a bending load were analyzed when Ni-Ti SMA was actuated by heating from temperature T1 below austenite start (A_S) to the temperature T2 of austenite finish (A_f).

5.2 Description of the model

An un-notched IHPC beam modeled is an epoxy beam with rectangular cross section with one (1) mm diameter embedded Ni-Ti shape memory alloy wire. The 150 mm length of the wire is embedded 7mm off the neutral axis of the beam. The reason for locating the SMA wire off the neutral axis is to improve bending flexural stiffness of the beam when martensite transforms to austenite and a compressive recovery force is developed in the Ni-Ti SMA wire. The matrix is a two dimensional (2D) model and the SMA wire is a one dimensional (1D) model. The IHPC beam is a 2D model. The beam epoxy matrix is anisotropic and the SMA wire is isotropic. It is proper for the IHPC beam to be treated as anisotropic model. The geometry and dimensions of the model are shown in figure 3.1(see page 31)

Ni-Ti SMA and epoxy matrix material properties and dimensions of the model for the analytical computations are presented in table 5.1.

The values of austenite start A_S, austenite finish A_f, austenite modulus E_A and martensite modulus E_M are presented in table 5.1 and have been determined experimentally in chapter two.

Table 5.1: Model material properties and dimensions

Material properties	**Ni-Ti SMA**	**Epoxy** (polyurethane 60D)
Prestrain of SMA, ε_L	0.03	-
Max recovery strain, ε_{max}	0.08	-
A_S (ºC)	30	
A_f (ºC)	46	
E_A (Gpa)	16.0	-
E_M (Gpa)	11.5	-
E_m (GPa)	-	0.6
V_{SMA} (e-03)	12.56	-
V_m (e-03)	-	987.44
Model dimensions		
a (m)	0.03	
B (m)	0.01	
h (m)	0.007	
H (m)	0.025	
y (m)	0.0125	

5.3 Modeling of the Ni-Ti SMA wire

5.3.1 Approaches of modeling SMAs

Modeling of SMAs may be classified into two groups, the first is the macroscopic (phenomenological) model (Brinson, 1993; Brinson and Huang, 1996) in which phenomenological thermodynamics or/and curve fitting of experimental data are used. Many of them are based on experimental phase diagrams of SMA transformation where the transition regions of the martensite to the austenite or the austenite to the martensite are experimentally determined by plotting the stress-temperature diagram. In this approach, the martensite volume fraction is typically employed as an internal variable.

The second is the micromechanics based model (Lu and Weng, 1997). In this approach, SMAs crystallographic phenomena using the thermodynamic laws for describing phase transformation are used. These models consider the martensite variant as a transforming inclusion and use micromechanics to calculate the interaction energy due to the phase transformation in the material. Stresses and strains are obtained as averages over a volume in which many inclusions are considered representing the possible variants.

Most of the current micromechanics models can only predict the SMA behaviour qualitatively and can not easily be used for engineering applications because of the included variables such as free energy which are not easily quantified. However, macroscopic phenomenological models are quite accurate because the phase diagram is built on experimental data. They have a relatively simple expression including only quantifiable engineering variables and material constants. They have been widely accepted for engineering application of SMAs (Auricchio et al. 2003).

5.3.2 Recovery stress equation in the Ni-Ti SMA

In this thesis, modeling of the SMA wire was done by application of macroscopic (phenomenological) approach.

The model is based on the work done by Tanaka, (1986) who developed an equation of an explicitly model consisting of general state variables, strain, temperature and martensite fraction as follows:

$$d\sigma/dt = E(\partial\varepsilon/\partial t) + \Theta(\partial T/\partial t) + \Omega\,(\partial\,\xi\,/\partial t) \quad \text{---------- (5.1)}$$

Where σ is the Piola- Kirchhoff stress, ε is the Green strain, E is the Young's modulus, Θ is the modulus of thermal expansion, T is the temperature, ξ is the martensite volume fraction, t is the time and Ω is the SMA material transformation modulus.

The model developed by Tanaka describes SMA behaviour qualitatively with limitations to engineering applications. Liang and Rogers (1990) further improved this model to quantitatively describe the SMA behaviour by proposing a new set of empirical equations in a simple cosine form for kinetics of phase transformation. Brinson (1993) pointed out that Liang's and Rogers model does not properly feature SMA material behaviour at any temperature below martensite starting temperature M_s nor at higher temperatures when SMA material contains temperature induced martensite.

Brinson (1993) improved the Liang and Rogers model by splitting the martensite volume fraction ξ, into two components i.e. stress induced (detwinned) single variant martensite ξ_S, and temperature induced (twinned) multiple variant martensite ξ_T, volume fractions as can be represented in the following equation:

$$\xi = \xi_S + \xi_T \quad \text{---------- (5.2)}$$

The improved model can be represented by a constitutive equation of non constant material functions as:

$$\sigma_{re} = E(\xi)\,\varepsilon - \Omega(\xi)\,\xi_S + \Theta(T-T_o) \quad \text{----------(5.3)}$$

Where:

σ_{re} -term represents compressive recovery stress resulting in the SMA material,

E (ξ) ε - term represents the mechanical stress in the SMA material,

(Ω (ξ) ξ_s -term represents the transformation stress in the SMA material,

Θ($T-T_o$)- term represents the change of thermal stress in material.

T_o,T- terms represent initial and final temperature conditions of the SMA material.

The Young's modulus E(ξ) as a function of martensite volume fraction can be written as

$E(\xi) = E_A + \xi(E_M - E_A)$ ----------(5.4)

Where:

E_A= is the Young's modulus of the austenite

E_M= is the Young's modulus of the martensite

E_s= E_M at temperature T1 below austenite start A_S and $E_s = E_A$ at a temperature T2 of austenite finish A_f

The material transformation modulus Ω(ξ) as a function of martensite volume fraction can be written as:

$\Omega(\xi) = -\varepsilon_L E(\xi) = \varepsilon_L(E_A+ \xi(E_M - E_A))$ ----------(5.5)

ε_L = is the maximum recoverable martensite → austenite transformation strain which may be constant in a wide temperature range.

Considering the state of the Ni-Ti SMA during actuation where the material temperature T, is raised from the austenite start A_S to the austenite finish A_f temperature.

Applying one of the transformation kinetic equations obtained in Lin and Rogers's model (1991), the total martensite volume fraction ξ, in the SMA as a function of temperature can be obtained by the equation:

For change of phase from martensite to austenite (M→A);

$\xi(T) = 1$ for $T \le A_S + \sigma/ C_A$

$\xi(T) = 1- (T - A_S)/(A_f-A_S) + \sigma/ C_A (A_f-A_S)$ for $A_S + \sigma/ C_A < T < A_f + \sigma/ C_A$ ------(5.6)

$\xi(T) = 0$ for $T \ge A_f + \sigma/ C_A$

Where:

C_A = SMA material constant in austenite phase,

A_S = austenite starting temperature,

A_f = austenite finish temperature,

σ = axial mechanical stress applied in the SMA material, in the present work the axial stress in the SMA material is negligible, therefore σ = 0.

$\xi(T)$ = martensite volume fraction induced in the SMA material at temperature T.

The stress induced (detwinned) martensite fraction ξ_S in the SMA at any temperature can be obtained by the equation

$\xi_S(T)=\xi_{so}\xi(T)$----------(5.7)

The value of ξ_{So} represents initial stress induced (detwinned) martensite volume fraction in the SMA and can be calculated using a relation given by Tsoi et al. (2002) that the amount of single variant (detwinned) martensite volume fraction in the SMA material is directly proportional to the prestraining of the SMA. This relationship can be mathematically approximated as:

$\xi_{So} = \varepsilon_o/\varepsilon_{max}$ ----------(5.8)

where;

ε_o= initial prestrain of the SMA material (0.03 for this case)

ε_{max}= maximum transformation recoverable strain that can be attained by a shape memory alloy. It is taken as 0.08 (8%) for Ni-Ti alloy and 0.067 (6%) for Ni-Ti-Cu alloy.

By substituting equations (5.5) and (5.4) in equation (5.3) the net actuating stress in the SMA material can be represented by the following equation:

$\sigma_{re} =(E_A+ \xi(E_M - E_A))\varepsilon - \varepsilon_L(E_A+ \xi(E_M - E_A))\xi_S + \Theta(T-T_o)$----------(5.9)

Equation (5.9) represents resultant compressive recovery stress in the SMA material. It will be used in this SMA model and can be abbreviated as:

$\sigma_{re} = \sigma_{me} - \sigma_{tr} + \sigma_{th}$----------(5.10)

Where:

σ_{re} = total recovery stress in the SMA material

$\sigma_{me}=(E_A+ \xi(E_M- E_A))\varepsilon$ = total mechanical axial stress acting in the SMA wire.

$\sigma_{tr} = -\varepsilon_L(E_A+ \xi(E_M - E_A))\xi_s$ = total compressive transformation stress in the SMA due to the martensite → austenite transformation.

$\sigma_{th} = \Theta(T-T_o)$ = thermal expansion stress induced in the SMA wire.

The action and direction of stresses in the SMA material are illustrated in figure 5.1.

The mechanical stress and thermal expansion induced stresses are small compared to the transformation stress, there fore can be neglected. Equation (5.9) reduces to

$\sigma_{re} = - \varepsilon_L(E_A+ \xi(E_M - E_A))\xi_S$----------(5.11)

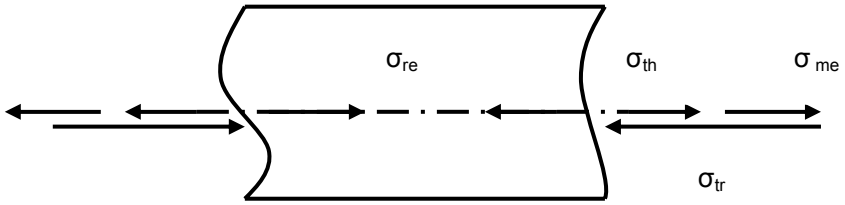

Figure 5.1: Stresses in the Ni-Ti SMA wire.

5.3.3 Instantaneous recovery stress state equation in the Ni-Ti SMA material.

In this section, the equation that describes the state of stress in the SMA material during the process of heating from austenite starting temperature (A_S) to austenite finishing temperature (A_f) is derived. Equation (5.11) can be modified to give the state of recovery stress $\sigma_{re}(T)$ in the SMA material at a given temperature T as;

$\sigma_{re}(T) = - \varepsilon_T(E_A + \xi(E_M - E_A))\xi_S$----------(5.12)

Where ε_T is the recovery strain at the temperature T.

The behaviour of recovery strain with increasing temperature is shown in figure 5.2. It is assumed that the recovery strain is linearly increasing with the increase of temperature. The value of recovery strain is assumed zero at the austenite starting temperature A_S and maximum ε_L at the austenite finish temperature A_f.

Applying the relationship of similar triangles, the transformation strain ε_T at temperature T can be expressed as:

$\varepsilon_T = \varepsilon_L(T - A_S)/(A_f - A_S)$----------(5.13)

Substituting equation (5.13) into equation (5.12) gives;

$\sigma_{re}(T) = -\varepsilon_L \xi_S (E_A + \xi(E_M - E_A)) (T - A_S)/(A_f - A_S)$----------(5.14)

It should be noted that the recoverable strain in the SMA wire is the initial prestrain, therefore it is approximated that ε_L =0.03.

Substituting the expressions for ξ and ξ_S, gives;

$\sigma_{re}(T) = -\varepsilon_L \xi_{So} [E_A + \{1-(T - A_S)/(A_f - A_S)\}(E_M - E_A)]\{(T - A_S)/(A_f - A_S)\}\{1- (T - A_S)/(A_f - A_S)\}$ --(5.15)

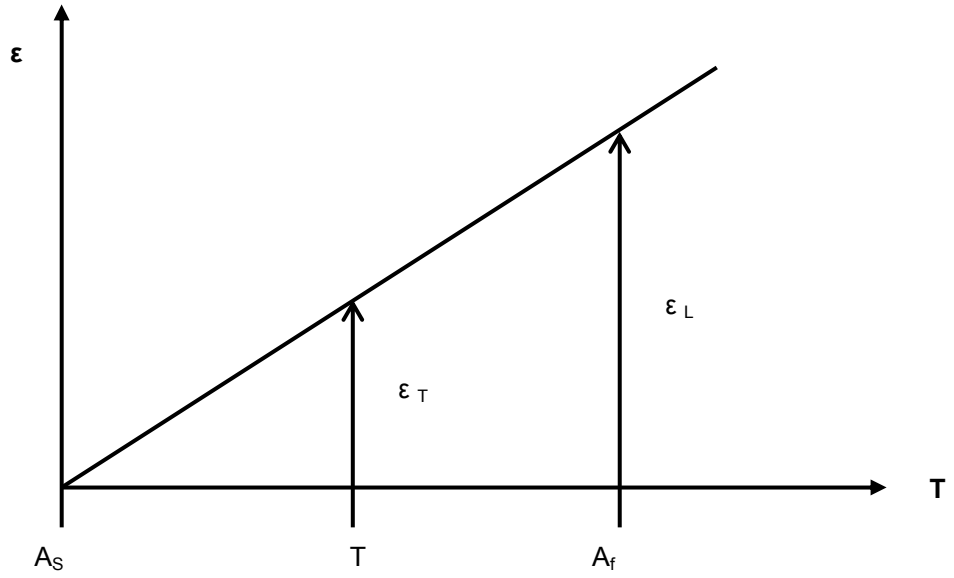

Figure 5.2: Recovery strain versus temperature in the Ni-Ti SMA

In this thesis the recovery stress and force were calculated in steps of 2ºC temperature increment from A_S to A_f . The total recovery stress and strain at the end of transformation were obtained by summing up the calculated values in temperature intervals of 2ºC (see table 5.2). The value of the transformation strain ε_T at 2ºC temperature interval was 3750 με. The total recovery force in the SMA wire denoted by F_{re} is obtained by the product of the cross section area of the SMA wire and the total recovery stress i.e.

$F_{re}(T) = A\sigma_{re}(T)$----------(5.16)

The values of the martensite fraction ξ, twinned martensite fraction ξ_S, Young's modulus E of the SMA, recovery stress $\sigma_{re}(T)$ and recovery force $F_{re}(T)$ generated by the SMA as functions of temperature were calculated using the derived equations. The values were calculated based on the actuating (heating) process from austenite start A_S = 30ºC to austenite finish A_f= 46ºC. Computed values are presented in table 5.2

Table 5.2: Martensite volume fraction, stress and force generated in the Ni-Ti SMA wire in the actuating process

T /ºC	ξ(T)	ξ_S(T)	ε_T/microstrain (10^{-6})	E(ξ)/GPa	σ_{re}(T)/MPa	σ_{re}(T)/MPa accumulative	F_{re} (T)/N
30	1	0.375	3750	11.5	0.0	0.0	0.0
32	0.875	0.328	3750	12.1	16.2	16.2	12.7
34	0.750	0.281	3750	12.6	14.9	31.1	24.4
36	0.625	0.234	3750	13.2	13.3	44.4	34.9
38	0.500	0.188	3750	13.8	11.6	56.0	43.9
40	0.375	0.141	3750	14.3	9.7	65.7	51.6
42	0.250	0.094	3750	14.9	7.6	73.3	57.6
44	0.125	0.047	3750	15.4	5.3	78.6	61.7
46	0	0	3750	16	2.7	81.3	63.9

5.4 Modeling of un-notched IHPC beam

5.4.1 Loading of un-notched IHPC beam

An un-notched IHPC beam (see figure 5.3) is loaded under four point bending, the beam is simply supported. The bending loads act transversely (perpendicular) to the longitudinal axis of the beam. The Ni-Ti SMA recovery force F_{re} acts axially along the axis of the Ni-Ti SMA wire and parallel to the longitudinal axis of the beam. When the SMA wire is actuated, the compressive recovery force in the Ni-Ti SMA wire will bend the beam hence creating a compressive stress in the upper portion of the beam which will oppose the tensile stress generated by the four point loading of the beam.

5.4.2 Assumptions made

The following assumptions were made:

- The IHPC beam is straight with a constant cross section.
- Planes normal to the axis of un-deformed IHPC beam remain normal to the axis of the deformed IHPC beam.
- In the model it is assumed that there is a perfect bond along the SMA wire - epoxy matrix interface, therefore there is continuity of strain along the interface. The stress is discontinuous along the interface.
- The total strain of the IHPC beam at any point from the neutral axis includes mechanical, thermal and recovery (transformation) strain.
- The effect of the cross section area of the SMA wire on the second moment area of the IHPC beam cross section about the z-z axis is neglected. It is assumed that the

second moment area of the cross section of the IHPC beam about z-z axis is equal to that of the epoxy matrix.

5.4.3 Equations for the bending moment, bending stress and bending strain in un-notched IHPC beam.

The un-deformed IHPC beam with embedded Ni-Ti SMA wire is illustrated in figure 5.3. Figure 5.4 illustrates a deformed IHPC beam under the action of bending and recovery forces when the Ni-Ti SMA wire is actuated. Main forces on the IHPC beam are the four point bending forces F acting transversely on the IHPC beam, recovery force F_{re} acting axially in the IHPC beam at a distance h=7mm from the neutral axis.

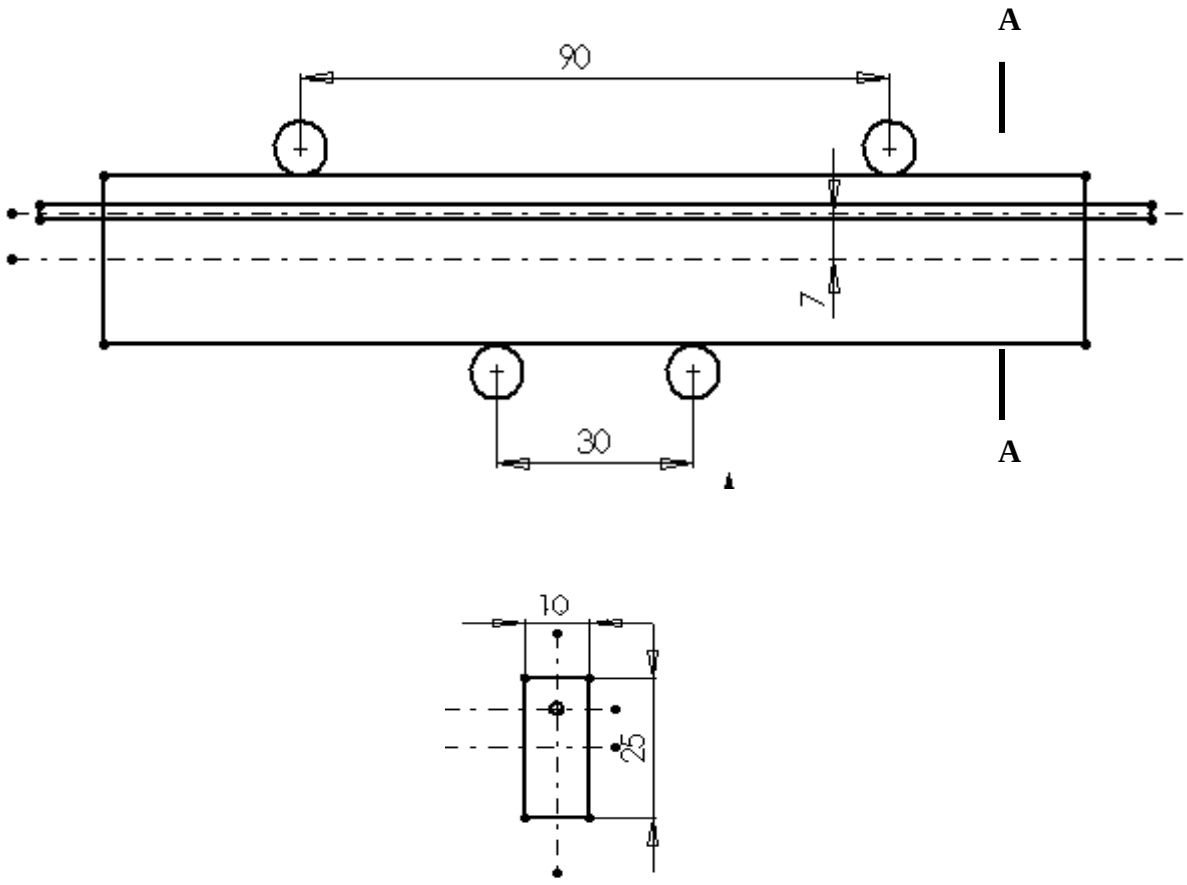

Figure 5.3: **IHPC beam in un-deformed configuration and Ni-Ti SMA wire un-actuated.**

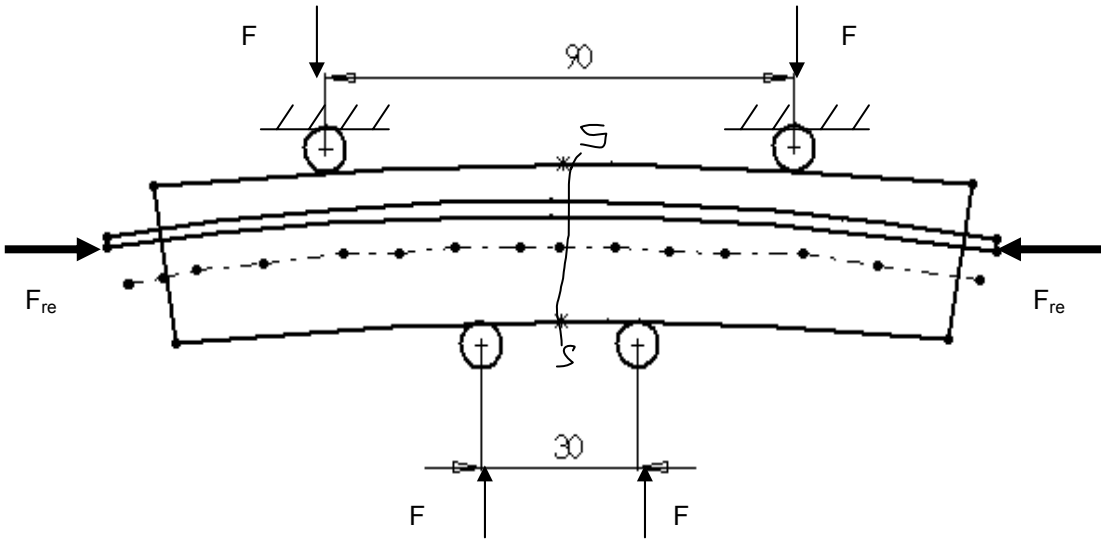

Figure 5.4: IHPC beam in a deformed configuration and Ni-Ti SMA wire actuated

An element of an arbitrary length x cut from a deformed IHPC beam at section s-s in figure 5.4 is taken for analysis. The forces and moments on the element are illustrated in figure 5.5. The element is subjected to external forces F and the net recovery force F_{re} exerted by the SMA wire on the IHPC beam. The recovery force is compressive and acts axially at a distance h from the neutral axis. The IHPC beam is subjected to internal bending moment M(x), shear force Q(x) at a section point. Under equilibrium of the element, taking anticlockwise moments as positive, taking summation of moments about a point on the section s-s along the neutral axis and equate to zero gives:

$-M(x)- F_{re}.h + F.x- F(x-a) = 0$

$M(x)= F.a - F_{re}.h$ ----------(5.17)

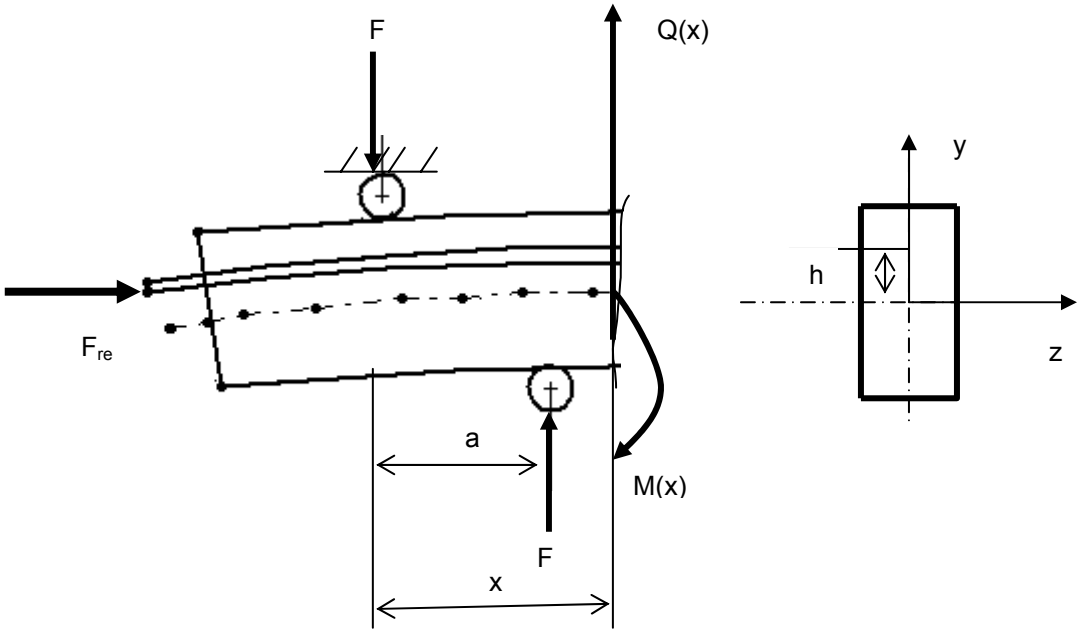

Figure 5.5: Beam element

Considering equilibrium of the element under forces in the vertical (y-axis) gives:

$F-F+Q(x) = 0$

$Q(x) = 0$ ---------- (5.18)

Equation (5.17) tells us that the embedded SMA recovery force F_{re} reduces the bending moment in the IHPC beam induced by the applied external forces F. Hence in this context the SMA wire increases the bending flexural stiffness of the IHPC beam. The magnitude of induced flexural stiffness increases with the distance h of SMA location from the neutral axis in the positive y- axis. Location of the SMA wire at a distance h in the negative y-axis will increase the bending moment in the IHPC beam, and therefore in this context it will decrease the flexural stiffness.

Equations (5.17) and (5.18) indicate that in a four point loading along the mid span of the IHPC beam (at x = a, to x = a + b), the bending moment is constant and the shear force is zero.

The bending stress in the IHPC is obtained by:

$\sigma_b = (M(x)/I_{zz})y$ ----------(5.19)

where by;

σ_b= bending stress in the IHPC beam

M(x) = bending moment on the IHPC beam at length x from the origin about the z-axis

$= F.a- F_{re}.h$

I_{zz} = area second moment of the cross section of the IHPC beam about the z- axis

$= BH^3/12$ for a rectangular cross section. B and H are the IHPC beam section width and height respectively.

y= the length from the neutral axis of the IHPC beam to the point of consideration measured positive outside and negative inside the bending curve.

Substituting the values in equation (5.19), the bending stress can be expressed as:

$\sigma_b = \{(F.a- F_{re}.h) / (BH^3/12)\}y$ ---------- (5.20)

By Hooke's law, the bending strain ε_b in the IHPC beam can be expressed as:

$\varepsilon_b= \sigma_b/E_c$ ----------(5.21)

where;

E_c= Young's modulus for the IHPC beam,

$E_c = E_sV_s + E_mV_m$ ---------- (5.22)

The quantities E_s and E_m are the Young's modulus of the SMA material and epoxy matrix respectively. V_s and V_m are the volume fractions of the SMA and the epoxy matrix respectively. It should be noted that the value of E_s depends on the temperature and state/phase of Ni-Ti SMA material and can be defined using equation (5.4)

Substituting equations (5.20) and (5.22) in equation (21) gives:

ε_b ($(E_A + \xi(E_M - E_A))V_s + E_mV_m)$ $(BH^3/12)/ay + F_{re}.h/a = F$ or

$\varepsilon_b = [\{(F.a - F_{re}.h)/(BH^3/12)\}/((E_A + \xi(E_M - E_A))V_s + E_mV_m)]y$ ---------- (5.23)

Equation (5.23) can be abbreviated as:

$\varepsilon_b.=\{(F.a - F_{re}.h)/ E_cI\}y$---------- (5.24)

The term $E_cI=((E_A + \xi(E_M - E_A))V_s + E_mV_m)(BH^3/12)$ is the flexural stiffness of the IHPC beam.

The Young's modulus E_c and the flexural stiffness E_cI of the IHPC beam at elevated temperature T2 are affected by other factors such as martensite-austenite transformation or martensite volume fraction, temperature sensitivity of the epoxy matrix and debonding of the SMA-matrix interface.

- **Martensite volume fraction:** During actuation by heating the Ni-Ti SMA, transformation of martensite to austenite may not be complete. This can result to the Young's modulus of the SMA E_S being lower than the calculated one hence lower Young's modulus E_C and lower flexural stiffness E_CI of the IHPC beam. In this model the martensite-austenite transformation was assumed ideal, ie the Ni-Ti SMA was assumed to be completely in the austenitic phase at temperature T2.
- **Temperature sensitivity of the epoxy matrix:** As the SMA wire is actuated, via electric current resistive heating, the temperature along the SMA-epoxy interface starts increasing towards the glass transition temperature T_g of the epoxy matrix. As a result, the heated matrix softens along the interface. If the matrix is a good heat conductor the yield stress and Young's modulus E_m will decrease with the increasing temperature. In this model the heating temperature was 46ºC hence below 75ºC which is the glass transition temperature (T_g) of the epoxy matrix. In this model the effect of temperature sensitivity of the epoxy matrix to the Young's modulus of the IHPC beam was neglected.

- **Debonding of the SMA-epoxy matrix interface:** The process of heating the Ni-Ti SMA wire results in softening of the epoxy matrix along the interface. Hence the bonding strength of the composite is degraded at temperature T2. The significant effect of heating the Ni-Ti SMA wire on the SMA-matrix interfacial bonding has also been observed in the pullout test performed in this thesis (see chapter four) in which Pullout test results showed that actuating the SMA reduced the pullout load by 50%.

In this model, the experimental flexural stiffness of the IHPC beams at T2 was relatively lower than that of the analytical model at T2, this was due to the debonding that initiated along the SMA-matrix interface. For the analytical model to agree with experimental results, the effect of temperature on the SMA-matrix interfacial strength was taken into account. Based on the experimental data, a bonding factor K_b was introduced to the theoretical bending strain ε_b as follows:

$\varepsilon_{b,a} = \varepsilon_b/K_b + \varepsilon_{b,o}$ ----------(5.25)

where;

$\varepsilon_{b,a}$ is the actual bending strain,

$\varepsilon_{b,o}$ is a strain constant,

A strain constant in this case is the value of compressive bending strain induced in the IHPC beam by the SMA recovery force when the external applied load is zero. It is determined by the relation:

$\varepsilon_{b,o} = \varepsilon_b(F=0)$

Equation (5.24) can be substituted in equation (5.25) to give:

$\varepsilon_{b,a} = \{(F.a - F_{re}.h)/ E_cI\}y /K_b + \varepsilon_{b,o}$

$= \{(F.a - F_{re}.h)/ K_b E_cI\}y+\{(-F_{re}.h)/ E_cI\}y$

Arranging the above equation, the actual bending strain in the IHPC beam is given by:

$\varepsilon_{b,a} = (F.a -(1+ K_b)F_{re}.h)y/K_b.E_cI$----------(5.26)

The above equation can be written in the expanded form as:

$\varepsilon_{b,a} = [\{(F.a- (1+ K_b)F_{re}.h)/(BH^3/12)\} / K_b ((E_A + \xi(E_M - E_A))V_s + E_mV_m)]y$

where;

$K_b.E_cI = K_b((E_A + \xi(E_M - E_A))V_s + E_mV_m)(BH^3/12)$ is the effective flexural stiffness of the IHPC beam that depends on bonding between SMA wire and epoxy matrix at temperature T2.

$F.a - (1+ K_b)F_{re}.h$ is the effective bending moment induced in the IHPC beam

Equation (5.26) for the bending strain induced in the IHPC beam reduces to the bending strain equation for the polymeric virgin (PV) beam under the following conditions:

- Since the PV beam contains no Ni-Ti SMA, then E_s=0 and F_{re}=0.
- It is assumed that no debonding takes place in the PV beam, hence the bonding factor K_b =1.

The actual bending strain equation for the IHPC beam reduces to that of PV beam as follows:

$\varepsilon_{b,a} = (F.a /.E_m I)y$----------(5.27)

A C++ program (see appendix D) was written and used for the computations. The program was formulated to compute variation of martensite fraction, recovery stress and force in the Ni-Ti SMA wire, flexural stiffness EI for un-notched IHPC beam with increasing temperature of the Ni-Ti SMA, from austenite start A_s to austenite finish A_f. Also, the program computes the bending strain resulting from bending force F applied on un-notched IHPC and PV beams.

Variations of the martensite fraction, Young's modulus of the Ni-Ti SMA, Young's modulus of the IHPC beam and the flexural stiffness of the IHPC and PV beams with the temperature of the SMA material are presented in table 5.3. The responses of strain and the flexural stiffness EI for IHPC and PV beams to the actuation temperature were calculated and presented in table 5.4.

Table 5.3: Variation of martensite fraction ξ(T), Young's modulus of Ni-Ti SMA E(ξ), Young's Modulus of IHPC beam E_C and flexural stiffness E_CI of the IHPC beam with temperaure

T /ºC	ξ(T)	ξ_S(T)	E(ξ)/GPa	E_C/GPa	I/m^4	E_CI/Nm^2	K_bE_CI/Nm^2
30	1	0.375	11.5	0.737	1.302x10^{-8}	9.59	7.70
32	0.875	0.328	12.1	0.744	1.302x10^{-8}	9.69	7.75
34	0.750	0.281	12.6	0.751	1.302x10^{-8}	9.77	7.82
36	0.625	0.234	13.2	0.758	1.302x10^{-8}	9.87	7.89
38	0.500	0.188	13.8	0.766	1.302x10^{-8}	9.97	7.98
40	0.375	0.141	14.3	0.772	1.302x10^{-8}	10.05	8.04
42	0.250	0.094	14.9	0.779	1.302x10^{-8}	10.15	8.12
44	0.125	0.047	15.4	0.786	1.302x10^{-8}	10.23	8.18
46	0	0	16	0.793	1.302x10^{-8}	10.33	8.27

Table 5.4: Results for applied force F, bending strain ε and flexural stiffness EI on the model

FORCE F/N	BENDING STRAIN ε/microstrain		
	PV BEAM $T1 < A_S$	IHPC BEAM $T1 < A_S$	IHPC BEAM $T2 = A_f$
0	0	0	-1216.09
2.5	120.04	97.7	-1102.65
5.0	240.08	195.4	-989.21
7.5	360.12	293.1	-875.76
10.0	480.15	390.8	-762.34
12.5	600.19	488.5	-648.90
15.0	720.23	586.2	-535.46
17.5	840.27	683.9	-422.03
20.0	960.31	781.6	-308.59
22.5	1080.35	879.3	-195.15
25.0	1200.39	977.7	-119.21
27.5	1320.42	1074.7	31.72
FLEXURAL STIFFNESS EI/Nm^2	7.81	9.59	8.27

5.5 Analytical results

Variations of the martensite fraction, the flexural stiffness of the IHPC and PV beams and recovery stress/force with the temperature of the Ni-Ti SMA were plotted. The bending strain induced in the un-notched IHPC beam against external force F as predicted by equation (5.26) was plotted within two temperature conditions, T1 below austenite start A_S and T2 of austenite finish A_f. The plotted results are presented in figures 5.6 - 5.9.

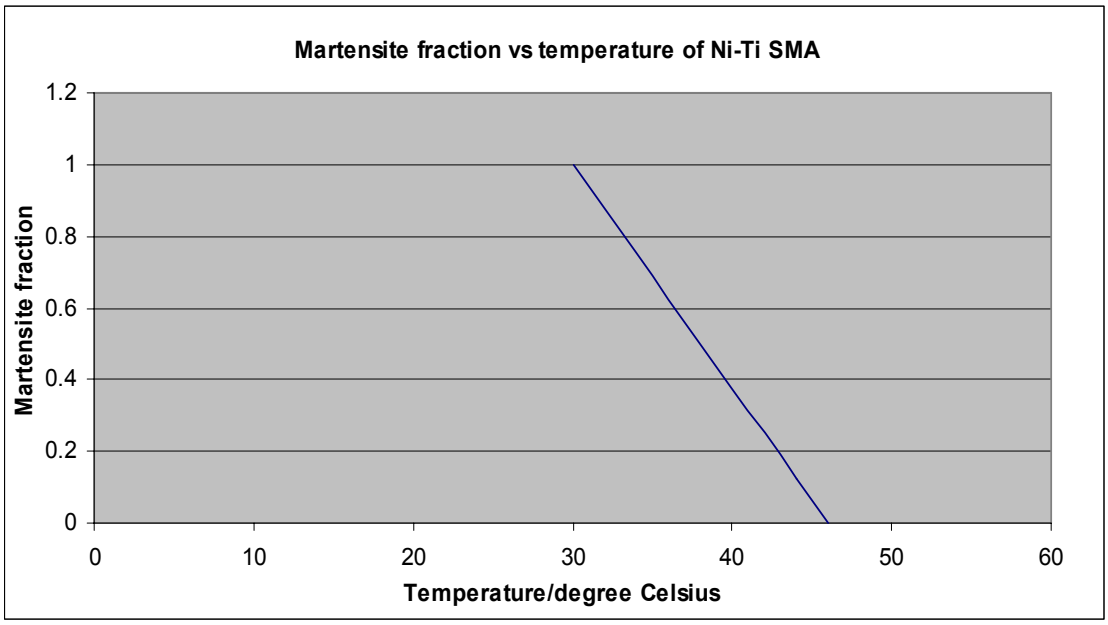

Figure 5.6: Martensite fraction versus actuation temperature of Ni-Ti SMA

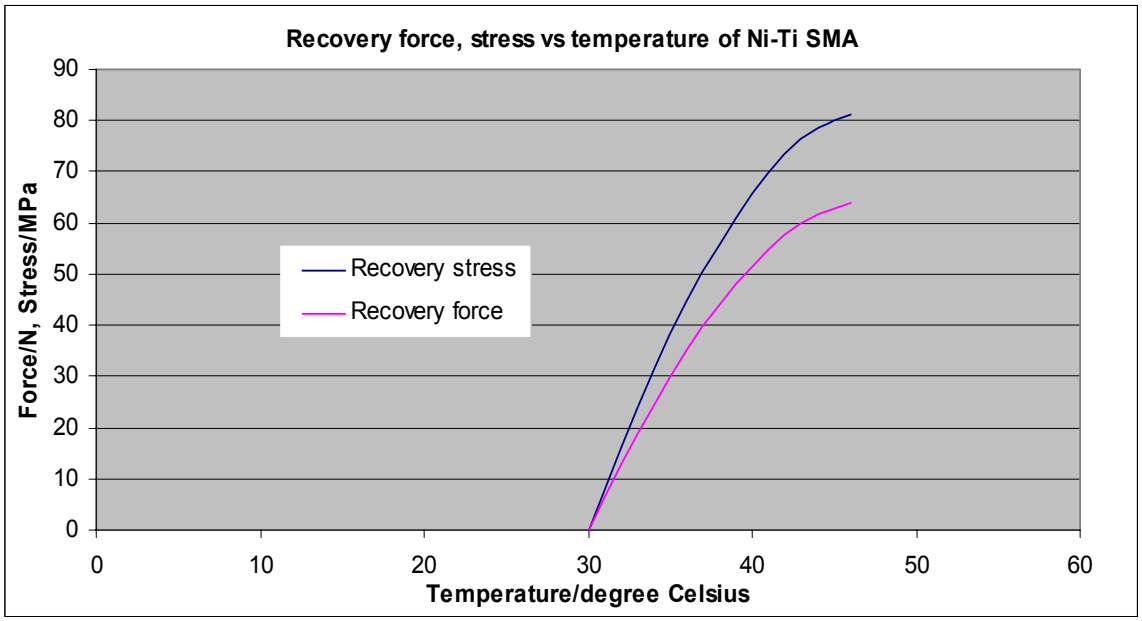

Figure 5.7: Recovery force, stress versus temperature of Ni-Ti-SMA

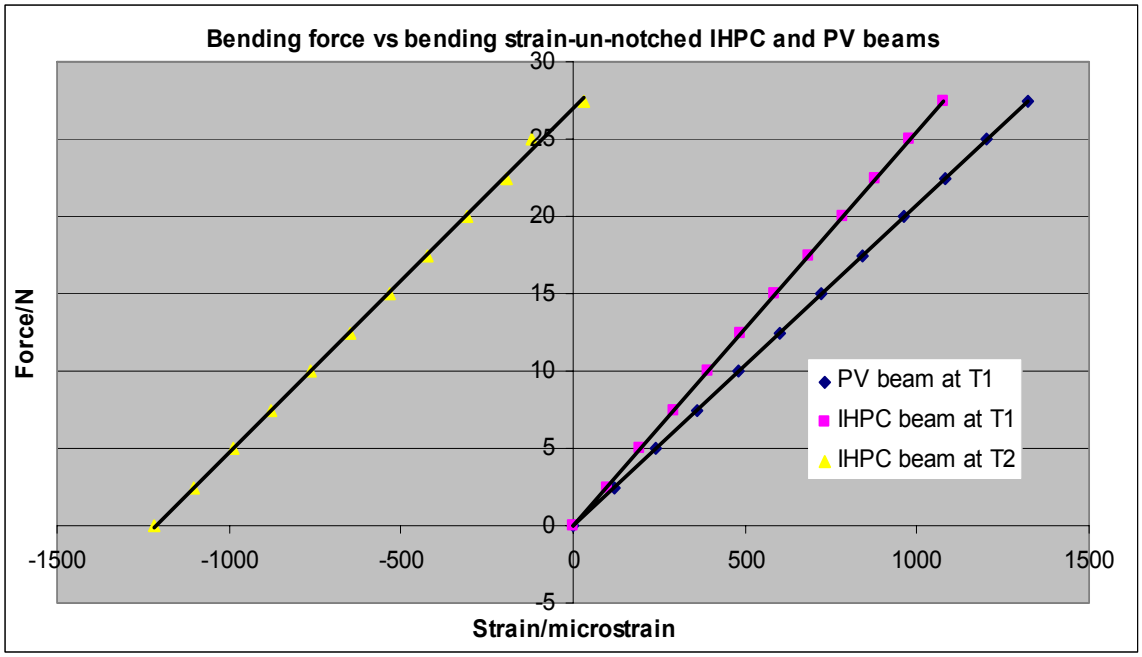

Figure 5.8: Bending force versus strain

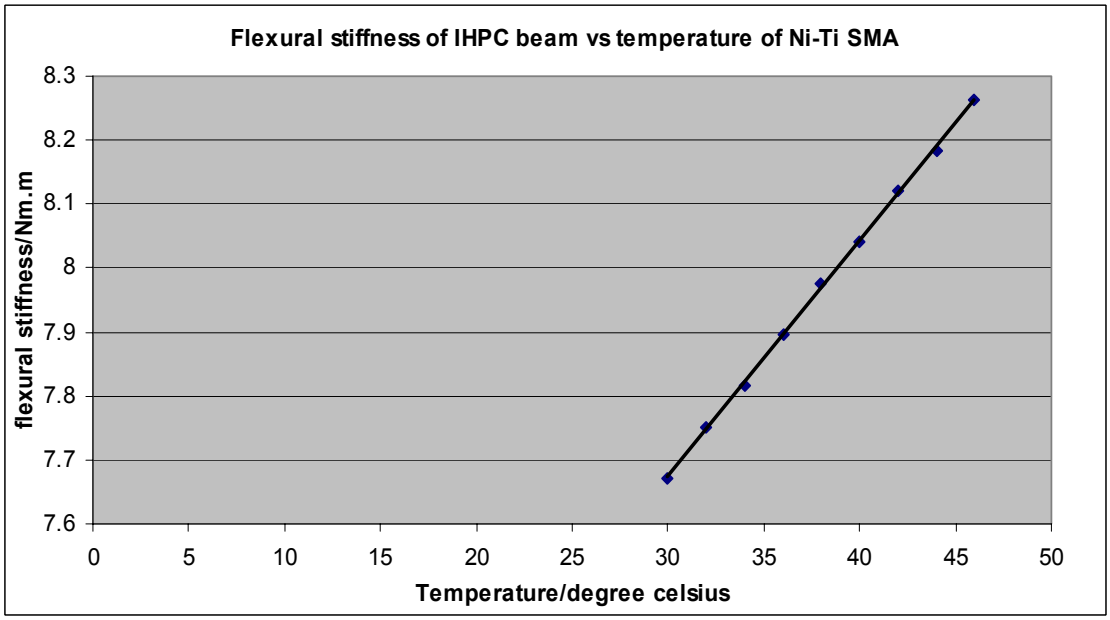

Figure 5.9: Flexural stiffness of IHPC beam versus actuation temperature of Ni-Ti SMA

CHAPTER SIX

DISCUSSION OF RESULTS

6.1 Introduction

This chapter discusses the experimental and analytical results obtained in this thesis. It covers a detail discussion of results obtained in the pullout test, the four point bending test performed on un-notched IHPC and PV beams and on notched IHPC and PV beams. Also results of analytical modeling of un-notched IHPC and PV beams done to compare with experimental results are discussed.

The pullout test was done to determine the strength of the matrix-SMA interface. The four point bending tests were done to determine the effect of actuated Ni-Ti SMA on the flexural stiffness EI and mode I fracture stress intensity factor K_{IC} of the IHPC beam. The increase of values of EI and K_{IC} would stiffen the beam and enhance healing by retarding crack growth and recovery of strain induced by applied load.

6.2 Experimental results

6.2.1 Results of the pullout test

Results of a pullout test (see figure 4.8 page 45) showed that actuation of the SMA decreased debonding load at temperature T2 of austenite finish A_f by 50% compared to the debonding load at temperature T1 below austenite start A_S. At temperature T1, the debonding load was 120N. At temperature T2, debonding load was 60N. It was expected that contraction of actuated SMA wire would induce compressive forces in the beam matrix hence increase debonding load, but the results did not fulfill the expectation. The reason being that heating of the Ni-Ti SMA wire resulted in softening and weakening of the matrix -SMA wire interface.

Actuation of the Ni-Ti SMA wire by resistive heating significantly decreased the debonding load of the SMA-matrix interface from120N to 60N, but increased debonding extension from 12mm to 23mm until complete fracture. The reason for the IHPC beam yielding further until failure at temperature T2 was that due to heating of the Ni-Ti SMA, the SMA-matrix interface temperature increased, the matrix material softened and

became more ductile along the interface. The increase of ductility of the matrix along the interface exhibited a higher elongation under a pullout load.

It was also noted that for the pullout test performed at temperature T1, after attaining a maximum load of 120N, the matrix material debonded completely and could not resist any more load while the pullout test performed at temperature T2 showed that after attaining a maximum load of 60N, debonding along the SMA-matrix interface initiated, but the material did not debond completely as it had been observed in the pullout test performed at temperature T1. Instead, with a gradual drop of the load, material offered some resistance before complete failure. The resistance was due to compressive recovery stress induced by the Ni-Ti SMA in the beam.

6.2.2 Results of bending test of un-notched IHPC and PV beams

Results of the bending test of un-notched IHPC and PV beams (see figure 4.9 page 45) showed that at temperature T1, the force versus strain curve for the IHPC beams had steeper gradient than that of the PV beams' curve. At temperature T1, the flexural stiffness EI was 6.90 Nm^2 for the PV beams and 8.23 Nm^2 for the IHPC beams.

Results showed that the force versus strain curve for the IHPC beams at temperature T2 had steeper gradient than that of the PV beams' curve at temperature T1.The flexural stiffness EI was 6.90 Nm^2 for the PV beams at temperature T1 and 7.2 Nm^2 for the IHPC beams at temperature T2. The value of EI for IHPC at T2 was 4.3% greater than that of PV at T1.

It was noted that the IHPC beams at temperature T2 had a lower flexural stiffness than that of the IHPC beams at temperature T1. The reason is that at temperature T2, the IHPC beams softened along the SMA-matrix interface during heating the Ni-Ti SMA. Interfacial debonding initiated and a large fraction of the load was transferred to the matrix.

Within the loading range of 0-25N, actuated IHPC beams at temperature T2 accommodated a bending load with a compressive strain, while the IHPC and PV beams at temperature T1 accommodated the bending load with a tensile strain. The compressive strain in the IHPC beams was induced by the compressive recovery force generated by actuated Ni-Ti SMA.

Considering the load versus deflection curves for un-notched IHPC and PV beams (see figure 4.10 page 46), it was noted that within the loading range of 0-15N, actuation of the Ni-Ti SMA wire increased the load accommodated by the un-notched IHPC beams at temperature T2 by 50% over the load accommodated by the IHPC beams at temperature T1.

6.2.3 Results of bending test of notched IHPC and PV beams

Results of the four point bending test performed on the notched IHPC and PV beams (see figure 4.11 page 46) showed that when the notched PV beams were loaded at a temperature T1 (below austenite start A_S), the PV beams fractured at a force of 93N with a corresponding critical stress intensity factor K_{IC} of 4.21MN/m$^{3/2}$. When the IHPC beams were loaded at a temperatureT1 (below austenite start A_S), the beams fractured at a force of 321N with a corresponding critical stress intensity factor K_{IC} of 8.64MN/m$^{3/2}$. When the IHPC beams were loaded at a temperature T2 (of austenite finish A_f), the IHPC beams fractured at a force of 268N with a corresponding critical stress intensity factor of 12.17MN/m$^{3/2}$. The value of K_{IC} for IHPC at T2 was 189% over that of PV at T1.

The bending load versus crack length curve (see figure 4.12 page 47) revealed that at a temperature T1 (below the austenite start A_S) the notched PV beams showed a linear curve up to a force of 75N, afterwards the crack was unsteady and propagated at approximately constant bending load up to fracture. Results showed that at T1 the notched IHPC beams showed a linear curve up to a force of 225N, afterwards the crack was unsteady and propagated at a small increase of the bending load up to fracture. At a temperature T2 (of austenite finish A_f), the notched IHPC beams showed approximately a linear curve with a steady crack propagation up to a fracture load of 268N. Stability of the crack growth in the beam was a result of induced compressive recovery stress of the actuated Ni-Ti SMA.

The bending load versus deflection curves (see figure 4.13 page 47) showed that at temperature T2, within the loading range of 0-200N, the flexural stiffness EI of notched IHPC beams increased by 20% over that of the notched IHPC beams at temperature T1. Afterwards the flexural stiffness decreased towards that of IHPC beams at T1.The reason for the decrease of the flexural stiffness was softening along the SMA-matrix interface upon heating the Ni-Ti SMA.

Experimental results showed that actuation of the Ni-Ti SMA could generate a significant recovery stress. The recovery stress induced a compressive stress in the matrix that

increased the flexural stiffness and mode I stress intensity factor of the IHPC beam. The Ni-Ti SMA wire stiffened and enhanced healing of beam by retarding crack growth and recovery of strain. The stiffening of the IHPC beam was limited by the SMA-matrix interfacial debonding.

6.3 Analytical results

In chapter five analytical modeling was performed to determine the effect of actuated Ni-Ti SMA on the flexural stiffness of the un-notched IHPC beams. Theoretical values for bending load, strain response and the flexural stiffness EI of the beams at two temperature conditions T1 (below austenite start A_S) and T2 (of austenite finish A_f) were determined and plotted.

Results (see in figure 5.6 page 64) showed that as the Ni-Ti SMA wire is heated from a temperature of austenite start A_S (30 ºC) to the temperature of austenite finish A_f (46 ºC) the martensite fraction decreases. The martensite fraction decreases from 1 at 30 ºC to 0 at 46 ºC. This implies of course that in the heating process, the Ni-Ti SMA material undergoes phase transformation from martensite to austenite.

Results (see figure 5.7 page 64) showed that the recovery stress and force in the Ni-Ti SMA wire prestrained by 3% increased linearly with the increase of temperature between austenite start A_S and austenite finish A_f. The maximum stress of 81.3 MPa (force of 63.9N) was generated in the Ni-Ti SMA at austenite finish A_f temperature of 46ºC.

The bending force versus strain curves (see figure 5.8 page 65) showed that at temperature T1 the flexural stiffness EI of the PV beam was 7.81 Nm^2 and that of IHPC beam was 9.59 Nm^2. At temperature T2 the flexural stiffness of the IHPC beam was 8.27 Nm^2. The results showed that the flexural stiffness for IHPC beam increased by 7.1% at T2 over that of the PV beam at T1.

6.4 Comparison between experimental and analytical results

The bending force versus bending strain curves for experimental and analytical data were combined and compared. As can be seen in figures 6.1 and 6.2, at temperature T1 there was a close agreement between experimental and analytical results for the PV beams and the IHPC beams.

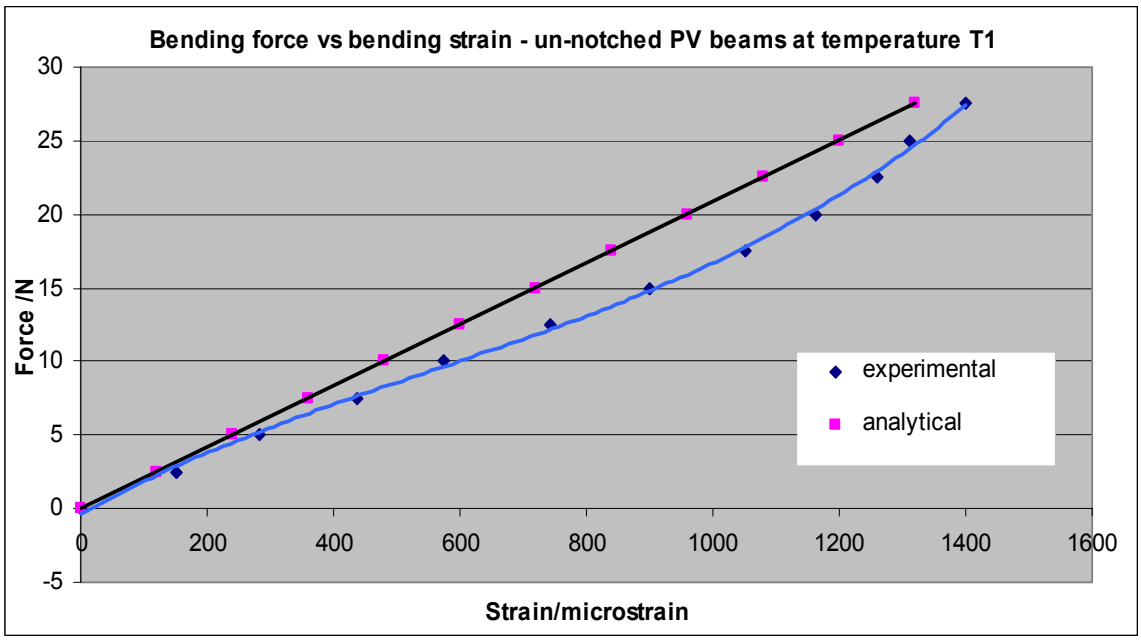

Figure 6.1: Bending force versus strain - PV beams at T1

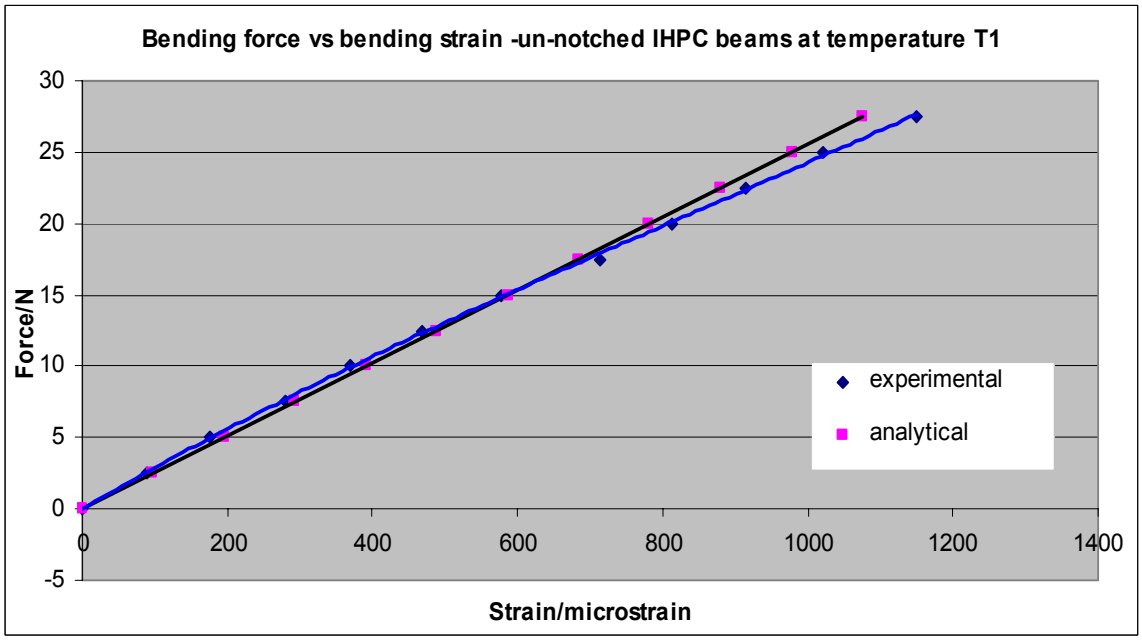

Figure 6.2: Bending force versus strain - IHPC beams at T1

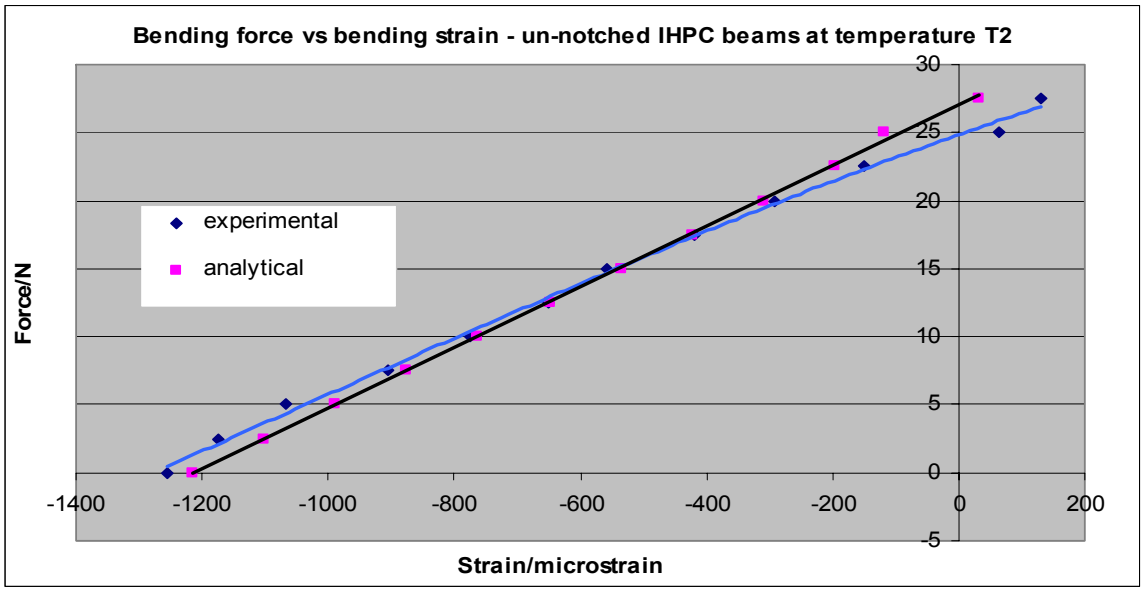

Figure 6.3: Bending force versus strain- IHPC beams at T2

Comparison between experimental and analytical results for the IHPC beams under four point loading at temperature T2 is shown in figure 6.3. Due to the matrix sensitivity to the temperature change, the heating of the Ni-Ti SMA wire started softening the epoxy matrix along the SMA-matrix interface. As a result, debonding initiated along the SMA-matrix interface, the experimental flexural stiffness of the IHPC beams at T2 was relatively lower than that of the analytical model at T2. Based on the experimental data, the effect of debonding in the analytical model was accounted for. In order for the analytical model to agree with experimental results, a bonding factor K_b = 0.8 was applied to equation 5.26 (see page 61). Analytical model agreed with experimental results. Comparison between experimental and analytical results is summarized in table 6.1.

Table 6.1: Comparison between experimental and analytical results-bending of un-notched IHPC and PV beams

	FLEXURAL STIFFNESS, EI (Nm^2)		
TYPE OF BEAM	EXPERIMENTAL	ANALYTICAL	Percentage error (%)
PV beams at room temperature T1< A_S	6.90	7.81	13.2
IHPC beams at room temperature T1< A_S	8.23	9.59	16.5
IHPC beams at elevated temperature T2= A_f	7.20	8.27	14.9

CHAPTER SEVEN

CONCLUSION AND RECOMMENDATIONS

7.1 Conclusion

In this thesis, an intelligent hybrid polymeric composite (IHPC) beam with healing ability was developed and tested. The IHPC beam developed consisted of a 3% prestrained 1mm diameter Ni-Ti shape memory alloy (SMA) actuator embedded in the polymeric host matrix. The function of the embedded Ni-Ti shape memory alloy was to enhance intelligence and healing ability to the IHPC beam. Upon application of electric current resistance heating, the Ni-Ti SMA actuator contracts as a result of Martensite → Austenite phase transformation of the Ni-Ti SMA. Contraction of the SMA in the IHPC beam was utilized to stiffen and enhance healing by retarding crack growth and recovery of the strain induced in the IHPC beam by applied load. Ability of the IHPC beam to retard crack growth and recovery of strain was experimentally quantified through determination of the flexural stiffness EI and mode I fracture stress intensity factor K_{IC} of the IHPC beam at elevated temperature T2 (austenite finish A_f) of the Ni-Ti SMA.

Ni-Ti SMA, 1mm diameter wire specimens were prepared. The specimens were heat treated to stabilize transformation temperatures. Transformation temperatures of the SMA (austenite start A_s and austenite finish A_f) were experimentally determined. Hybrid Polymeric beam specimens embedded with Ni-Ti SMA wires were manufactured in the laboratory.

A pullout test was performed to determine the matrix-SMA interfacial critical debonding load. The objective of the pullout test was to determine the strength of matrix-SMA interface of the manufactured IHPC beam. The critical load obtained was used as a guideline to set the maximum bending load in the bending test. The test was done at two temperature conditions, T1 and T2. The results showed that upon heating the Ni-Ti SMA, the pullout load at T2 decreased by 50% compared to the pullout load at T1.

A four point bending test was performed to determine the flexural stiffness EI of the un-notched intelligent hybrid polymeric composite (IHPC) beams and un-notched polymeric

virgin (PV) beams at the two temperature conditions, T1 and T2. The values of the flexural stiffness for the IHPC and PV beams were compared.

The results showed that actuation of the Ni-Ti SMA increased the flexural stiffness EI of the un-notched IHPC beams at elevated temperature T2 by 4.3% over the value of EI for the PV beams at temperature T1.

The four point bending test was performed to determine the mode I fracture stress intensity factor K_{IC} of the notched IHPC and PV beams at the two temperature conditions, T1 and T2. The values of the mode I fracture stress intensity factor were compared. The results showed that actuation of the Ni-Ti SMA increased the fracture stress intensity factor K_{IC} of IHPC beams at T2 by 41% over the value of K_{IC} for IHPC beams at T1. The fracture stress intensity factor K_{IC} of IHPC beams at T2 was 189% over that of PV beams at T1.

An analytical model was used to compare with experimental results for un-notched IHPC and PV beams. The Lin and Rogers (1991) model equation was applied to predict the martensite volume fraction in the Ni-Ti SMA as a function of temperature. The Brinson (1993) model was applied to formulate a constitutive relation for recovery stress and force generated in the Ni-Ti SMA. Equations for the bending strain and the flexural stiffness of un-notched IHPC and PV beams as functions of temperature were developed.

A comparison between experimental and analytical results on the bending load versus strain was done. Results showed good agreement for un-notched IHPC and PV beams at T1. For the un-notched IHPC beam at T2, the experimental flexural stiffness EI was relatively lower than the value of EI determined based on the analytical model. This was contributed by softening and debonding of the SMA-matrix interface upon heating the Ni-Ti SMA wire. For the analytical model to agree with experimental results, the effect of heating the Ni-Ti SMA wire from T1 to T2 on the analytical model was taken into account. A bonding factor K_b =0.8 was introduced to the analytical bending strain equation in order to improve analytical results accuracy.

Results obtained in this thesis have shown that application of embedded Ni-Ti SMA actuator in the hybrid polymeric composite host matrix could enhance intelligence and healing ability to the IHPC beam. Upon heating the Ni-Ti SMA, the IHPC beam with the embedded Ni-Ti SMA actuator was able to contract as a result of Martensite-Austenite phase transformation of the Ni-Ti SMA. Contraction of the embedded Ni-Ti SMA stiffened the IHPC beam, enhanced healing by retarding crack growth and recovery of strain induced by applied load.

Throughout this work, measures were taken to reduce debonding of the SMA – matrix interface. These include predetermining the pullout load, intermittent heating of the Ni-Ti SMA wire and selecting the Ni-Ti SMA with actuation austenite finish temperature (A_f) below the glass transition temperature T_g of the polymeric host matrix. However interfacial debonding to some extent remained as the challenge to this work.

Results obtained in this thesis promise that application of Ni-Ti shape memory alloy can improve in-service safety and reliability of the hybrid polymeric composite structures.

7.2 Recommendations

In this thesis comparison between experimental and analytical work showed that heating the Ni-Ti SMA wire from the temperature $T1<A_S$ to $T2 = A_f$ degraded the SMA-matrix interfacial strength. In future, more work is needed to develop a constitutive relation on the variation of the bonding factor K_b with other variables such as the martensite volume fraction and the actuation temperature in the interval $A_S <T<A_f$.

Actuation of the shape memory alloy by heating can be detrimental to the composite matrix and to the SMA-matrix interface. This is due to the temperature changes and resulting stresses in the composite material. More research is required to overcome this by either choosing the shape memory alloy (SMA) with appropriate composition or prior heat treatment so that the resulting SMA actuator can be transformed to the austenite state at a lower temperature.

The size of the Ni-Ti SMA wire used throughout this research was 1mm in diameter. In future, work should be done on how the size (diameter), number of wires and the orientation of the wires in the matrix can improve the flexural stiffness and ability to retard crack growth in the hybrid polymeric composite beam.

For all experiments performed, the bending load applied on the beam specimens was a static load. In future work, investigation on healing of the hybrid polymeric composite beam using shape memory alloy should be extended to dynamic/fatigue load.

There is a need to investigate the use of Ni-Ti SMA for healing other polymeric composites that can provide better adhesive forces along the SMA-matrix interface than polyurethane epoxy (60D). The better adhesiveness along the SMA-matrix interface will provide improved bonding and healing.

LIST OF REFERENCES

1. Auricchio, F, Marfia, S and Sacco, E, 2003
Modelling of SMA materials: training and two way memory effects
Computers and Structures 81 2301-2317

2 Bhattacharyya, A. & Lagoudas, D.C 1997
A stochastic thermodynamic model for the gradual thermal transformation of SMA polycrystals, Journal of *Solids and Structures,* 6, pp. 235-250.

3. Baz, A, Tampe L, 1989, Active control of buckling of flexible beams.
Proc. Of ASME, Design Technical conference, Montreal, Canada, page 211-8.

4. Bleay, SM, Loader, CB, Hawyes, VJ, Humberstone, L and Curtis, PT, 2001.
A smart repair system for polymer matrix composites. *Composites A*. 32 1767-1776

5. Brinson, LC and Huang, MS, 1996
Simplifications and comparisons of shape memory alloy constitutive models
Journal of Intelligent materials Syst. Structures 7 104-14

6. Brinson, LC, 1993
One dimensional constitutive behaviour of shape memory alloys: thermo mechanical derivation with non-constant material functions *Journal of Intelligent materials Syst. Structures* 4 229-42.

7. Burton, DS, Gao, X and Brinson, LC, 2006.
Finite element simulation of self-healing shape memory alloy composite
Mechanics of Materials 38 525-537

8. Chen X, Dam, MA, Ono, K Mal, AK, Shen, H, Nutt, SR, Sheran K and Wudl, F, 2002
A. Thermally Remendable Cross-Linked Polymeric composites.
Material Science 295 (5560) 1698-1702.

9. Chen, LP and Si, NC, 2006
Influence of thermo mechanical training deformations on TWSME in Ni-Ti-Cu alloy spring. *Journal of Alloys and Compounds* XXX XXX-XXX

10. Derek A Hebda and Scott R White, 1995.
Effect of training conditions and extended thermal cycling on nitinol two-way shape memory behavior, *Smart Materials and Structures* Vol.4 No4 298-304

11 Eggeler, G, Khalil-Allafi, J, Gollertham, S, Somsen, C, Schmahl, WS and Sheptyakov, D, 2005. On the effect of aging on martensitic transformations in Ni-rich NiTi shape Memory alloys, *Smart Materials and Structures*, Vol. 14 No5 S186.

12 Gao, YC, 1988
Fracture of fiber-reiforced materials
Journal of Applied Mathematics and Physics (ZAMP) 39:551-72

13. Hayes, SA, Jones, FR, Marhiya, K, Zhang, W, 2005
Self-healing Composite Materials. *Proc. 15th Int. Conference on Composite Materials*, Durban, south Africa, 27-June- 01-July2005.

14. Huang, W 1998,
Effects of internal stress and martensite variants on phase transformation of Ni-Ti shape memory alloy. *Journal of Material Science Letter* 17 1843-4

15. Jackson,CM, 1972
55-Nitinol-the alloy with a memory: its physical metallurgical properties and applications. NASA-SP5110

16. Kessler, MR, Sottos, NR and White, SR,2003. Self healing structural composite materials Composites Part A: *Applied Science and Manufacturing* Vol. 34,Issue 8, 743-753

17. Khalil-Allafi, J, Schmahl, WW and T-Reinecke, 2005. Order parameter evolution and random free energy coefficients for the B2---R-phase transition in NiTi shape memory alloy, *Smart Materials and Structures*, Vol. 14 No5 S192

18. Lagoudas, DC and Tadjbakhsh, IG, 1993.
Deformation of active flexible rods with embedded line actuators.
Smart Materials and Structures 2 71-81

19. Lahoz,R and Puertolas, JA, 2004
Training and two–way shape memory effect in Ni-Ti alloys: influence on thermo parameters. *Journal of Alloys and Compounds* 381 130-136

20. Lee, JY, Buxton, GA, and Balazs, AC, 2004
Using nano particles to create self healing composites *JCHEM PHYS* 121 (11) 5533-5540

21. Liang, C, Rogers, CA, 1990
One dimensional thermomechanical constitutive relations for shape memory material, *Journal of Intelligent materials and Structures* 20 207-34

22. Lin, MW and Rogers, CA. 1991,
Analysis of the stress distribution in a shape memory alloy composite beam.
AIAA/ASME/ASCE/AHS/ASC 32nd Structures, *Structural dynamics and materials* Conference, AIAA-91-1164-CP, 8-10 April Baltimore: Maryland, page 169-77.

23. Lin, Y, Favier, D and Orgeas, L, 2005. Mechanistic simulation of martensite reorientation deformation of polycrystalline NiTi Shape memory alloy, *Smart Materials and Structures*, Vol. 14 No5 S207

24. Lu, ZK and Weng, GJ, 1997
Martensitic transformation and stress-strain relations of shape memory alloys.
Journal of Solids 45 1905-28

25. Michaud, V, 2004.
Can shape memory alloy composites be smart?
Scripta Materialia 50 249-253

26 Miller, DA, Lagoudas, DC, 2001.
Influence of cold work and heat treatment on the shape memory effect and plastic strain development of Ni-Ti, *Material Science and Engineering A* 308 161-175

27 Mukhawana, MD, 2005
Effects of thermo- mechanical cycling and aging on quasi-plastic material response exhibited by Ni-Ti shapory alloys. (M Tech Thesis)

28. Muller, I and Seelecke, S, 2001. Analysis, Modeling and simulation of Multi scale problems. *Math. & Comp. Modeling*,34, Pergamon Press, Oxford, New York

29. Muthumani, K 2002,
Structural Application of Smart Materials.
Smart Materials Bulletin Vol. 2002 11 10-12

30. Name, T-H, Park, S-M, Kim, T-Y and Kim, Y-W, 2005.
Microstructures and shape memory characteristics of Ti-25Cu (%) alloy ribbons.
Smart Materials and Structures, Vol. 14 No5 S239

31. Nemat-Nasser, S, and Wei-Guo Guo, 2006.
Super elastic and cyclic response of NiTi SMA at various strain rates and temperatures. *Mechanics of Materials* 38 463-474

32. Philander, O, 2004
The Development of a Computational Design Tool for uses in the design of Actuator Systems consisting of NiTi Shape Memory Alloy Wires Harnessing the Shape Memory Effect. (D.Tech Thesis).

33. Poon, C-K, Lau, K-T, and Zhu, L-M, 2005.
Design of pull-out stresses for prestrained SMA wire/polymer hybrid composites *Composites: Part B* 36 25-31

34. Poon, C-K, Zhou, L-M, Jin, W and Shi, S-Q, 2005. Lecture notes on interfacial debond of shape memory alloy composites, *Smart Materials and Structures*, Vol.14 No4, N29.

35. Rustighi, E, Brennan, MJ, and Mace, BR, 2005.
A shape memory alloy adaptive tuned vibration absorber: Design and implementation *Smart Material and Structures* 14 19-28

36. Shimamoto, A, Furuya, Y and Taya, M, 1997.
Active control of crack-tip stress intensity by contraction of shape memory TiNi fibers embedded in epoxy matrix composite. *Smart Materials and Structures*.

37. Shimamoto, A, Zhao, HY and Abe, H, 2004.
Fatigue crack propagation and local crack tip strain behaviour in NiTi shape memory fiber reinforced composite, *International Journal of fatigue* 26 533-542

38 Tanaka, K, 1986.
A thermo mechanical sketch of shape memory effect: one - dimensional tensile behaviour, *Res.Mech*. 18 251-63

39. Thompson, SP and Loughlan, J 2000,
The control of the post buckling response in thin composites using smart technology.Thin Walled Structures 36 4 231-63.

40. Thompson, SP, Loughlan, J, 2001
Enhancing the post-buckling response of a composite panel structure utilising shape memory alloy actuators- a smart structural concept *Composite Structures,* 51 21-36

41 Trask, RS and Bond, IP, 2006.
Biomimetic self –healing of advanced composite structures
Smart Materials and Structures 15 704-710

42. Tsoi, KA, Schrootenand, J and Stalmans, R, 2003.
Part I: Thermo mechanical characteristics of shape memory alloys
Material Science and Engineering A 368 286-298

43. Tsoi, KA, Stalmans, R and Schrooten, J, 2002.
Transformation behaviour of constrained shape memory alloys
Acta Materialia 50 3535-3544

44. Umezaki, E, 2000
Improvement in separation of SMA from matrix in SMA embedded structures.
Materials Science and Engineering A 285 363-369.

45. Wang, X and Hu, G, 2004.
Stress Transfer for an SMA fiber pullout from an elastic matrix and related bridging Effect, *Composites: Part A* 36 1142-1151

46. Wenyi yan, Chun Hui Wang, Xin Ping Zhang and Yin-Wing Mai, 2002. Effect of transformation volume contraction on the toughness of super elastic shape memory alloys (SMA), *Smart Materials and Structures*, Vol. 11, No6 947-987.

47 Wenyi Yan, Chun Hui Wang, Xin Ping Zhang and Yin-Wing Mai, 2003. Theoretical modeling of the effect of plasticity on reverse transformation in super elastic shape memory alloys. *Material Science and Engineering* A 354 146-157.

48. Yang, D, 2000.
Shape memory alloy and hybrid composites advanced materials for the 21st Century, *Materials and Design* 21 503-505

49. Zako, M and Takano, N, 1999.
Intelligent material systems using epoxy particles to repair microcracks and delamination damage in GFRP, *J Int. Mat. Sys. & Struc.*10 (10)836-841

50 Zheng, YJ, Cui, LS and Schrooten , J, 2004.
Basic design guidelines for SMA/epoxy smart composites
Material Science and Engineering A 390 139-143

LIST OF BIBLIOGRAPHY

1 Anderson, TL 1995.
Fracture Mechanics. Fundamentals and Applications. Second edition
CRC Press LLC-USA , page 419 - 445.

2 Boresi, Arthur P and Schmidt, Richard J, 2003.
Advanced Mechanics of Materials, sixth edition USA, John Wiley & Sons,
page 608 - 664.

3 Broek, D, 1986.
Elementary Engineering Fracture Mechanics, fourth revised edition,
Kluwer Academic Publishers, Dordrecht, page 179 -181.

4 Collister, William D jr, 2003.
Material Science and Engineering, an introduction, sixth edition.
USA, John Wiley & Sons, page 451- 566.

5 Crane, FAA and Charles, JA, 1984.
Selection and use of Engineering Materials , Letchworths-Herts,
Butter worths, page 54 – 80.

6 Francois, D Pineau, A and Zaoui, A, 1998.
Mechanical Behaviour of Materials, Volume1.Netherlands, Kluwer Academic
Publishers, page 122 -127.

7 Han, Patricia, 1992.
Tensile testing, ASM International, page 33 - 40.

8 Hannah, RL, Reed, SE, 1982
Strain gage users' hand book, Elsevier Science Publishers Ltd. and Society for
Experimental Mechanics page 13 -22.

9 Hearn, EJ, 1997
Mechanics of Materials 2, Third Edition
ButterWorth-Heinemann

10 Iremonger, MJ, 1982
BASIC stress analysis, Butterworth &Co. (Publishers) Ltd, page 55 - 65.

11 Johnson, W, 1972
Impact Strength of Materials, Edward Arnold (Publishers) Limited, UK,
page 250-280.

12 Measurements Group, 1982
TECH NOTE
Calibration of Photoelastic Plastics for Two and Three – Dimensional Modal
Analysis- TN705 – page 5
Measurements Group, INC
Raleigh, North Carolina 27611, USA

13 Mike Ashby and Kara Johnson, 2000.
Materials and Design. The Art and Science of Material selection in product design.
Butterworth Heinemann-UK, page 177-178.

APPENDIX A

Experimental results

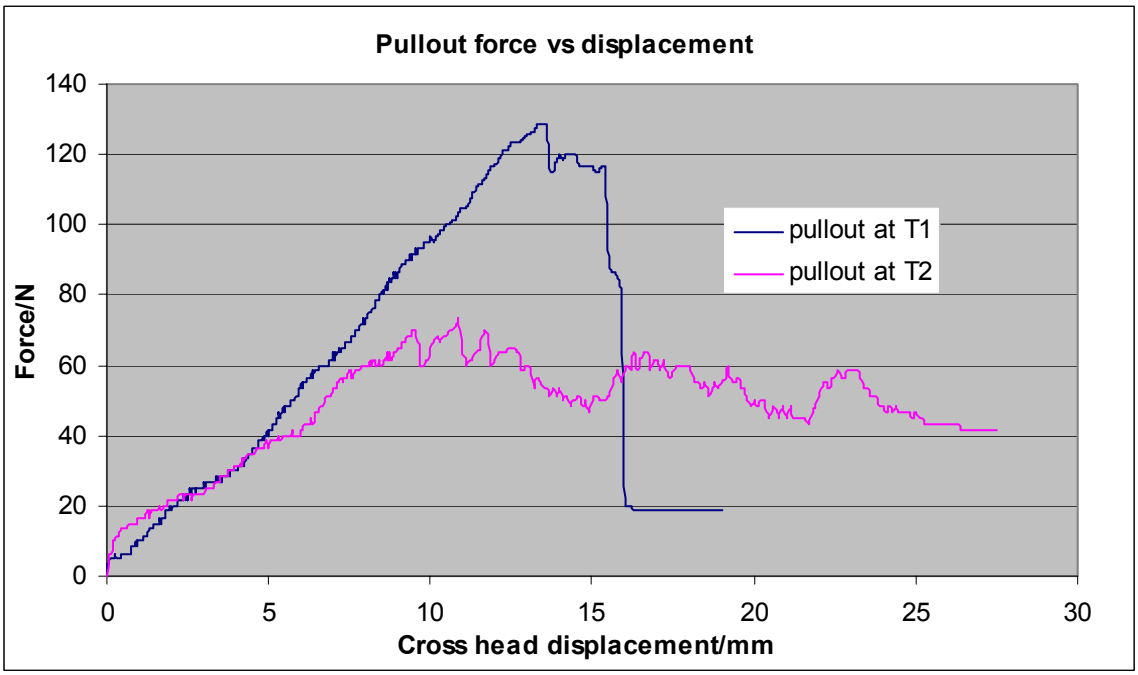

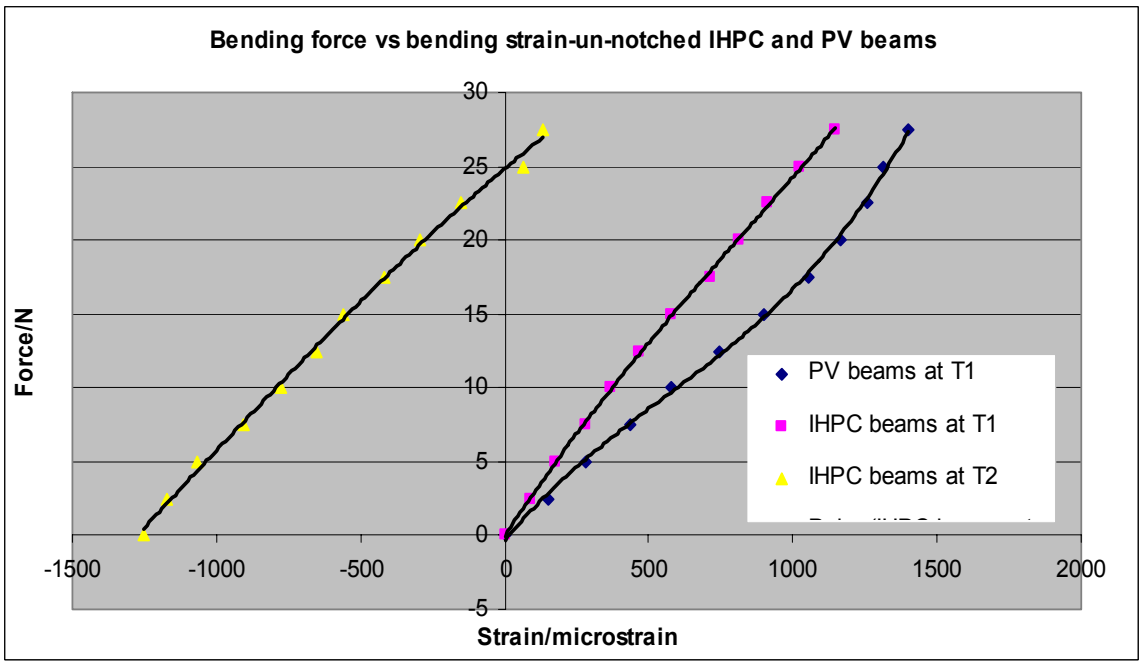

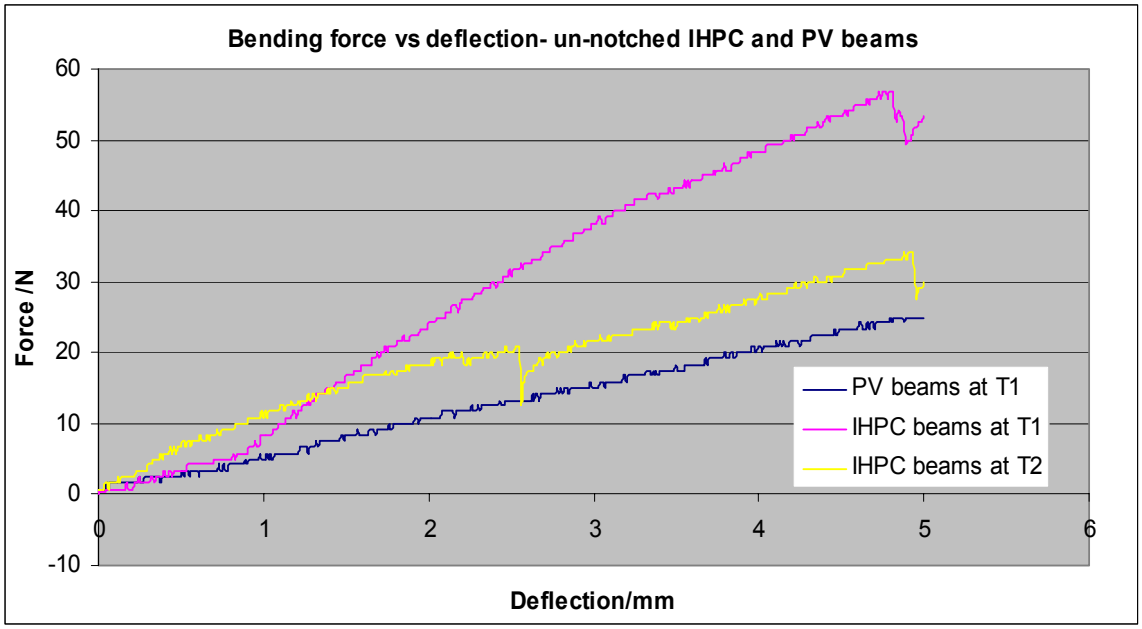
Bending force vs deflection- un-notched IHPC and PV beams
Force /N
Deflection/mm
PV beams at T1
IHPC beams at T1
IHPC beams at T2
60
50
40
30
20
10
0
-10
0
1
2
3
4
5
6

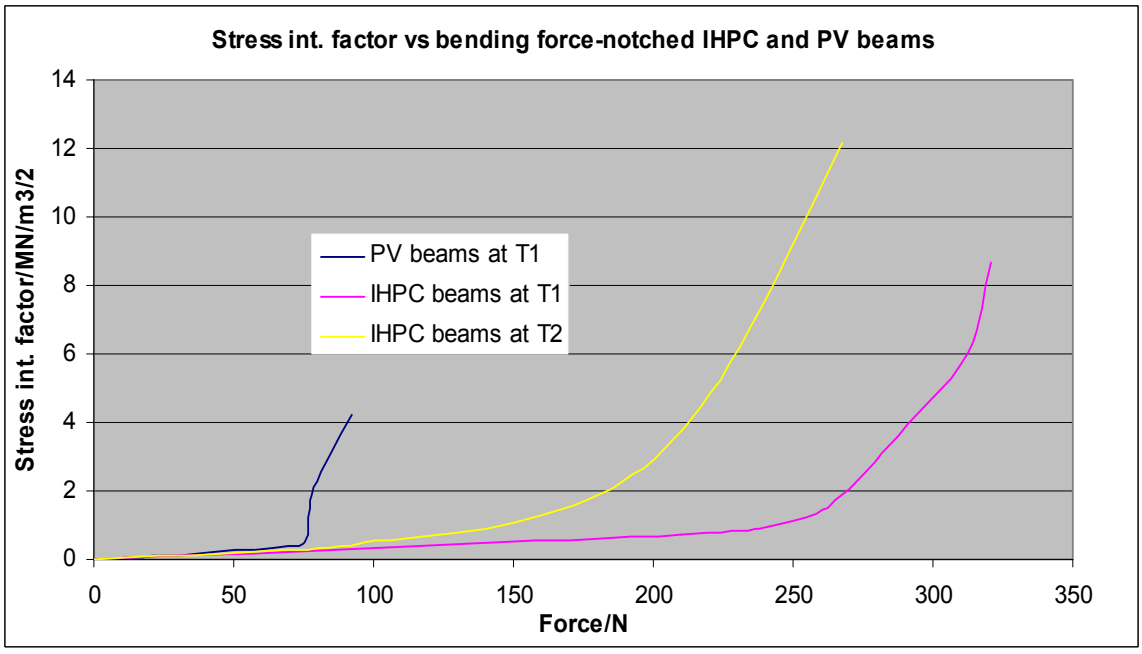
Stress int. factor vs bending force-notched IHPC and PV beams
Stress int. factor/MN/m3/2
Force/N
PV beams at T1
IHPC beams at T1
IHPC beams at T2
14
12
10
8
6
4
2
0
0
50
100
150
200
250
300
350

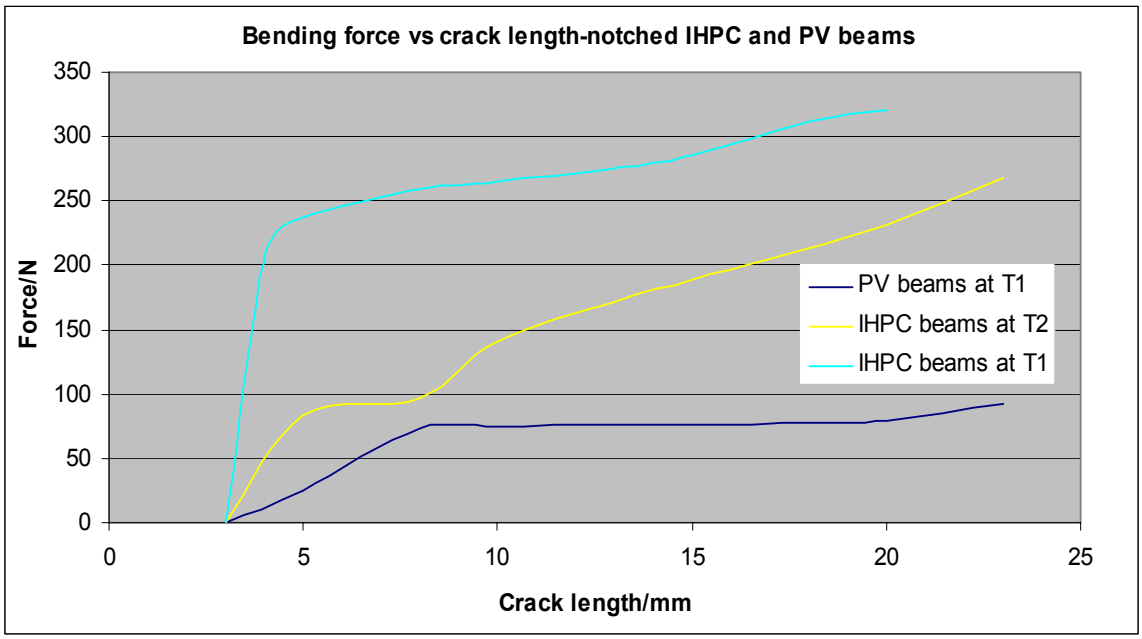
Bending force vs crack length-notched IHPC and PV beams
Force/N
350
300
250
200
150
100
50
0
0
5
10
15
20
25
Crack length/mm
PV beams at T1
IHPC beams at T2
IHPC beams at T1

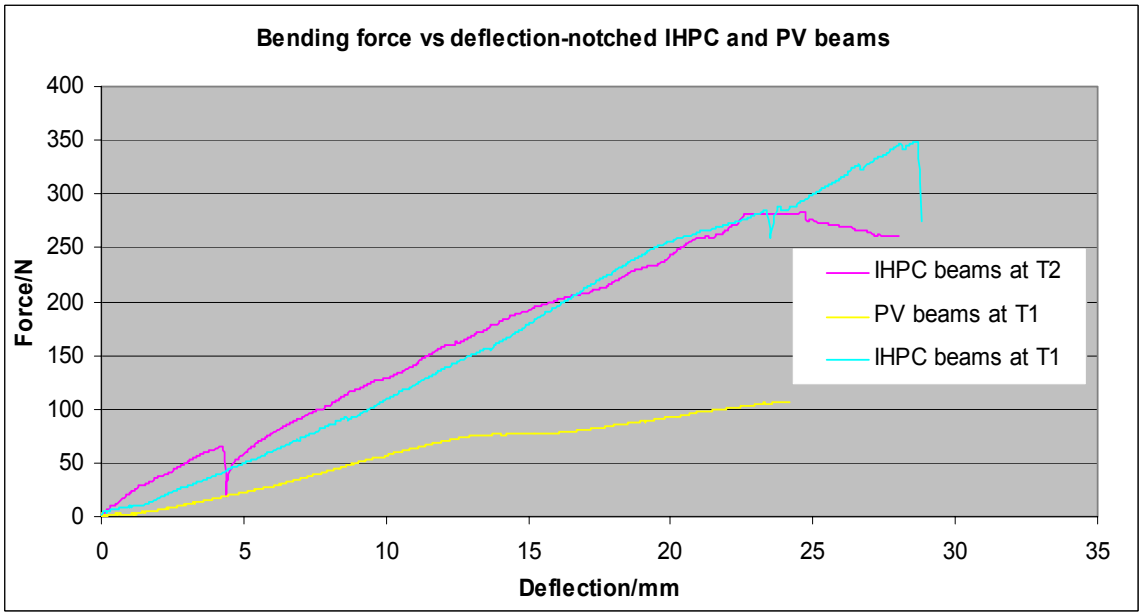
Bending force vs deflection-notched IHPC and PV beams
Force/N
400
350
300
250
200
150
100
50
0
0
5
10
15
20
25
30
35
Deflection/mm
IHPC beams at T2
PV beams at T1
IHPC beams at T1

APPENDIX B

Analytical results

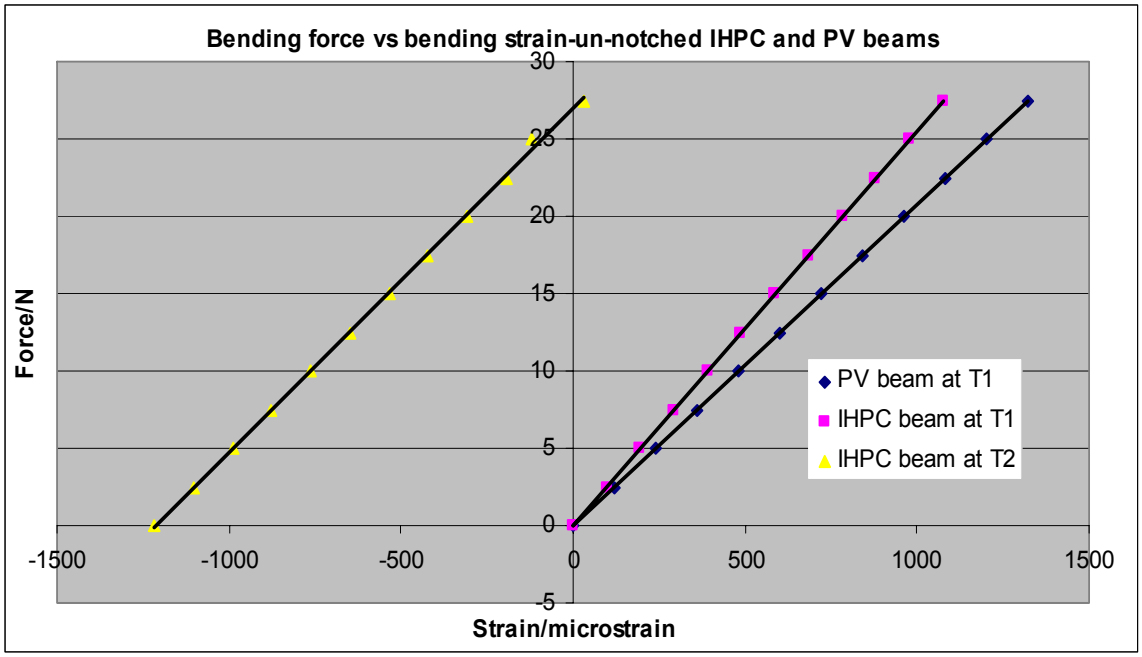

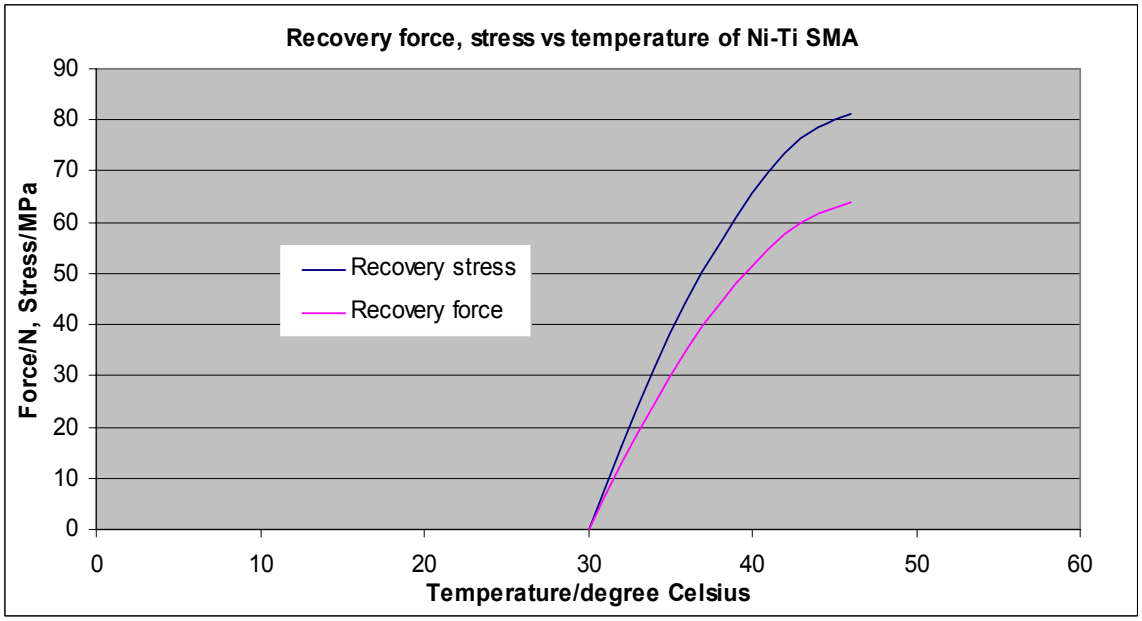

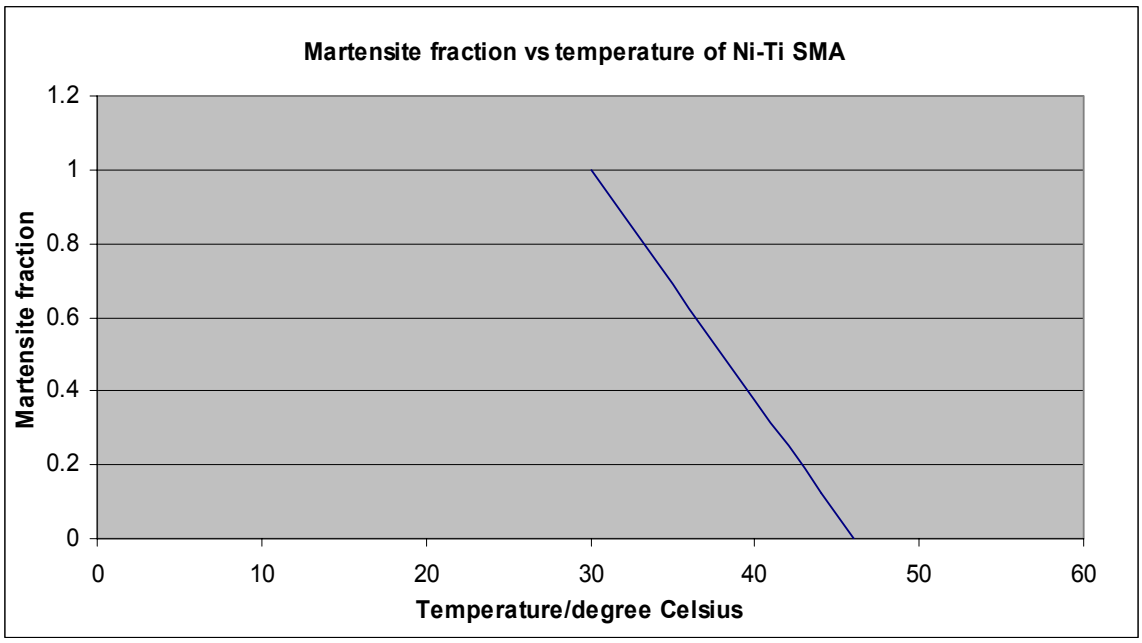
Martensite fraction vs temperature of Ni-Ti SMA
Martensite fraction
1.2
1
0.8
0.6
0.4
0.2
0
0
10
20
30
40
50
60
Temperature/degree Celsius

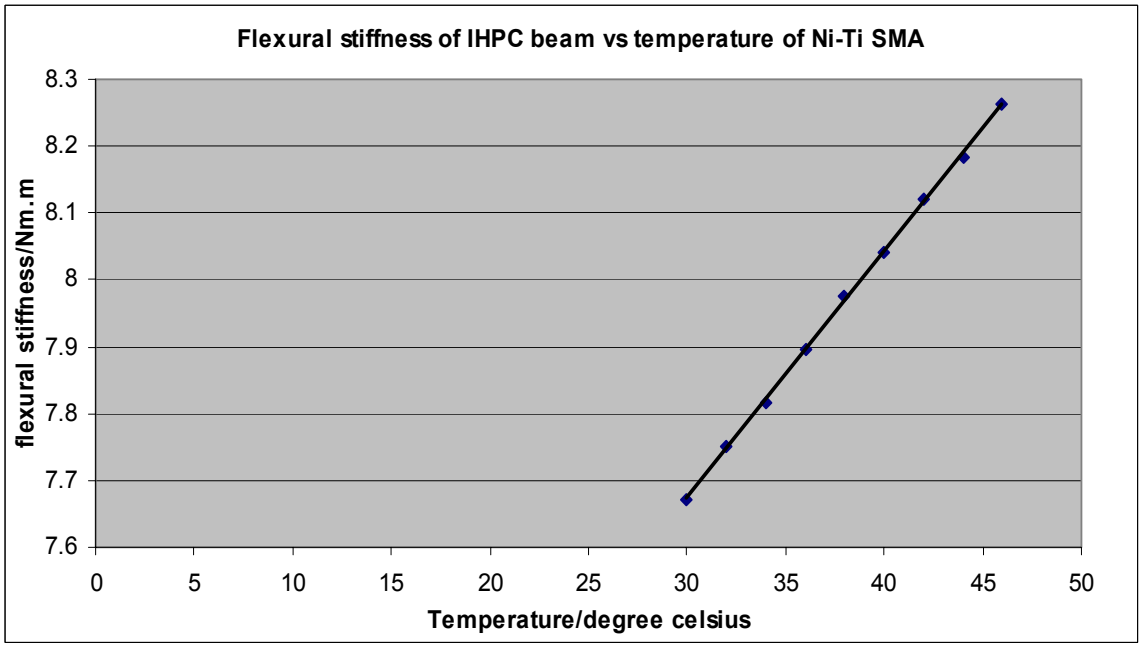
Flexural stiffness of IHPC beam vs temperature of Ni-Ti SMA
flexural stiffness/Nm.m
8.3
8.2
8.1
8
7.9
7.8
7.7
7.6
0
5
10
15
20
25
30
35
40
45
50
Temperature/degree celsius

APPENDIX C

Comparison between experimental and analytical results for un-notched IHPC and PV beams

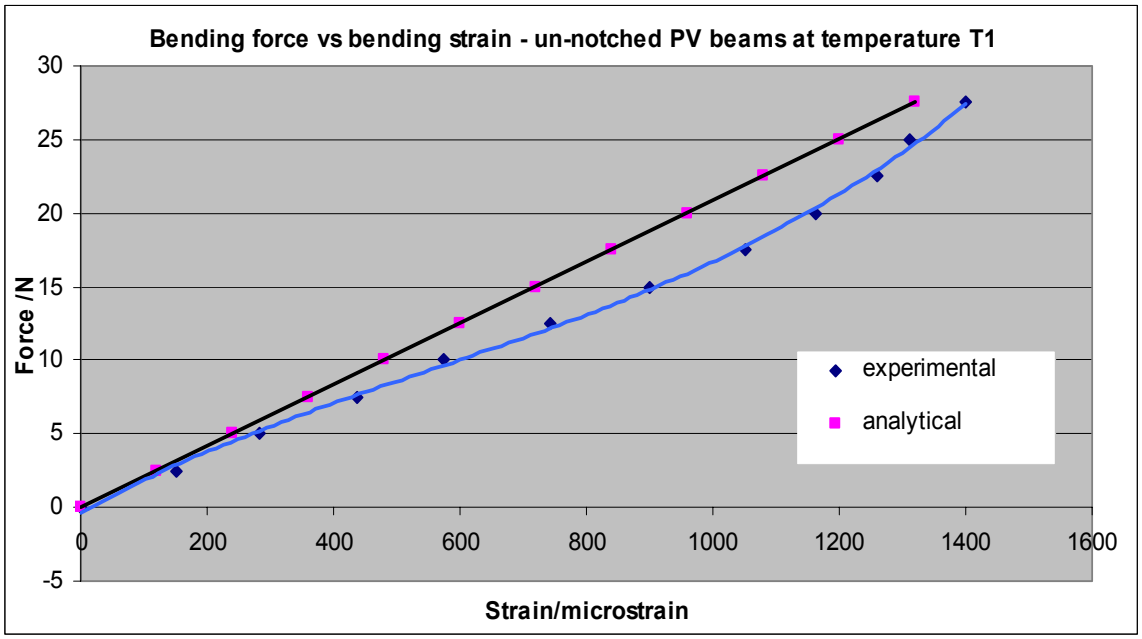

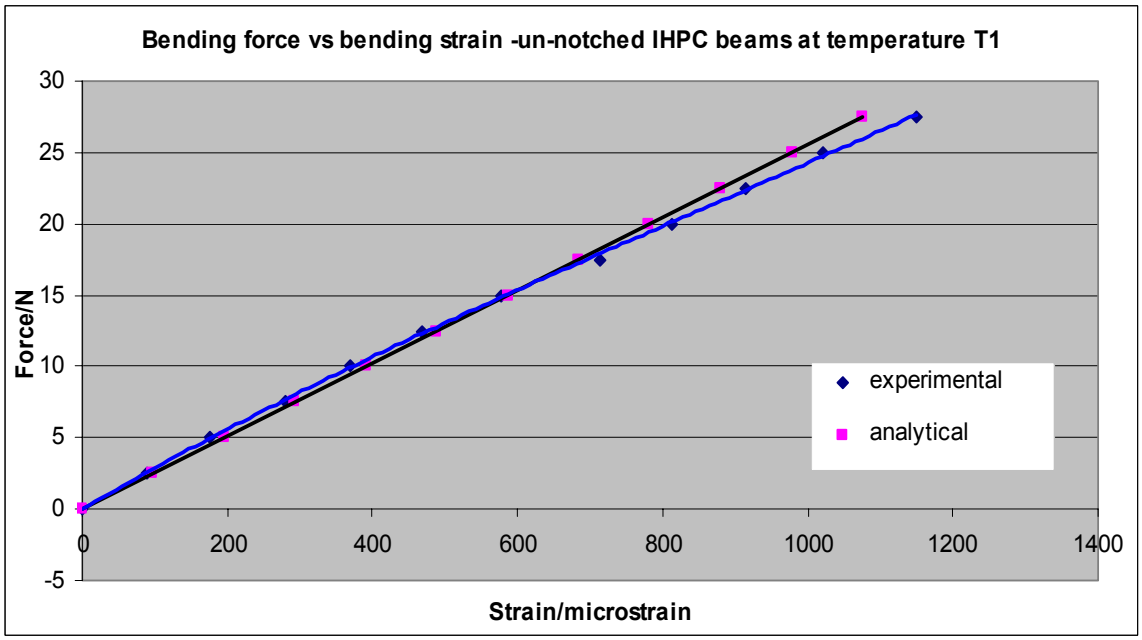

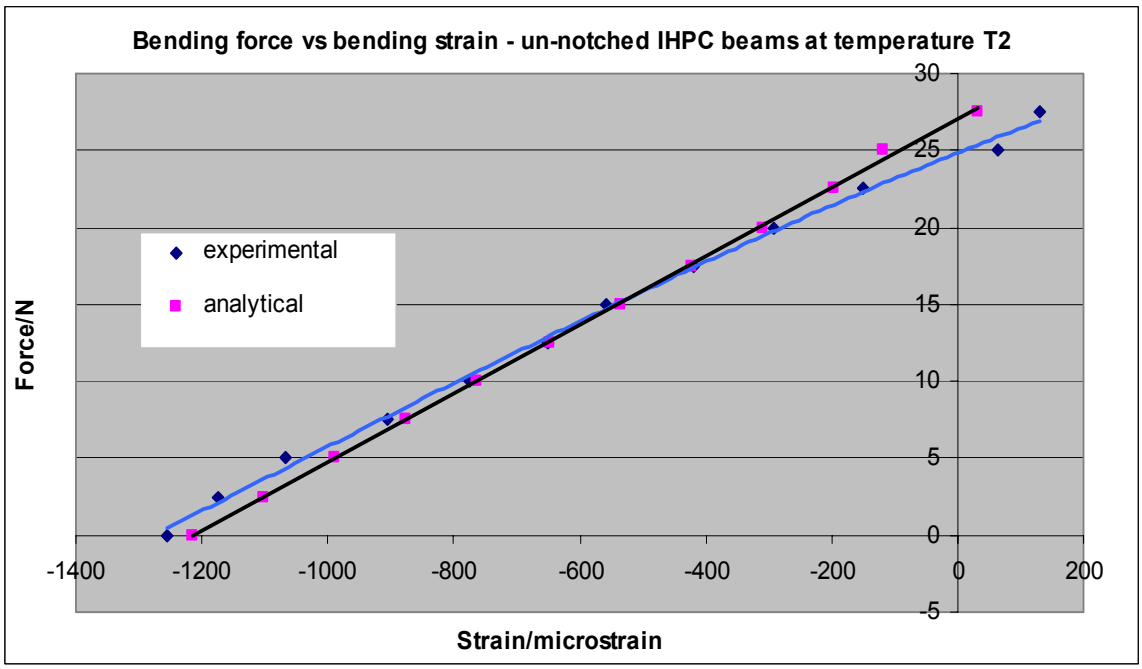
Bending force vs bending strain - un-notched IHPC beams at temperature T2
Force/N
Strain/microstrain
experimental
analytical
30
25
20
15
10
5
0
-5
-1400
-1200
-1000
-800
-600
-400
-200
0
200

APPENDIX D

C++ Program for analytical computation

D.1 Martensite fraction, Young's modulus of SMA, recovery stress and force in SMA as functions of temperature

```
// C++program: martensite fraction, stress and force generated in SMA
// Author: w m mwita, stud no. 206212089
// Date: 01-November-2007
#include <cstdlib>
#include <iostream>
#include "matrix.h"
#include <math.h>
#define SWAP(p,q) {dum=(p)=(q); (q)=dum;}
using namespace std;
int main(int argc, char *argv[])

{
   // Declare the variables
   int i;
   float initial_strain, max_strain;
   float M_initialtwinfraction,M_twinfraction, M_fraction;
   float A_start, A_finish;
   float E_sma, E_austenite, E_martensite;
   float force_sma, sum,stress_sma , wire_radius,temp;

   // Assign  values for austenite and martensite Young's Modulus
    E_austenite=16.0e09;
    E_martensite=11.5e09;

    // Assign prestraining properties of SMA
    initial_strain=0.03;
    max_strain=0.08;
    wire_radius=0.0005;
   // Assign austenite transformation temperatures of SMA
```

```
    A_start=30;
    A_finish=46;

    // Calculate martensite fraction, stress and force generated in SMA.
  M_initialtwinfraction=initial_strain/max_strain;
  cout<<"  "<<"Temp(C)"<<"    "<<"M_fraction"<<"   "<< "M_twinfraction" <<"
"<<"E_sma"<<"   "<<"Stress_sma(Pa)"<<"    "<<"Force_sma(N)"<<"\n";
  cout<<"\n ";

   temp=30,sum=0;
  for(i=1;i<=9;i++)
  {
    M_fraction=1-(temp- A_start)/(A_finish-A_start);
    M_twinfraction=M_initialtwinfraction*M_fraction;
    E_sma=E_austenite+M_fraction*(E_martensite-E_austenite);
    stress_sma=initial_strain*E_sma*M_twinfraction/8;
    sum=sum+stress_sma;
    stress_sma=sum;
    force_sma=stress_sma*3.14*wire_radius*wire_radius;

    cout<<"  "<<temp<<"   "<<M_fraction<<"   "<< M_twinfraction <<"    "<<E_sma<<"
"<<stress_sma<<"   "<<force_sma<<"\n";
    temp=temp+2;

  }
  cout<<"\n ";

 system("PAUSE");
return EXIT_SUCCESS;
}
```

----------END OF PROGRAM----------

D.2 Bending moment, flexural stiffness, stress and strain in IHPC and PV beams

```
// C++program: bending moment, flexural stiffness, stress and strain for IHPC and PV beams
// Author: w m mwita, stud no. 206212089
// Date: 01-November-2007

#include <cstdlib>
#include <iostream>
#include "matrix.h"
#include <math.h>
#define SWAP(p,q) {dum=(p)=(q); (q)=dum;}
using namespace std;
int main(int argc, char *argv[])

{
   // Declare the variables
   int i,j,k;
   float M_fraction;
   float A_start, A_finish,bond_factor;
   float E_sma, E_austenite, E_martensite,E_matrix,E_composite;
   float force_sma, force_applied,stress_sma , wire_radius,temp;
   float moment_bend, stress_bend, strain_bend,fs;
   float I,B,H,a,h,y,L;

   // Declare volume fractions of sma wire and epoxy matrix
   float V_sma,V_matrix;
   // Assign values for volume fractions
   V_sma=12.56e-3; V_matrix=987.44e-3;

   // Assign initial values for Young's Modulus
    E_austenite=16.0e9;
    E_martensite=11.5e9;
    E_matrix=0.60e9;
    wire_radius=0.0005;
    bond_factor=0.8;
   // Assign austenite transformation temperatures of Ni-Ti SMA
    A_start=30;
    A_finish=46;
```

```
    // Assign loading dimensions
    a=0.030;
    h=0.007;
    y=0.0125;
    L=0.090;
    // Assign beam sectional properties
    B=0.010;
    H=0.025;
    //Compute sectional second moment of area I
    I=B*H*H*H/12;

    // calculate bending, moment,stress, and strain at loading  points
  cout<<"POLYMERIC VIRGIN (PV) BEAM  AT ROOM TEMPERATURE-27 CELCIUS
"<<"\n";

  cout<<"force_applied"<<"  "<<"moment_bend"<<"  "<<"stress_bend"<<"
"<<"strain_bend"<<"  "<<"\n";
   force_applied=0;
          for(k=1;k<=12;k++)
         {
           moment_bend=force_applied*a;
           stress_bend=moment_bend*y/I;
           strain_bend=stress_bend/E_matrix;

           cout<<"   "<<force_applied<<"   "<<moment_bend<<"   "<<stress_bend<<"
"<<strain_bend<<"   "<<"\n";
        force_applied=force_applied+2.5;
         }
           cout<<"\n";

           fs=E_matrix*I;
  cout<<"flexural stiffness for the virgin beam is "<<fs<<"\n";
  cout<<"\n";

  cout<<" IHPC BEAM AT ROOM TEMPERATURE-27 CELCIUS"<<"\n";
  cout<<"force_applied"<<"  "<<"moment_bend"<<"  "<<"stress_bend"<<"
"<<"strain_bend"<<"  "<<"\n";
```

```
  force_applied=0;
  E_composite=E_martensite*V_sma+E_matrix*V_matrix;
        for(k=1;k<=12;k++)
        {
         moment_bend=force_applied*a;
         stress_bend=moment_bend*y/I;
         strain_bend=stress_bend/E_composite;
         cout<<"   "<<force_applied<<"   "<<moment_bend<<"   "<<stress_bend<<"
"<<strain_bend<<"   "<<"\n";
         force_applied=force_applied+2.5;
        }
         cout<<"\n";
         fs=E_composite*I;
        cout<<"flexural stiffness for the composite beam is "<<fs<<"\n";
         cout<<"\n";

  cout<<" IHPC BEAM AT ELEVATED TEMPERATURE-46 CELCIUS"<<"\n";
  temp=46;

   cout<<"force_applied"<<"  "<<"moment_bend"<<"  "<<"stress_bend"<<"
"<<"strain_bend"<<"  "<<"\n";
   cout<<"\n";
   M_fraction=1-(temp- A_start)/(A_finish-A_start);
   E_sma=E_austenite+M_fraction*(E_martensite-E_austenite);

  force_sma=63.9;
  E_composite=bond_factor*(E_sma*V_sma+E_matrix*V_matrix);

        force_applied=0;
        for(j=1;j<=12;j++)
        {
         moment_bend=force_applied*a-force_sma*h*(1+bond_factor);
         stress_bend=moment_bend*y/I;
         strain_bend=stress_bend/E_composite;
         cout<<"  "<<force_applied<<"  "<<moment_bend<<"  "<<stress_bend<<"
"<<strain_bend<<"  "<<"\n";
```

```
            force_applied=force_applied+2.5;
            cout<<"\n";
          }
         cout<<"\n";
         fs=E_composite*I;
         cout<<"flexural stiffness for the composite beam is "<<fs<<"\n";
         cout<<"\n";
 system("PAUSE");
return EXIT_SUCCESS;
}
```

----------END OF PROGRAM----------

D.3 C++ program output for analytical computation

```
 Temp(C)   M_fraction   M_twinfraction   E_sma   Stress_sma(Pa)   Force_sma (N)

  30   1   0.375   1.15e+010   1.61719e+007   12.6949
 32   0.875   0.328125   1.20625e+010   3.10144e+007   24.3463
 34   0.75   0.28125   1.2625e+010   4.43298e+007   34.7989
 36   0.625   0.234375   1.31875e+010   5.59204e+007   43.8975
 38   0.5   0.1875   1.375e+010   6.55884e+007   51.4869
 40   0.375   0.140625   1.43125e+010   7.3136e+007   57.4118
 42   0.25   0.09375   1.4875e+010   7.83655e+007   61.5169
 44   0.125   0.046875   1.54375e+010   8.10791e+007   63.6471
 46   0   0   1.6e+010   8.10791e+007   63.6471

 Press any key to continue . . .

POLYMERIC VIRGIN (PV) BEAM AT ROOM TEMPERATURE-27 CELCIUS
force_applied  moment_bend  stress_bend  strain_bend
  0   0   0   0
  2.5   0.075   72000   0.00012
  5   0.15   144000   0.00024
  7.5   0.225   216000   0.00036
  10   0.3   288000   0.00048
  12.5   0.375   360000   0.0006
  15   0.45   432000   0.00072
  17.5   0.525   504000   0.00084
  20   0.6   576000   0.00096
  22.5   0.675   648000   0.00108
  25   0.75   720000   0.0012
  27.5   0.825   792000   0.00132

flexural stiffness for the virgin beam is 7.8125

 IHPC BEAM AT ROOM TEMPERATURE-27 CELCIUS
force_applied  moment_bend  stress_bend  strain_bend
  0   0   0   0
  2.5   0.075   72000   9.77061e-005
  5   0.15   144000   0.000195412
  7.5   0.225   216000   0.000293118
  10   0.3   288000   0.000390824
  12.5   0.375   360000   0.00048853
  15   0.45   432000   0.000586236
  17.5   0.525   504000   0.000683943
  20   0.6   576000   0.000781649
  22.5   0.675   648000   0.000879355
  25   0.75   720000   0.000977061
  27.5   0.825   792000   0.00107477

flexural stiffness for the composite beam is 9.5951
```

IHPC BEAM AT ELEVATED TEMPERATURE-46 CELCIUS
force_applied moment_bend stress_bend strain_bend

0 -0.80514 -772935 -0.00121772

2.5 -0.73014 -700934 -0.00110429

5 -0.65514 -628934 -0.000990855

7.5 -0.58014 -556934 -0.000877422

10 -0.50514 -484934 -0.00076399

12.5 -0.43014 -412934 -0.000650558

15 -0.35514 -340934 -0.000537125

17.5 -0.28014 -268934 -0.000423693

20 -0.20514 -196934 -0.00031026

22.5 -0.13014 -124934 -0.000196828

25 -0.0551401 -52934.5 -8.33956e-005

27.5 0.0198599 19065.5 3.00368e-005

flexural stiffness for the composite beam is 8.26483

Press any key to continue . . .

APPENDIX E

Experimental data

BENDING OF UN-NOTCHED PV BEAMS AT T1<A_S				
FORCE F/N	**BENDING STRAIN/microstrain ON STRAIN GAUGES**			
	SPECIMEN1	**SPECIMEN2**	**SPECIMEN3**	**AVERAGE**
0	0	0	0	0
2.5	145	151	154	150
5	180	279	287	282
7.5	443	436	432	437
10	576	572	577	575
12.5	741	748	740	743
15	900	903	894	899
17.5	1052	1050	1054	1052
20	1160	1170	1161	1164
22.5	1263	1254	1266	1261
25	1307	1318	1308	1311
27.5	1420	1385	1390	1401
BENDING OF UN-NOTCHED IHPC BEAMS AT T1<A_S				
0	0	0	0	0
2.5	84	87	93	88
5	178	173	174	175
7.5	282	285	276	281
10	368	366	370	368
12.5	466	473	465	467
15	580	576	575	577
17.5	716	709	715	713
20	810	817	812	813
22.5	918	909	916	914
25	1022	1025	1016	1021
27.5	1043	1050	1054	1149
BENDING OF UN-NOTCHED IHPC BEAMS AT T2>A_f				
0	-1249	-1261	-1252	-1254
2.5	-1173	-1174	-1178	-1175
5	-1069	-1067	-1062	-1066
7.5	-908	-900	-907	-905
10	-777	-776	-769	-774
12.5	-652	-647	-653	-650
15	-563	-562	-549	-558
17.5	-410	-425	-422	-419
20	-300	-290	-289	-293
22.5	-149	-155	-147	-150
25	69	67	59	65
27.5	134	132	125	130

BENDING OF NOTCHED PV BEAMS AT T1 <A_S					
BENDING FORCE F/N				AVERAGE CRACK LENGTH a/mm	STRESS INTENSITY FACTOR K_I/MN/$m^{3/2}$
SPEC1	SPEC2	SPEC3	AVERAGE		
0	0	0	0	3	0
24	28	23	25	5	0.095
72	73	75.5	73.5	8	0.384
74	74	77	75	10	0.482
75	77	77.5	76.5	13	0.695
76	77	78	76.8	15	0.917
76.5	78	78	77.5	18	1.483
78	78.5	79	78.5	20	2.113
91.5	92	94	92.5	23	4.209
FRACTURE STRESS INTENSITY FACTOR K_{Ic}/MN/$m^{3/2}$					**4.209**
BENDING OF NOTCHED IHPC BEAMS AT T1 <A_S					
0	0	0	0	3	0
209	211.1	210	210	4	0.709
239	236.7	237	237.5	5	0.904
257	260	258.5	258.5	8	1.351
267	264.5	263.6	265	10	1.701
277	273.5	274.5	275	13	2.499
283.7	287	284.5	285	15	3.404
310.1	311.8	315.7	312.5	18	5.979
325	320	318	321	20	8.642
FRACTURE STRESS INTENSITY FACTOR K_{Ic}/MN/$m^{3/2}$					**8.642**
BENDING OF NOTCHED IHPC BEAMS AT T2 >A_f					
0	0	0	0	3	0
87	85	80	84	5	0.319
95	97	98	96.5	8	0.504
140	139	141	140	10	0.899
172	173	168	171	13	1.554
185	190	191.6	189	15	2.258
202	209	204	205	17	3.329
233.5	230	229.5	231	20	6.219
270	268	264.5	267.5	23	12.174
FRACTURE STRESS INTENSITY FACTOR K_{Ic}/MN/$m^{3/2}$					**12.174**

APPENDIX F

Material properties for Ni-Ti shape memory alloy wire and 60D epoxy matrix

Material properties	**Ni-Ti SMA**	**Epoxy** (polyurethane 60D)
Prestrain of SMA, ε_L	0.03	-
Max recovery strain, ε_{max}	0.08	-
A_S(ºC)	30	
A_f(ºC)	46	
E_A (Gpa)	16.0	-
E_M (Gpa)	11.5	-
E_m (GPa)	-	0.6
V_{SMA}(e-03)	12.56	-
V_m(e-03)	-	987.44
CTE	6.6 e-06/ ºC	90e-06/ ºC
Yield strength, σ_Y (MPa)	550	40
Glass trans. Temp T_g, (ºC)	-	75
Density (kg/m^3)	6500	1100
Elongation at fracture (%)	10	20
Poison ration, v	0.3	0.33
σ_{UTS} (MPa)	1150	-
Melting point (ºC)	1300	-
Resistivity (micro-Ohm.cm)	80 -100	-
K_{IC} (MN/m$^{3/2}$)	-	0.5 - 3.0
Model dimensions		
a (m)	0.03	
B(m)	0.01	
h (m)	0.007	
H(m)	0.025	
y (m)	0.0125	